12-2018

New Methods for the Optical Detection of Trace Compounds and the Delivery of a Chemical Oxidant

Roberto Alan Federico-Perez
University of Tennessee

To the Graduate Council:

I am submitting herewith a dissertation written by Roberto Alan Federico-Perez entitled "New Methods for the Optical Detection of Trace Compounds and the Delivery of a Chemical Oxidant." I have examined the final electronic copy of this dissertation for form and content and recommend that it be accepted in partial fulfillment of the requirements for the degree of Doctor of Philosophy, with a major in Chemistry.

Ziling Xue, Major Professor

We have read this dissertation and recommend its acceptance:

Michael J. Sepaniak, Tao Wu, Bin Zhao

Accepted for the Council:
Carolyn R. Hodges

Vice Provost and Dean of the Graduate School

(Original signatures are on file with official student records.)

New Methods for the Optical Detection of Trace Compounds and the Delivery of a Chemical Oxidant

A Dissertation Presented for the

Doctor of Philosophy

Degree

The University of Tennessee, Knoxville

Roberto Alan Federico-Perez

December 2018

Dedication

To my husband, Fernando.

Thank you for all the love and support. I look forward to our new adventures.

Acknowledgements

Reaching the end of this chapter was only possible with the help of many people along the way. First, I would like to thank my research advisor, Dr. Zi-ling Xue, for his guidance during my graduate studies. His patience, mentoring, and genuine passion for knowledge were valuable assets that not only helped me shape my professional career for the past five years, but also allowed me to grow as a person. I would also like to extend my gratitude to the rest of my committee, Drs. Michael Sepaniak, Bin Zhao, Tao Wu, and Svetlana Zivanovic for their constructive feedback and advice. A special thank you to Dr. Sepaniak for having me as a teaching assistant in one of his courses, which was probably the teaching assignment I enjoyed the most. Also, my sincere appreciation to Dr. Frank Vogt for his support to one of my projects, and for the fruitful conversations that helped me understand my research.

I could not emphasize enough how important it was for me to have great people to work with when I first joined the Xue group. I will always have fond memories of the times we would all have lunch together and talk about our lives inside and outside of the laboratory. We did not have a very large table, but we somehow managed to make it work. I would like to give them all a sincere thank you, in strict order of our almost constant seating arrangement everyday around noon: Tabitha Cook, Kendhl Seabright, Thomas Carpenter, Samuel Rosolina, Jonathan Fong, Adam Lamb, Shelby Stavretis, and Seth Hunter.

I would like to specially thank Jonathan Fong for showing me the ropes of the research during my first semester, and Adam Lamb for his immeasurable support on

Part 4 of this work, and his willingness to share his knowledge. Also, it was a great pleasure having Samuel Rosolina as a lab mate and constantly learning from his dedication and determination. I would like to thank him for his help to my research and for his continuous friendship after leaving the group. To Kendhl Seabright, thank you for your kindness and support during the first semesters of graduate school. It was definite more amenable knowing I had someone else sharing my experience as a new member of the analytical group. Also, a very special mention to Shelby Stavretis. Our conversations everyday were instrumental on navigating these last semesters of the program. I am excited to see what the future has planned for her and to continue our friendship on this new chapter. To the current group members, Duncan Moseley, Peter Pham, Zhiming Liu, Clay Mings, and Chelsea Widener, I wish you all the best on the rest of our journey. I am sure a fulfilling career is on the way for all of you.

I would like to take the opportunity to thank my family, friends, and other people that have been there for me before I even started my graduate studies. To my parents, Beatriz and Roberto, know that I am forever indebted to you for shaping me into the person I am today. To my brother, Jonathan, I am happy to see the person you have become, and I am excited to see where life takes you next. To my aunt, Clarisa, and my grandfather, Reynaldo, thank you for being great role models that I will always look up to. To my friend, Milagros, thanks for always picking up the phone when I needed it the most. To my undergraduate advisor, Dra. Clara R. Alvarez-Chavez, thank you for believing in me. Finally, to my husband Fernando, thank you for always listening and for having plenty of understanding for me these past years. Our best years are ahead of us, and I am excited to share them with you.

Lastly, I would like to thank the University of Tennessee for accepting me into its graduate program, and to Chevron, UT Research Foundation and National Science Foundation for partial support of my PhD studies.

Abstract

Biogenic amines are known indicators of spoilage in food. Indole in particular is a chemical used extensively to indicate seafood freshness. Levels higher than 25 µg [micrograms]/100 g shrimp mark early decomposition, according to the US Food and Drug Administration. We developed an optical probe based on an Ehrlich-type reaction to detect indole in shrimp. The probe is based on the reaction of *p*-dimethylaminobenzaldhyde (DMAB) with indole, generating red β[beta]-bis(indolyl)methane (BIM). Color development is observed by the naked eye after exposure to indole. When using UV-Visible spectroscopy as a detection method, the limits of detection and quantification are of 0.05 and 0.16 µg mL^{-1} [per milliliter], respectively. These limits lead to quantification of less than 25 µg [micrograms] indole/100 g shrimp, when recovery is accounted for. Moreover, an inexpensive handheld colorimeter can be used to perform optical measurements of indole by the probe with similar sensitivity. In addition, studies to confirm the structure of BIM were conducted. The β-position of two indole molecules is involved in the reaction with one DMAB molecule, yielding the product β[beta]-bis(indolyl)methane (BIM).

Determination of amines in aviation fuels is of interest as these species reduce fuel stability when present in higher concentrations. Since anilines and indoles are species of major presence in fuels, we have explored their simultaneous determination by the probe using a chemometric calibration with Classical Least Squares and Principal Component Regression.

In-situ chemical oxidation (ISCO) is an approach for remediation of polluted groundwater by the release of oxidants directly into the contaminated zone. We have developed a system for the controlled release of potassium persulfate from pellets of diatomaceous earth for the oxidation of organic contaminants, obtaining a continuous delivery for up to 21 h. In addition, this approach was used to release Fe^{2+} [iron two plus] ions for *in-situ* activation of persulfate. Controlled-released persulfate and Fe^{2+} ions from the pellets have been used for batch treatment of 15 mg L^{-1} [per liter] trichloroethylene (TCE) aqueous solution, giving residual TCE concentration of < [less than] 0.06 mg L^{-1} after 6 h and degradation of 93% TCE after 2 h.

Table of Contents

List of Tables

List of Figures

List of Schemes

Nomenclature and Abbreviations

A	Absorbance
AOP	Advanced oxidation process
b	Pathlength
BIM	β-Bis(indolyl)methane
BFB	Bromofluorobenzene
c	Concentration
CLS	Classical Least Squares
°C	Degree Celsius
DART	Direct Analysis in Real Time
DI	Deionized
DMAB	*p*-Dimethylaminobenzaldehyde
EC	Ethyl cellulose
EPA	Environmental Protection Agency
EtOH	Ethanol
EtOAc	Ethyl acetate
ε	Molar absorptivity
g	Grams
GC-MS	Gas chromatography-mass spectrometry
h	Hour
ISCO	*in-situ* chemical oxidation
K	Kelvin

λ	Wavelength
L	Liter
m	Meter
MeOH	Methanol
mM	Milimolar
M	Molar
mol	Moles
MΩ	Megaohm
min	Minute
mg	Miligram
mg L^{-1}	Miligrams per liter
mL	Mililiter
nm	Nanometer
NMR	Nuclear magnetic resonance
PCR	Principal Component Regression
PEG	Poly(ethyleneglycol)
PMMA	Poly(methylmetacrylate)
PS	Polystyrene
PTSA	*p*-Toluenesulfonic acid
R^2	Coefficient of determination
RSD	Relative standard deviation
rpm	Revolutions per minute
s	Second

t	Time
TCA	Trichloroacetic acid
TCE	Trichloroethylene
TEOS	Tetraethylorthosilicate
THF	Tetrahydrofuran
TMOS	Tetramethylorthosilicate
UV-Vis	Ultraviolet-visible
wt%	Weight percent
µg	Microgram
µg mL^{-1}	Micrograms per microliter
µL	Microliter

Part 1

Introduction and background

1.1. Foreword

Development of novel sensing mechanisms has been one of most active research areas, providing alternatives for chemical analyses that have been traditionally carried out by complex methods or instrumentation. An example is the use of optical detection with thin-film sensors or probes. Numerous applications of optical thin-film sensors have been reported in the literature, ranging from pH determination [1, 2] to the detection of gases [3, 4], metals [5, 6], and organic compounds [7, 8].

Control of food quality using new analytical techniques is an area of interest, as several parameters such as moisture, bacterial count, and other biomarkers are routinely monitored for quality assurance in the manufacturing processes [9]. Among these biomarkers, amines are a common indicator of bacterial breakdown of protein. Indole in particular has been observed in seafood and is correlated to seafood decomposition [10-12]. Amines are also analytes of concern in matrices such as fossil fuels, due to their effect on the storage stability [13,14]. Part of the research in this dissertation explores the determination of indole in food and fuel matrices, respectively. We have developed spectroscopic methods for indole analyses using doped polymer thin-film probes in shrimp and fuel matrices. In addition, colorimetric analysis of indole in shrimp has been developed using an inexpensive, hand-held color scanner (Color Muse™ [https://colormuse.io/]) coupled to cell phones.

Non-selective advance oxidation processes (AOPs) have been actively studied to treat a wide variety of organic pollutants in ground and wastewater [15]. *In-situ* chemical oxidation (ISCO) is a form of AOPs that rapidly treats contaminants [16]. Common ISCO oxidants include persulfates such as $K_2S_2O_8$, hydrogen peroxide, and permanganate.

However, these oxidizing species often have short lifetimes, limiting their applications [16]. Sustainable delivery of these oxidative species has been actively explored [17-19]. This dissertation also reports the development of a controlled release system involving the pelletization of persulfate and $FeSO_4$ in diatomaceous earth. The system performance has been studied using trichloroethylene as the target pollutant.

1.2. Analysis techniques used in the research

1.2.1. UV-visible spectroscopy

Irradiation of a molecule with light can result in the absorption of a photon. This leads to the transition from the ground state to an excited state [20]. Presence of delocalized electrons in organic compounds affects absorption in the UV-visible range of 180-800 nm. Functional groups leading to the absorption in the ultraviolet and visible region are called chromophores. For molecules in solution, vibrational states are affected by the solvent, causing the appearance of absorption bands rather than distinct peaks [21].

Beer's law shows a quantitative relationship between the concentration of a species and its absorbance of light at a specific wavelength:

$$A = \varepsilon b C \qquad \text{Eq. 1}$$

where A corresponds to absorbance, ε is the molar absorptivity ($M^{-1}\,cm^{-1}$), b is the optical pathlength (cm), and C is the concentration of the analyte (M). A typical UV-Vis spectrophotometer includes a light source and a monochromator. The light after the

monochromator then goes through a cuvette containing a solution of the analyte, and the intensity of the beam emerging from the analyte is then measured.

1.2.2. Color space

In color space, colors are described by their location in 3-dimensional (3D) geometric arrangements. Several color spaces have been proposed since the 18th century as our understanding for color perception has evolved [22]. An early theory by Young and Helmholtz proposed that human vision relied on the presence of sensors in the eye that are sensitive to three starting colors [23]. This *tristimulus* theory of color would eventually lead to the development of modern conventional color spaces. Since the observation of color is not uniform among individuals, one of the early tasks of the *Commision Internationale de l'Eclaraige* (CIE) was the development of a color space based on a standard observer. In 1931, the CIEXYZ color space was introduced, describing color by the coordinates in a sphere whose three axes are mutually perpendicular [24]. Each axis corresponds to a stimulus on the human eye to a certain region of the visible spectrum. However, a major disadvantage of this system was the lack of correlation between the geometric distance of two tones and their empirical perception among different colors [24]. In an effort to overcome this drawback and to unify the different schemes available for controlling color, the CIELAB space was developed in 1976 and it became popular for the specification of color differences.

The CIELAB system describes three parameters, L^*, a^*, and b^* (Figure 1.1). L^* provides a measurement for lightness in a scale of 0-100, where zero corresponds to absolute black and 100 to white. The a^* axis represents the green-red character ($a^* < 0$

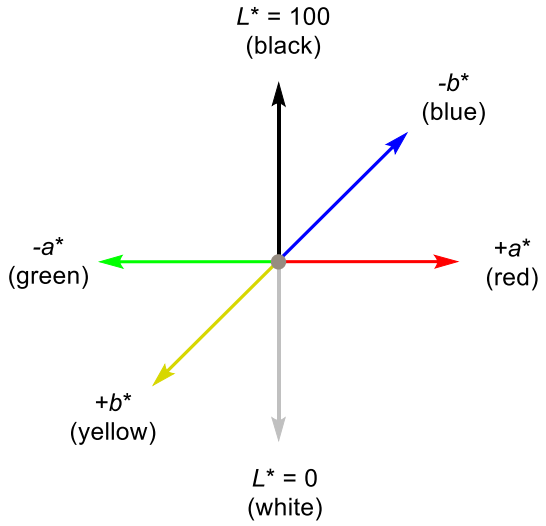

Figure 1.1. CIELAB color space.

green, $a^* > 0$ red), while b^* denotes blue-yellow components ($b^* < 0$ blue, $b^* > 0$ yellow). Applications of this device-independent color space, particularly correlating CIELAB parameters to food quality parameters, can be found in the literature [25]. For example, for the estimation of anthocyanins in juice [26].

1.2.3. Gas chromatography

Chromatography is currently the most extensively used separation method. In the same way as extraction techniques, it consists of the partition of a solute between two phases. However, chromatography involves the immobilization of one of them, the stationary phase [20]. The solutes flow between the stationary and mobile phases through a separation column, eluting at different times depending on the distribution between them.

Separation of a compound between stationary and mobile phases is governed by thermodynamic and kinetic factors. Thermodynamics affects the distribution constant

K_c, which is the ratio between equilibrium constants of the solute in the stationary and mobile phase. The magnitude of this distribution constant is affected by intermolecular and interionic forces between the phases, including Van der Waals forces and ionic interactions, hydrogen bonding, and charge transfer [27]. Kinetics affects the dispersion of the analyte on the column. As the stationary phase becomes increasingly wider during the elution process, the solutes tend to spread more, causing peaks to broaden [26]. An efficient chromatographic process considers parameters from both thermodynamic and kinetic effects in order to attain an optimal resolution amongst the analytes' peaks.

In gas chromatography (GC), the mobile phase is an inert gas, while the stationary phase is usually an open tubular column. GC is suitable for the separation of volatile compounds. The sample is injected with an air-tight syringe or autosampler into the injection port, where it is transported by the carrier gas along the capillary column. The column is contained inside the oven, which regulates the temperature of the elution and has a direct effect on the separation efficiency. A temperature gradient is regularly used to achieve an optimal balance between the resolution and elution time. A detector is coupled to the instrument to generate a measurable signal of the analytes eluting from the column.

Several detectors are available that vary in performance. While some of them are considered universal based on the wide response to several analytes, others respond selectively only to certain categories of compounds. The mass spectrometer (MS) is a universal detector that relies on the ionizing the analyte, followed by a fragmentation of the resulting ions. These are then distributed and detected based on their mass-to-

charge ratio (m/z). MS can provide information useful both for quantitative and qualitative analysis [28]. A diagram of a typical GC instrument is presented in Figure 1.2.

1.2.4. Overview of sol-gel process

The sol-gel process refers to a series of reactions leading to the synthesis of ceramic or glass-like solids from small molecules as starting materials. Common precursors include organic silane alkoxides such as tetramethylorthosilicate $Si(OMe)_4$ (TMOS) and tetraethylorthosilicate $Si(OEt)_4$ (TEOS). Inorganic precursors include sodium metasilicate Na_2SiO_3 [29]. Sol-gel synthesis involves an initial hydrolysis step, where O- H bonds are formed, and a condensation phase in which an expansion of the

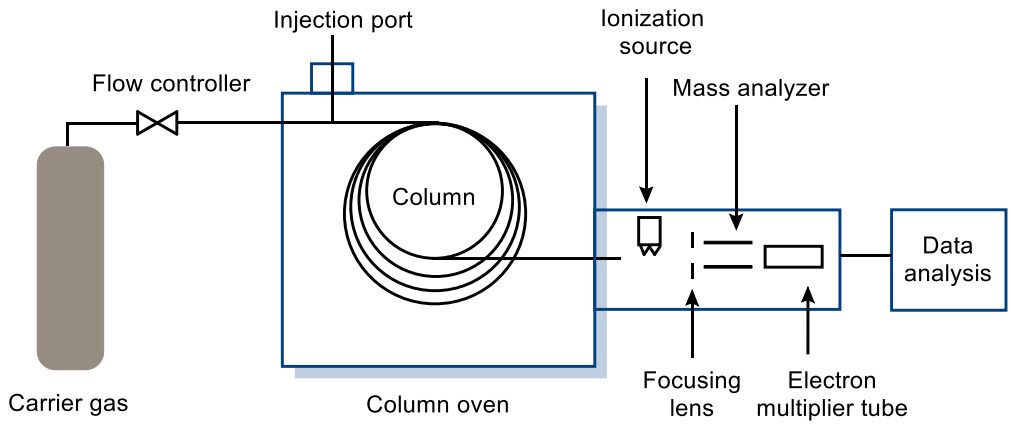

Figure 1.2. Basic diagram of typical GC-MS instrumentation.

molecular network occurs (Scheme 1.1). A drying or curing period then follows to expel water from the gel [30].

Several factors affect the gel formation. The hydrolysis step is typically catalyzed by either an acid or a base, resulting in gels with different characteristics [29]. Gelation times vary depending on the concentration of acid or base, temperature, water fraction and solvent [31].

1.3. Summary of dissertation parts

There are two central themes in this dissertation. Parts 2-4 focus on the development and application of an optical thin-film probe for the detection of indole and aniline. Part 5 reports our studies of the control release of potassium persulfate and Fe^{2+} for contaminant remediation.

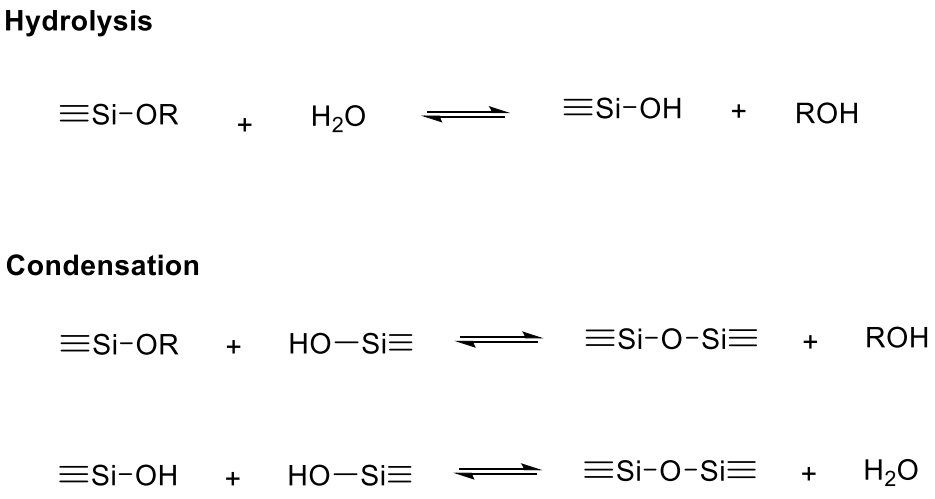

Scheme 1.1. General sol-gel process.

1.3.1. Part 2

We have studied the incorporation of an Ehrlich-type reaction in an optical probe for the assessment of shrimp freshness. Simplex optimization is performed to enhance the probe response. An organic solvent has been used to extract indole from shrimp and expose the probe to the recovered organic fraction. A limit of detection (LoD) of 0.05 mg L^{-1} is calculated for UV-Vis spectroscopic detection. Additionally, a CIELAB portable colorimeter has been used as a detection technique, achieving an LoD of 0.31 mg L^{-1}. Interference studies and the effect of film thickness are discussed, along with a comparison of other reports in the literature.

1.3.2. Part 3

Part 3 describes the use of the probe for the detection of indole and aniline in kerosene for potential applications in aviation fuels. We have explored the differences in the response of the probe to indole and aniline. Studies to estimate the selectivity of one analyte over the other are presented. In addition, we discuss attempts to achieve the simultaneous determination of both analytes by chemometric techniques (e.g., classical least squares and principal component regression).

1.3.3. Part 4

Studies to clarify the sensing mechanism in Parts 2-3 are presented here. Numerous reports in the literature give conflicting structures for the colored product from the reaction between indole and *p*-dimethylaminobenzaldehyde (DMAB). Part 4 discusses our studies of the product, including its synthesis and characterization. We

have found that the reaction occurs at the β position of indole. The 2:1 (indole:DMAB) stoichiometry of the reaction is confirmed. These findings are used in Parts 2-3 of the dissertation to assess the maximum saturation of the thin-film probe and the probability of other indole-like species to react with DMAB in the probe.

1.3.4. Part 5

Initial studies to develop pellets for the control release of persulfate are described. The effects of sol-gel coatings and mixtures on the pellets made with diatomaceous earth on the release of the oxidant have been investigated. To initiate the oxidative process by persulfate, we have investigated the use of Fe^{2+} ions as an activator and studied its control release. Furthermore, we have studied the use of such control-release pellets in the degradation of trichloroethylene (TCE) in water, reducing its concentration from 15 mg L^{-1} to below the limit of detection.

1.3.5. Part 6

A summary of the dissertation is presented with emphasis in potential commercial applications and recommendations for future work.

References

[1] S. de Marcos, O.S. Wolfbeis, Optical sensing of pH based on polypyrrole films, Anal. Chim. Acta 334 (1996) 149-153.

[2] L.R. Allain, K. Sorasaenee, Z. Xue, Doped thin-film sensors via a sol-gel process for high-acidity determination, Anal. Chem. 69 (1997) 3076-3080.

[3] Y. Tang, E.C. Tehan, Z. Tao, F.V. Bright, Sol-gel-derived sensor materials that yield linear calibration plots, high sensitivity, and long-term stability, Anal. Chem. 75 (2003) 2407-2413.

[4] C. Cantalini, M. Post, D. Buso, M. Guglielmi, A. Martucci, Gas sensing properties of nanocrystalline NiO and Co_3O_4 in porous silica sol-gel films, Sens. Actuators B 108 (2005) 184-192.

[5] P.C.A. Jerónimo, A.N. Araújo, M.C.B.S.M. Montenegro, C. Pasquini, I.M. Raimundo Jr, Direct determination of copper in urine using a sol-gel optical sensor coupled to a multicommutated flow system, Anal. Bioanal. Chem. 380 (2004) 108-114.

[6] S.A. Wallington, T. Labayen, A. Poppe, N.A.J.M. Sommerdijk, J.D. Wright, Sol-gel entrapped materials for optical sensing of solvents and metal ions, Sens. Actuators B 38 (1997) 48-52.

[7] C.I. Li, Y.H. Lin, C.L. Shih, J.P. Tsaur, L.K. Chau, Sol-gel encapsulation of lactate dehydrogenase for optical sensing of L-lactate, Biosens. Bioelectron. 17 (2002) 323-330.

[8] K. Ertekin, S. Cinar, T. Aydemir, S. Alp, Glucose sensing employing fluorescent pH indicator: 4-[(*p*-N,N-dimethylamino)benzylidene]-2-phenyloxazole-5-one,

Dyes Pigm. 67 (2005) 133-138.

[9] E. Ohashi, I. Karube, Sensors for the food industry, Food Control 4 (1993) 183-188.

[10] R. Mendes, A. Huidobro, E.L. Caballero, Indole levels in deepwater pink shrimp (Parapenaeus longirostris) from the Portuguese coast. Effects of temperature abuse, Eur. Food Res. Technol. 214 (2002) 125-130.

[11] R. Mendes, A. Goncalves, J. Pestana, C. Pestana, Indole production and deepwater pink shrimp (Parapenaeus longirostris) decomposition, Eur. Food Res. Technol. 221 (2005) 320-328.

[12] R.A. Benner, Jr., W.F. Staruszkiewicz, P.L. Rogers, W.S. Otwell, Evaluation of putrescine, cadaverine, and indole as chemical indicators of decomposition in penaeid shrimp, J. Food Sci. 68 (2003) 2178-2185.

[13] K.E. Dahlin, S.R. Daniel, J.H. Worstell, Deposit formation in liquid fuels. 1. Effect of coal-derived Lewis bases on storage stability of Jet A turbine fuel, Fuel 60 (1981) 477-480.

[14] M. Sobkowiak, J.M. Griffith, B. Wang, B. Beaver, Insight into the mechanisms of middle distillate fuel oxidative degradation. Part 1: On the role of phenol, indole, and carbazole derivatives in the thermal oxidative stability of Fischer−Tropsch/petroleum jet fuel blends, Energy Fuels 23 (2009) 2041-2046.

[15] C. Comninellis, A. Kapalka, S. Malato, A. Parsons Simon, I. Poulios, D. Mantzavinos, Advanced oxidation processes for water treatment: advances and trends for R&D, J. Chem. Technol. Biotechnol. 83 (2008) 769-776.

[16] R.L. Siegrist, In Situ Chemical Oxidation for Groundwater Remediation, New

York, NY: Springer Science+Business Media, New York, NY, 2011.

[17] C. Liang, C.-Y. Chen, Characterization of a sodium persulfate sustained release rod for in situ chemical oxidation groundwater remediation, Ind. Eng. Chem. Res. 56 (2017) 5271-5276.

[18] A. Kambhu, S. Comfort, C. Chokejaroenrat, C. Sakulthaew, Developing slow-release persulfate candles to treat BTEX contaminated groundwater, Chemosphere 89 (2012) 656-664.

[19] M.R. Dhananjeyan, E. Fine, J. Kiwi, Synthetic polymer delivery system: Sustained release of persulfate during the photo-oxidation of an azo-dye, J. Photochem. Photobiol. A. Chem. 136 (2000) 125-131.

[20] D.C. Harris, C.A. Lucy, Quantitative Chemical Analysis, W.W. Norton, New York, NY, 2016.

[21] D.A. Skoog, F.J. Holler, S.R. Crouch, L. Cengage, Fundamentals of Analytical Chemistry, Cengage Learning, Andover, 2014.

[22] R.G. Kuehni, Color Space and Its Divisions: Color Order from Antiquity to the Present, J. Wiley, Hoboken, NJ, 2003.

[23] D. Kernell, Colours and Colour Vision: An Introductory Survey, Colors and Color Vision, Cambridge: Cambridge University Press, 2016.

[24] A.D. Broadbent, Colorimetry, Methods A2 - Lindon, John C, Encyclopedia of Spectroscopy and Spectrometry, 2nd Ed., Academic Press, Oxford, 2010, pp. 372-379.

[25] V. Sant'Anna, P.D. Gurak, L.D. Ferreira Marczak, I.C. Tessaro, Tracking bioactive compounds with colour changes in foods - A review, Dyes Pigm., 98

(2013) 601-608.

[26] U.A. Fischer, R. Carle, D.R. Kammerer, Thermal stability of anthocyanins and colourless phenolics in pomegranate (Punica granatum L.) juices and model solutions, Food Chem. 138 (2013) 1800-1809.

[27] J.M. Miller, Chromatography: Concepts and Contrasts, 2nd ed., Hoboken, N.J.: Wiley, Hoboken, NJ, 2005.

[28] E. Stauffer, J.A. Dolan, R. Newman, Gas Chromatography and Gas Chromatography—Mass Spectrometry, in Fire Debris Analysis, Academic Press, Burlington, 2008, Ch. 8, pp. 235-293.

[29] L.A. Adams, R.O. Shaibu, R.E. Essien, A. Oki, Bentonite clay and waterglass porous monoliths via the sol-gel process, J. Met., Mater. Miner. 21 (2011) 1-6.

[30] L.L. Hench, J.K. West, The sol-gel process, Chem. Rev. 90 (1990) 33-72.

[31] A.H. Boonstra, T.N.M. Bernards, The dependence of the gelation time on the hydrolysis time in a two-step SiO_2 sol-gel process, J. Non-Cryst. Solids 105 (1988) 207-213.

Part 2

Optical probe for the analysis of trace indole in shrimp

This part is based on the following paper: Only minor revisions were made.

R.A. Federico-Perez, Z.-L. Xue, Optical probe for the analysis of trace indole in shrimp, Anal. Biochem. 557 (2018) 104-110.

R.A. Federico-Perez proposed the study, conducted experimental work, interpreted the results, and prepared the manuscript. Dr. Z.-L Xue supervised the work.

Abstract

Indole is a chemical from the decomposition of shrimp and is used extensively to indicate seafood freshness. US Food and Drug Administration (FDA) sets its concentration of <25 μg/100 g shrimp as the threshold for Class I (fresh shrimp). A novel optical probe is reported to quantitatively analyze trace indole in shrimp, including the Class I threshold concentration. Based on an Ehrlich-type reaction, UV-visible spectroscopic analysis of indole in petroleum ether gives a limit of detection (LoD) and quantification (LoQ) of 0.05 and 0.16 μg mL^{-1}, respectively. For 25 μg indole/100 g shrimp extracted into petroleum ether, the probe successfully detects it and the color change is visible to the naked eye. Analysis of the probe response by a UV-visible spectrometer leads to quantification of ≤25 μg indole/100 g shrimp, when recovery is accounted for. When a handheld colorimeter, based on the CIELAB color space, and a smartphone with Bluetooth connectivity are used, the probe demonstrates similar sensitivity for indole in shrimp. The current probe is made of 4-(dimethylamino)benzaldehyde (DMAB) and catalyst *p*-toluenesulfonic acid (PTSA) in thin films. Indole in shrimp samples after extraction reacts with DMAB to give red β-bis(indolyl)methane.

2.1. Introduction

Shrimp consumption has steadily increased, depending heavily on imports to meet the market needs [1]. Such high demand for imports has motivated the need for rapid methods to evaluate shrimp freshness. The US Food and Drug Administration (FDA) relies on organoleptic assessment for the quality classification of shrimp. However, quantitative indole determination is used for confirmation and classification of the seafood freshness. Indole is produced as a byproduct of the bacterial degradation of tryptophan residues in proteins by the enzyme tryptophanase, in addition to pyruvate and ammonium (Scheme 2.1). Numerous microorganisms are indole-positive, and this characteristic has been utilized as a test for phenotypical characterization of bacteria. Therefore, the presence of indole at high concentrations suggests a failure to meet Good Manufacturing Practices (GMPs) during harvesting and processing. The FDA categorizes shrimp quality in three distinctive classes. Class I (passable) corresponds to samples ranging from fresh to characteristic odors, with an indole concentration of <25 µg/100 g shrimp. Classes II and III are indicative of slight and definitive decomposition, respectively. Indole levels of >25 µg/100 g correspond to these two latter classes [2].

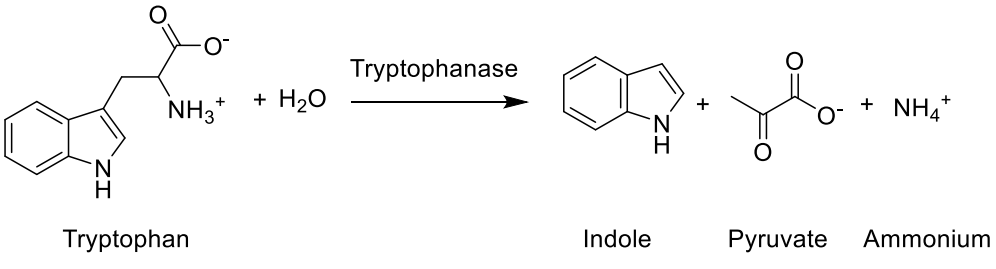

Scheme 2.1. Enzymatic degradation of tryptophan to indole by bacteria [12].

Methods for the determination of indole in shrimp and other fish products have been reported in the literature. In general, solvent extraction is coupled with colorimetric [3-5], fluorescence [6], voltammetric [7,8], HPLC [9,10] or GC (gas chromatography) detection [11]. Currently, HPLC with fluorescence detection prevails as the FDA recommended method for indole determination in shrimp [10]. The reported methods typically rely on instrumentation in a central location and are difficult to adapt into a rapid field test. In addition, the indole detection in the literature generally involves several time-consuming extraction steps. Snellings and coworkers have presented a simplified extraction technique that, when coupled to a *solution* test through a reaction with DMAB, colorimetrically quantitates indole in shrimp, achieving 68.7% derivatization of original indole [4].

Recently, color-sensing processes based on digital RGB (red, green, blue) parameters have been reported [13-16]. Digital cameras with the RGB parameters make it more convenient to analyze color development than desktop instruments. Nevertheless, a disadvantage of using RGB parameters is that it does not match closely with the human sense of color [17]. The CIELAB color space was first introduced in 1976, and it provides more uniformity than the RGB parameters in terms of visual color perception and position in a coordinate system when compared to earlier color spaces [18]. Each color is defined according to its contribution on three axes: L^* for lightness (0-100), a^* for red/green character (green < 0, red > 0), and b^* for blue/yellow character (blue < 0, yellow > 0). As a device-independent reference, the CIELAB color space has found numerous applications. Sant'Anna and coworkers offer a comprehensive review of the use of CIELAB parameters and their correlation to the content of bioactive

compounds by direct measurements on fruits and vegetables [19]. Several particularly portable CIELAB color readers are now available in the market. We have recently used a handheld colorimeter (Node Chroma™) and CIELAB for a quantitative, colorimetric probe to determine hydrogen sulfide gas concentration [20].

Simplex optimization evaluates the effect of several parameters on the performance of the analysis. Unlike univariable optimization procedures, where the influence of each factor is explored one at a time, the simplex algorithm reduces the number of experiments required to reach an optimal set of conditions [21]. The use of the basic simplex algorithm for the optimization of flow preconcentration systems, for example, has been shown [22,23].

Development of a solid sensor to detect indole *in vapor phase* has been reported [24,25], which mostly depends on the naked-eye detection of the color. To our knowledge, no optical probe for the detection of indole in solution has been reported. We have developed a thin-film probe for indole. Ethyl cellulose thin films, containing 4-(dimethylamino)benzaldehyde (DMAB) and an organic acid as catalyst for the Ehrlich reaction, is used for the probe. Formation of a color product in the probe is monitored by either a UV-visible spectrometer or a portable tristimulus CIELAB color reader (with a mobile phone through Bluetooth connectivity). The composition of the thin film probe has been optimized by the basic simplex algorithm. The new probe is highly sensitive, quantitatively analyzing trace indole in shrimp, including the Class I threshold concentration of <25 μg/100 g shrimp between “passable” and “slight decomposition.” The current optical probe offers a simpler, low-cost procedure for analysis of indole in shrimp with potential for field use than the HPLC-based method.

2.2. Materials and methods

Ethyl cellulose (90-110 mPa, TCI America), 4-(dimethylamino)benzaldehyde (DMAB, Certified ACS, Fisher), *p*-toluenesulfonic acid monohydrate (PTSA, Fisher, 99%), indole (Acros, 99+%), petroleum ether (certified ACS, Fisher, b.p. range 36-60 °C), trichloroacetic acid (Alfa Aesar, 99%) and ethanol (Decon Labs, 100%) were used as obtained. Spectra were collected in an Agilent 8453 UV-Visible spectrophotometer. *L*a*b** parameters were measured using a MUSE™ colorimeter (about $50) by Variable, Inc. (Chattanooga, TN, USA) [26]. A single-speed Waring blender E8100 (Eberbach corporation, Ann Arbor, MI, USA) was utilized on the extraction of indole from shrimp. GC-MS measurements were performed on a Hewlett-Packard HP 6890 Series GC system with a HP 5973 mass spectrometer detector, equipped with a HP-5ms Ultra Inert column (30.0 m × 0.25 mm i.d. × 0.25 µm film thickness). 2-methylindole (Alfa Aesar, 98+%) was used as an internal standard. Interference studies were carried out with skatole (3-methylindole, Alfa Aesar, 99%), catechol (Acros Organics, 99+%), melanin (MP Biomedicals), and 2-methylindole.

2.2.1. Probe fabrication

Ethyl cellulose (0.8 g) was dissolved in 15 mL of 1:1 ethanol/toluene by sonication. For a typical batch, 8.0 mg of DMAB was added to 1.0 g of the ethyl cellulose solution and 100 µL of a solution of PTSA in ethanol (0.1780 g mL^{-1} EtOH). The mixture was stirred for 15 min. Glass microscope slides were cut to obtain 1.2 × 0.8 cm^2 pieces. A film was deposited onto the glass slide by adding 60 µL of the polymer mixture to the surface of the slide that was spun at 2,500 rpm using an in-house spin

coater. The probe was dried in air overnight before weighing or use. Probes were stored in open air prior to use.

Two thicker Films A and B have also been prepared and studied in order to compare with the probe. Details of their preparation are given in supplemental materials.

2.2.2. Probe optimization

Basic simplex optimization was used to determine the formulation of the polymer mixture. A basic simplex method uses a sequence of displacements of an initial experimental design with the purpose of discarding areas of unfavorable performance. We used the absorbance of the probe after a 30 min exposure to 10 mL of 0.5 μg mL^{-1} indole to assess the performance of the formulation. The following three variables were optimized: DMAB, PTSA, and EC solution. Table 2.1 describes the original design conditions and the variation steps utilized to apply the basic algorithm. Additionally, a probe response vs. time profile showing the color development of the probe was constructed by exposing several probes under the same conditions as described above, but each with a different exposure time (2-70 min). A consistent exposure time was selected based on this profile.

Table 2.1. Initial values and variation steps for simplex optimization

Variable (per batch)	Initial value	Variation step
DMAB content (mg)	6.0	4.0
PTSA content (mg)	10.0	10.0
Ethyl cellulose content (mg)	800.0	200.0

2.2.3. Indole extraction

Commercial pre-frozen, head-off shrimp was obtained from a local supermarket. A sample of 20 g of peeled and deveined shrimp was spiked with 50 µL of 100 µg mL^{-1} stock solution of indole in petroleum ether (equivalent to 25 µg/100 g of shrimp). A 5% aqueous solution of trichloroacetic acid (10 mL) of and 50 mL of ice-cold petroleum ether were added to the spiked sample in a single-speed Waring blender with an aluminum foil lined cap and homogenized for 1 min. After rinsing the walls with DI water, the sample was blended for an additional 30 s. The mixture was distributed in six 10-mL conical tubes and centrifuged at 3,200 rpm for 10 min. The upper organic layer was recovered and the rest of the phases were homogenized again after adding 15 mL of petroleum ether. After a second centrifugation, the total recovered volume of petroleum ether was stirred with 50 mg of silica gel for 30 s. Volume of the organic phase was reduced to less than 10 mL under a nitrogen gas flow overhead. After concentration, each solution was added petroleum ether in a volumetric flask so its volume was 10.0 mL.

2.2.4. UV-Vis/CIELAB measurements

Probe calibration was conducted by exposing the coated glass slides to 10 mL of standard indole solutions at different concentrations for 30 min under magnetic stirring at 1,200 rpm. Spiked sample extracts were exposed in a similar fashion. Unspiked shrimp was extracted via the aforementioned procedure and used as a blank. Then, the probes were allowed to dry in air and UV-visible spectra were collected by placing the slides in a quartz cuvette with a 2-mm pathlength. The polymer film on the probe was positioned to face the incident beam. Four measurements on different points along the length of the probe surface were taken and absorbance data were averaged to account for potential variations throughout the film. A Savitzky-Golay filter with a 10-point window was applied on average spectra, then baseline subtraction and peak fitting were performed using the OriginPro 8.1 software. Absorbance maxima (540 nm) were recorded.

Similarly, CIELAB coordinates were obtained by placing the probe slides on a white background. The handheld colorimeter was calibrated with the manufacturer-supplied calibration cap before measurement. It was placed directly on top of the probes at 6 different points, and L^*, a^*, and b^* parameters were recorded to obtain average values. Illuminant and observer angle were set at D50 and 2°, respectively.

2.2.5. GC-MS determination

To establish a comparison, GC-MS analysis was performed at a constant flow rate of 1.0 mL min^{-1} using helium as a carrier gas. Temperature was ramped from 100 °C to 240 °C at 13.4 °C min^{-1}. Indole standards in petroleum ether (25 mL) were

prepared by diluting the corresponding volume of a 100 μg mL^{-1} stock solution of indole, adding 0.2 mL of 2-methylindole (1 μg mL^{-1}) as an internal standard, and diluting to the mark.

2.3. Results and discussion

2.3.1. Sensing mechanism

The probes show a visible gradient of the red color based on the Ehrlich-type reaction that correlates with increasing indole concentrations. The reaction with DMAB forms a red product β-bis(indolyl)methane (λ_{max} 536 nm, ε = 1.0×10^2 M^{-1} cm^{-1} in ethanol solution) that includes two indole moieties cleaved at the β position as a result of the nucleophilic addition onto DMAB (Scheme 2.2). There have been confusions in the literature regarding the nature of the reaction and structure of the product [27-31]. Reactions involving both 1:1 and 1:2 DMAB/indole have been reported [32,33]. In addition, different sites on the indole ring were reported for the reaction. We have recently confirmed the nature of both the site of the reaction and stoichiometry [34]. An extended discussion on this issue can be found in Part 4 of this dissertation.

Several polymers were tested to find a matrix that would give stable films upon exposure to potential solvents used in extraction (Table A1). After the polymers giving stable films were identified, the films were exposed to a concentrated indole solution (1% m/v) to determine whether indole would diffuse into the films. Ethyl cellulose in a 1:1 ethanol/toluene solution provided both film stability and an initial naked-eye response. It was selected as the polymer matrix for the probe for further optimization.

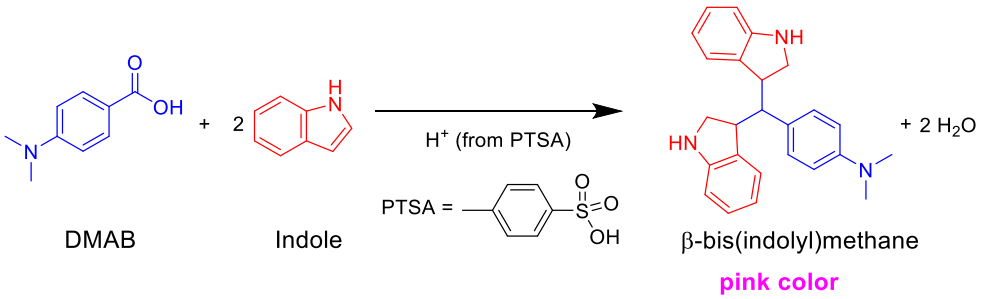

Scheme 2.2. Reaction of indole with DMAB forming pink-colored product β-bis(indolyl)methane. See Scheme 4.3 in which β-bis(indolyl)methane is formed from the reaction of DMAB with indole in solution with HCl as catalyst.

Given that the Ehrlich-type reaction is acid-catalyzed (Scheme 2.2), developing a formulation for the ethyl cellulose film containing both DMAB and an acid inside is essential for the sensing. Earlier formulations of the probe employed a diluted HCl solution in the films, which caused a non-uniform response over the probe surface. We then turned to solid organic acid *p*-toluenesulfonic acid (PTSA) and developed the current procedure and formulation to incorporate it into the probe. Unlike volatile HCl acid, non-volatile PTSA allows for consistent acid concentration in the probes.

2.3.2. Probe optimization

As a sequential method, simplex optimization implies the movement of an initial set of conditions across the experimental design in order to obtain an area of optimal response. We have applied it to optimize our probe formulation using absorbance at 540 nm as a response parameter. In theory, a larger amount of DMAB embedded into the film would translate into a larger linear range for our analysis. However, such

formulations with higher DMAB concentrations produced less transparent films compromising subsequent optical analysis. Thus, an initial set of values were chosen to optimize three variables in the formulation of the probe. By adding a variation step to each value using the basic simplex algorithm, a set of four experiments (hereafter denominated vertices) was obtained. The simplex comprises the geometrical figure delimited by *n+1* vertices, where *n* is the number of variables to optimize. In this manner, the 4 initial vertices (Table 2.2) were established and tested to determine the one with the lowest response. We utilized the basic simplex algorithm, in which the variation steps for each initial value are kept constant. Subsequent vertices were calculated by reflecting the experiment with the lowest absorbance (vertex *W*) through the rest of the vertices. The coordinates of this new reflected vertex (*R*) are obtained by Eq. 3.1:

$$R = 2M - W \qquad \text{Eq. 2.1}$$

M corresponds to the coordinates of the midpoint among the rest of the vertices. The coordinates of the midpoint can be calculated by Eq. 2.2:

$$M = \frac{1}{n} \sum_{j \neq i}^{n} v_j \qquad \text{Eq. 2.2}$$

where *n* represents the number of variables (*n* = 3 for this case) and *j* corresponds to each remaining vertex after discarding *W* (denoted here as *i*) [21].

Further reflection on the least favored vertices showed that optimal conditions correspond to those on initial vertex 3. Hence, all further tests were conducted utilizing the formulation described for experiment 3 (Table 2.2).

The response of the probe to 10 mL of 0.5 μg mL^{-1} indole in petroleum ether, which corresponds to the concentration of the indole solution extracted from 25 μg/100 g shrimp, was then tested by exposing ten probes to different times (*n = 1* for each exposure time). A probe response vs. time profile is shown in Figure 2.1. In about 20 min, the probe response started to level, reaching initial saturation. After 40 min, the

Table 2.2. Summary of simplex optimization experiments[a]

Experiment	Vertex	DMAB (mg)	PTSA (mg)	EC solution (mg)	Absorbance
1	*I*	6.0	10.0	800.0	0.038
2	*I*	10.0	10.0	800.0	0.018
3	*I*	8.0	18.7	800.0	0.097
4	*I*	8.0	12.9	964.0	0.039
5	*R*(2)	5.0	18.0	909.0	0.025
6	*R*(1)	11.0	18.0	909.0	0.024
7	*R*(3)	8.0	12.9	636.0	0.017

[a]*I*: initial, *R*: reflection; For example, *R*(2) is the vertex formed by reflection of 2 through 1,3, and 4.

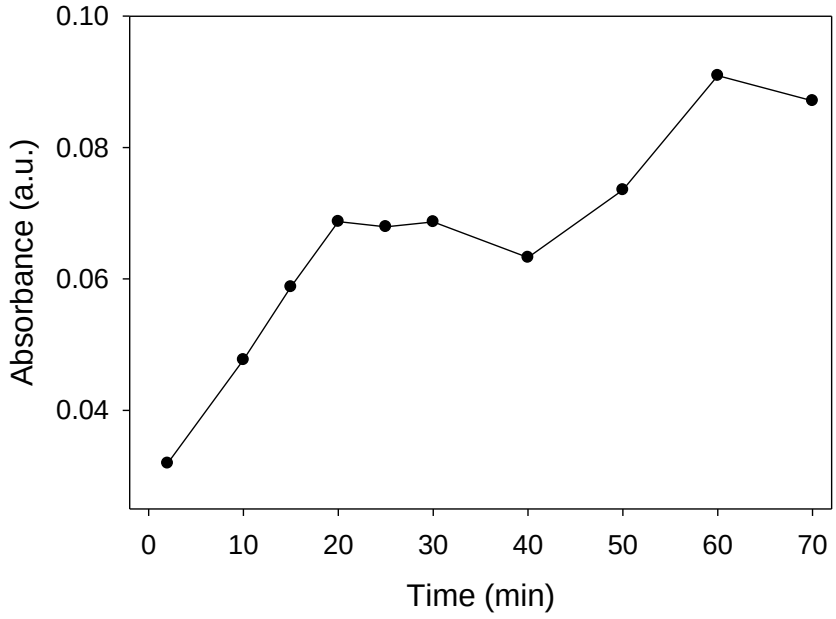

Figure 2.1. Probe response vs. time to 10 mL of 0.5 μg mL^{-1} indole solution in petroleum ether.

absorbance of the probe started to increase again. Given that DMAB is irreversibly depleted in the reaction with indole (Scheme 2.2), we think that film porosity perhaps increased after 40 min, exposing the remaining DMAB in smaller pores to indole, leading to the new response at the later stage. However, for consistency, we selected 30 min as the exposure time for subsequent tests of the probe.

2.3.3. Probe response to indole in petroleum ether solutions and analysis by visible spectroscopy

When the probe was exposed to 10 mL of 0.1-3.0 μg mL^{-1} indole solutions in petroleum ether, it gradually turned from colorless to pink, forming β-

bis(indolyl)methane. Photos of the probe to 0.1-3.0 μg mL^{-1} indole solutions are given in Figure 2.2.

The formation of the colored product in the probe is evidenced by the appearance of a peak at 540 nm (Figure 2.2-a). Absorbance at 540 nm shows a linear dynamic range between 0.1 and 3.0 μg mL^{-1} (Figure 2.5-b). At higher concentrations (>3.0 μg mL^{-1}), the probe reached the saturation of its response. Although a larger dynamic range was observed for 15 min exposure time (Appendix A, Figure A1), we have used 30 min for subsequent experiments due to its enhanced sensitivity. The limits of detection (LoD, $3\sigma/s$; s = slope of the calibration plot) and quantification (LoQ, $10\sigma/s$) for the probe are 0.05 μg mL^{-1} and 0.16 μg mL^{-1}, respectively.

GC-MS analysis of the 0.1 and 3.0 μg mL^{-1} indole solutions was performed to compare with that of the UV-visible spectroscopy. Results are given in the supplementary materials. A linear response (0.998) was observed in the range of 0.25-10 μg mL^{-1} (Figure A2), showing the LoD and LoQ of 0.14 μg mL^{-1} and 0.48 μg mL^{-1}, respectively. Unlike the probe's response, the GC-MS analysis failed to detect <0.25 μg mL^{-1} indole solutions. In other words, sensitivity of the probe by UV-visible spectrometer is higher. In particular, as analyzed below, the probe sensitivity is adequate to analyze indole in Class I (fresh shrimp). Our probe, however, showed a shorter linear range when compared to GC-MS.

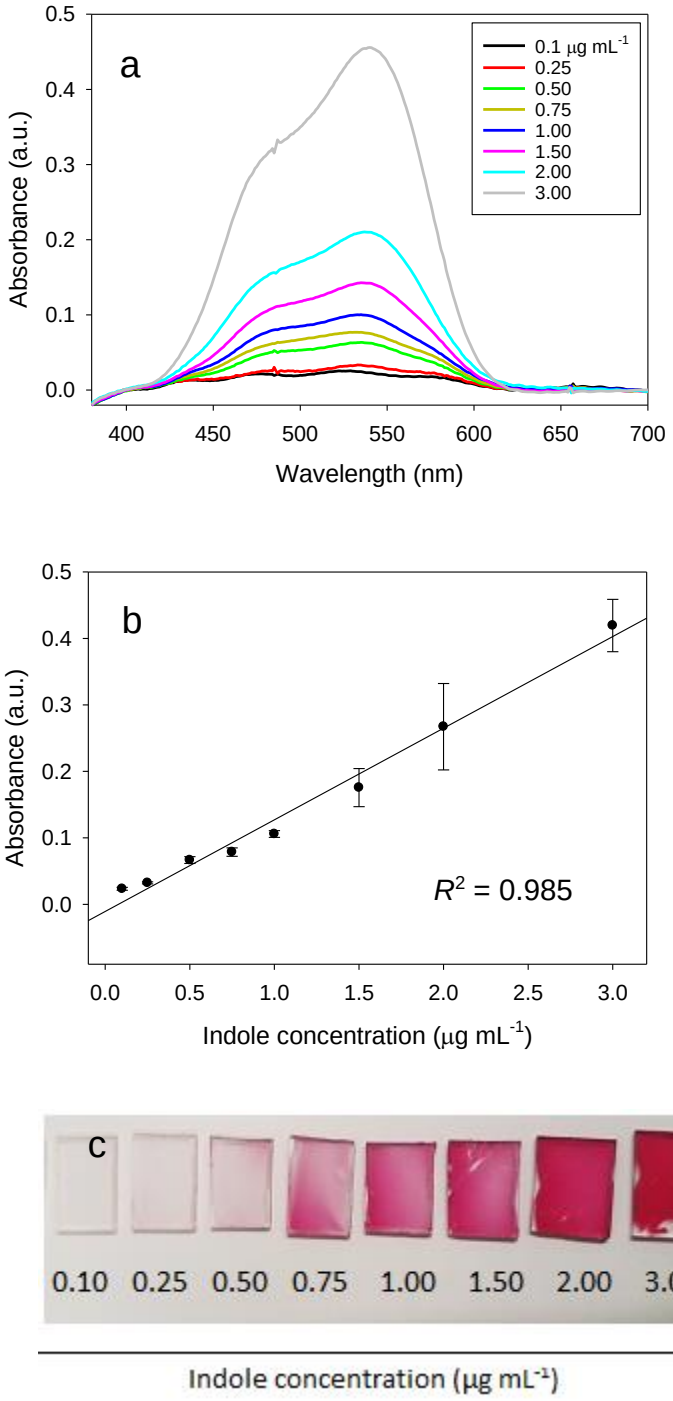

Figure 2.2. (a) Visible spectra of the probe showing response to increasing indole concentrations. (b) Calibration plot using the absorbance at 540 nm. (c) Photos of the probe to 0.1-3.0 μg mL^{-1} indole solutions.

2.3.4. CIELAB detection

Probe response by the CIELAB color space using the portable colorimeter MUSE^{TM} was also evaluated, showing a good correlation (R^2 = 0.990) on the *a** (the red/green axis) parameter (Figure 2.3-a). The *L** (lightness) values on Figure 2.3-b showed a negative correlation (R^2 = 0.982), as the probe became more opaque upon exposure to higher indole concentrations. The *a** values are thus preferred than the *L** parameters. No correlation was observed for the *b** values (Figure A3).

For the values on the *a** axis, the LoD and LoQ are 0.31 and 1.02 μg mL^{-1}, respectively. These limits are larger than those using the Agilent 8453 UV-Visible spectrophotometer. In other words, the portable colorimeter is not as sensitive as the spectrophotometer, although the colorimeter is much cheaper and easier to use [35]. The lower sensitivity by the colorimeter is perhaps expected since it is based on reflectance from the polymer surface. The absorbance spectroscopy is more sensitive, because of a longer pathlength from the film of the probe. It should be pointed out, however, that the sensitivity of the MUSE portable colorimeter to the probe is adequate for the analysis of indole extracted from Class I (fresh) shrimp, as the discussion below shows. Its low cost ($50) and cell phone connectivity are particularly attractive.

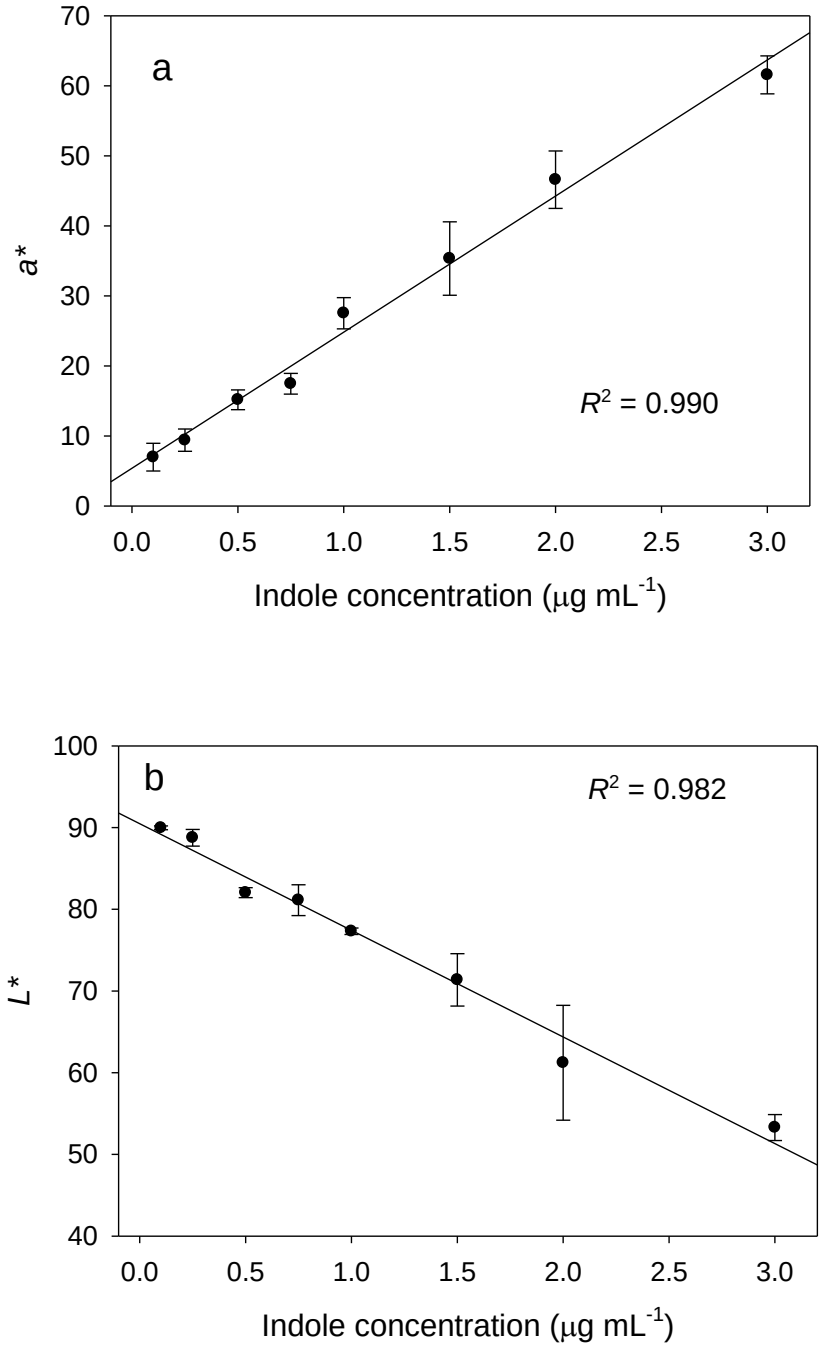

Figure 2.3. (a) Calibration plot with a* axis values showing correlation with indole concentration. (b) Calibration plot with the L* axis values.

2.3.5. Effect of film thickness

Tests have shown that the process to make the probe gives the thinnest film. The tests are given in supplementary materials. In order to find the effects of film thickness on sensor response, we have fabricated two different thicker films (Films A and B) than our probe. Film A, with the mass of 0.85 ± 0.23 mg (n = 7), was prepared by adding a second layer of the polymer mixture on top of Film A through spin-coating at 2,500 rpm. Film B, with the mass of 1.90 ± 0.29 mg (n = 7), was fabricated by direct drop-coating of the polymer mixture (25 µL) onto the substrate without spinning, followed by drying overnight. Using the mass of 0.64 ± 0.07 mg of the probe, it is estimated that Films A and B are about 1.3 and 3 times, respectively, of the thickness of the probe. Table 2.3 summarizes the calibration parameters for each probe in the range of 0.1-3.0 µg mL^{-1} of indole for both UV-visible and CIELAB color space detection.

Even though the thicker Films A and B have a longer optical pathlength, they are both less sensitive than the regular thin film. It is not clear why. Perhaps the regular thin film makes the preconcentration of indole in the film easier and more efficient. In

Table 2.3. Effect of film thickness on probe response

Probe	UV-Vis detection		CIELAB detection	
	Equation	R^2	Equation	R^2
Probe	$y = 0.172x - 0.037$	0.990	$y = 19.0x + 3.354$	0.991
Film A	$y = 0.156x - 0.026$	0.992	$y = 17.5x + 1.560$	0.993
Film B	$y = 0.100x - 0.013$	0.994	$y = 14.9x + 0.325$	0.994

addition, even with the same amount of indole in the film, the regular thin film with the smallest film volume would have highest indole concentration, leading to formation of more pink-colored product β-bis(indolyl)methane. This may explain the larger absorbance and *a** values and higher slopes for the regular thin film. Figures A4 and A5 (Appendix A) shows calibration plots for thicker Films A and B.

2.3.6. Interference studies

The effects of skatole (3-methylindole), melanin, catechol, and 2-methylindole as potential interferences have been studied. Although indole has been reported as the primary product in the decomposition of L-Trp, indole-3-acetic acid (IAA) may also be generated as a metabolite by the following path: Trp → IAA → skatole (3-methylindole) [4, 36]. Guo and coworkers have reported that no reaction is observed between IAA and DMAB at room temperature [37]. Nevertheless, skatole can potentially form a purple product with DMAB (λ = 580 nm) under certain conditions at a slower rate than indole [4, 38]. Jensen and coworkers have shown that the metabolic degradation of tryptophan results in indole as a primary product, with the production of skatole at 15-20% of L-Trp [36]. Therefore, we exposed the probe to a mixture of 5:1 indole/skatole (0.5 and 0.1 μg mL^{-1}, respectively). Our results show no significant skatole interference. There is <5% variation in the probe response to the mixture than the indole alone (Table 2.4).

Melanin has been reported to form colored products with DMAB after alkali fusion [39]. The presence of melanin in shrimp can be justified by a condition called melanosis, where brown spots are observed on the shrimp surface [40]. Our solubility test of

melanin, however, shows that it does not dissolve in water or petroleum ether. Consequently, it is unlikely to partition into the organic layer after the indole extraction.

We have studied the effect of catechol since it can act as a precursor in the synthesis of some melanins [41]. We have exposed our probe to 0.1 mg L^{-1} catechol. The tests show no reaction between our probe and catechol (and no color development). In addition, when our sensor is exposed to a mixture of catechol/indole, the probe showed no significant variation (<5%, Table 2.4).

We have also similarly investigated the effect of 2-methylindole, an indole analog. It does lead to larger variation (20%), as its β position as indole itself is available for the reaction with DMAB. However, since 2-methylindole is not a natural metabolite in tryptophan degradation [42], it is not expected to affect the current analysis of indole in shrimp.

Table 2.4. Probe response to indole 0.5 μg mL^{-1} with the presence of interferents

Interferent	Mean absorbance (*n = 3*)
None	0.053 ± 0.002
Skatole (0.1 μg mL^{-1})	0.051 ± 0.002
Catechol (0.1 μg mL^{-1})	0.051 ± 0.003
2-methylindole (0.1 μg mL^{-1})	0.064 ± 0.015

2.3.7. Indole extraction

In order to test the probe performance, shrimp samples were spiked with a standard solution of indole. Previous works have reported a wide range of solvent extraction methods, including steam distillation, ethyl acetate, petroleum ether, and hexanes [3-11]. Petroleum ether was used, as the ethyl cellulose film on the probe surface is stable in petroleum ether solutions. Other solvents caused ethyl cellulose to dissolve. Initially, petroleum ether was used with an aqueous carbonate buffer ($NaHCO_3/Na_2CO_3$, pH 9.6) which was a protein precipitating agent that Chambers had reported [11]. However, adding petroleum ether to the shrimp sample in the buffer caused the sample to gelate after homogenization, impeding subsequent collection of the petroleum ether solution for analysis. We then used a 5% aqueous solution of trichloroacetic acid (TCA) [3,4] to promote protein denaturation and indole release from the sample matrix. No gel formation was observed with TCA.

After extraction, the petroleum ether phase is light orange in color, which is indicative of the presence of astaxanthin (Figure 2.4). This carotenoid is taken by shrimp through its diet. Astaxanthin contributes to the characteristic red-orange pigmentation of shrimp [43] and has antioxidant activity. In a control test with no indole, no reaction was observed between DMAB and astaxanthin upon exposure to shrimp extract. However, astaxanthin is an interferent in indole detection by the current probe, as the carotenoid adsorbs to the probe surface and obstructs the optical measurements as the probe becomes more opaque. This interference is particularly significant, when the extract was concentrated and astaxanthin remained in solution, since it can partially dissolve the film due to its lipophilic nature.

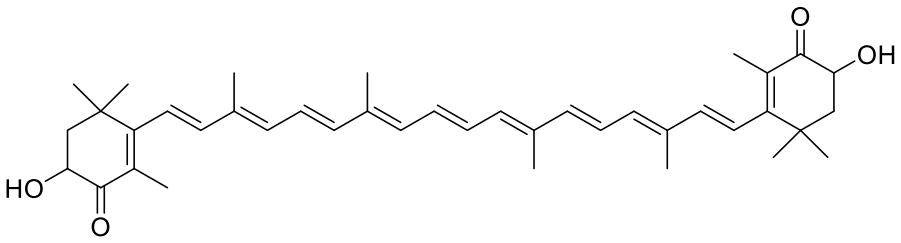

Figure 2.4. Astaxanthin.

Several solids, including silica gel, alumina gel, and ethyl cellulose, poly(2-vinylpiridine), and poly(4-vinylpyridine), were tested to adsorb astaxanthin in the petroleum ether solutions, thus removing it from the extract. Disappearance of the extract solution color was monitored by UV-visible spectroscopy. Only alumina and silica showed a significant decrease in the peak of astaxanthin at 467 nm (Figure A6) and silica was the more effective than alumina, allowing subsequent detection of indole extracted from shrimp samples. Silica is effective in removing astaxanthin from the petroleum ether extract probably because surface Si-OH forms hydrogen bond with the –OH and C=O groups in astaxanthin. Adsorption with silica eliminated the need for further filtration steps as previously performed in reported extraction protocols [3,4,9,10].

With the procedure described above, indole spiked in 20 g of shrimp samples at the 25 µg/100 g shrimp level (Class I) was successfully analyzed by the probe using either the UV-visible spectrometer or the MUSE^{TM} colorimeter. Change of the probe color to pink, when exposed to the petroleum ether extract, was also clearly observable to the naked eyes. Such a 20-g shrimp sample was expected to give 0.5 µg mL^{-1} of indole in the petroleum ether extract. Using the UV-visible spectrometer and the

calibration plot in Figure 2.2-b, the indole concentration was 0.31 µg mL^{-1}, giving a mean recovery of (62.1 ± 2.6)% (*n* = 3; relative standard deviation (RSD) of 4.2%). Given that the recovery is consistent throughout repetitions, a correction factor (62.1%) may be applied for such tests [44]. The recovery is comparable to 68.7% that Snellings and coworkers reported [4]. Our additional tests showed that the silica gel, used to remove astaxanthin, also adsorbed indole in petroleum ether solutions (Figure A6), probably through H bonds between Si-OH and the N atom on indole. The –OH and C=O groups in astaxanthin and N-H group in indole both form hydrogen bond with silica. Thus, removal of the former by the silica gel inevitably leads to some loss of the latter.

In addition, some indole may be left in the aqueous TCA solution when petroleum ether was used to extract it. In other words, both the use of the silica gel and TCA solution probably contributes to loss of indole in the extraction processes, giving the current 62.1% recovery. It should be pointed out, however, the procedure reported here has been optimized. In particular, the petroleum ether extract from the aqueous TCA solution is compatible with the thin film formulation on the probe, as discussed earlier. Other solvent mixtures dissolved the thin films on the probe. For the tests with 20 g shrimp at the 25 µg/100 g shrimp level, 0.31 µg mL^{-1} indole in the petroleum ether extract is significantly above the LoD (0.05 µg mL^{-1}) and LoQ (0.16 µg mL^{-1}) of the current probe. When the MUSE^{TM} colorimeter (the *a** value) was used to analyze indole in the petroleum ether extract, the recovery was consistently 51.2 ± 2.3% (*n* = 3; RSD of 4.5%). Although the colorimeter is more convenient to use than the desktop Agilent UV-visible spectrometer, the recovery here may suggest that it is less sensitive than the spectrometer.

2.3.8. Comparison with reported indole analyses

The current method shows several advantages in comparison with reported approaches in indole detection and assessment of shrimp freshness. Electrochemical detection of indole by flow injection shows a limit of detection of 6.3×10^{-7} mol L^{-1} (0.074 μg mL^{-1}) [8], which is above the limit of the current probe. The incubation time of our probe is comparable to those using colorimetric *solutions* to analyze indole. Darko et al. show a hydroxylamine-based test that incorporates two consecutive incubation times of 15 and 30 min prior to measurement [42]. A DMAB-based solution test by Snellings et al. requires a 15 min period [4]. When reducing the exposure time to 15 min, our probe shows a comparable linear range (Figure A2) to that of a commercial quantitative indole assay kit [45]. Furthermore, solution colors in the reported tests fade away [45,46]. In contrast, our probe response does not fade and is not constrained to a limited time window.

It should also be pointed out that the use of the CIELAB colorimeter in the current work significantly enhances the portability of the probe for field use, making it much easier to analyze the freshness of shrimp than the traditional chromatography that is not only much more expensive but also requires a centralized location to conduct the analysis. Sample handling is simple for the current probe, as no acidic solution is used and large batches of the probe can be made at a time. For solution tests using DMAB, handling acid solutions is needed [3,4,33].

2.4. Conclusion

The procedure presented herein represents a sensitive method to determine shrimp quality using indole concentration as a parameter. Naked-eye detection of the color development correlates accordingly with either a visible spectrometer or with a portable CIELAB space-based colorimeter, showing a direct correlation between the *a** parameter and the analyte concentration with a simple linear calibration. The probe incorporates sensing system with preconcentration of indole after a simple solvent extraction and, coupled with a handheld device, provides a simpler, low-cost, field test to determine if the indole level is in the Class I (passable). It can be adapted into a rapid test as an alternative to the FDA-approved process, involving indole extraction followed by HPLC-fluorescence analysis with dedicated, expensive instrument and trained personnel in a central location.

References

[1] A. Marvasti, D. Carter, Domestic and imports sources of supply to the US shrimp market and anti-dumping duties, J. Econ. Stud. 43 (2016) 1039-1056.

[2] Food and Drug Administration, FDA – Philippines MOU regarding food products exported to the U.S., 2015. https://www.fda.gov/InternationalPrograms/Agreements/MemorandaofUnderstanding/ucm107620.htm (accessed on Oct. 24, 2017).

[3] W.L. Cheuk, G. Finne, Modified colorimetric method for determining indole in shrimp, J. Assoc. Off. Anal. Chem. 64 (1981) 783-785.

[4] S.L. Snellings, N.E. Takenaka, Y. Kim-Hayes, D.W. Miller, Rapid colorimetric method to detect indole in shrimp with gas chromatography mass spectrometry confirmation, J. Food Sci. 68 (2003) 1548-1553.

[5] G. Tantillo, R. Augelli, G. Tiecco, Method for rapid determination of indole in fish products, Ind. Aliment. (Pinerolo, Italy) 35 (1996) 519-521.

[6] C. Ponder, Fluorometric determination of indole in shrimp, J. Assoc. Off. Anal. Chem. 61 (1978) 1089-1091.

[7] J.M. Pingarron Carrazon, A.J. Reviejo Garcia, L.M. Polo Diez, Determination of indole in shrimps by differential-pulse voltammetry in an emulsified medium, Analyst (London) 115 (1990) 869-871.

[8] C. Gomez-Gil, A. Gonzalez-Cortes, L. Agui, P. Yanez-Sedeno, J.M. Pingarron, Voltammetric behavior of indole at carbon fiber microelectrodes in organic solvents: Application to the determination of indole in food samples, Indian J. Chem. A 42 (2003) 727-732.

[9] T.L. Chambers, W.F. Staruszkiewicz, Jr., High-pressure liquid chromatographic method for indole in shrimp: development of method and collaborative study, J. Assoc. Off. Anal. Chem. 64 (1981) 592-602.

[10] H. Schulz, Determination of indole and skatole in seafood using high performance liquid chromatography (HPLC), Z. Lebensm. Unters. Forsch. 183 (1986) 331-334.

[11] T.L. Chambers, Modification of the AOAC gas-liquid chromatographic method for indole in shrimp: collaborative study, J. Assoc. Off. Anal. Chem. 65 (1982) 842-845.

[12] T. Sasaki-Imamura, A. Yano, Y. Yoshida, Production of indole from l-tryptophan and effects of these compounds on biofilm formation by fusobacterium nucleatum ATCC 25586, Appl. Environ. Microbiol. 76 (2010) 4260-4268.

[13] S.-M. Kang, S.-C. Jang, Y.S. Huh, C.-S. Lee, C. Roh, A highly facile and selective Chemo-Paper-Sensor (CPS) for detection of strontium, Chemosphere 152 (2016) 39-46.

[14] K. Bae, J. Lee, G. Kang, D.-S. Yoo, C.-W. Lee, K. Kim, Refractometric and colorimetric index sensing by a plasmon-coupled hybrid AAO nanotemplate, RSC Adv. 5 (2015) 103052-103059.

[15] R.J. Meier, S. Schreml, X.-d. Wang, M. Landthaler, P. Babilas, O.S. Wolfbeis, Simultaneous photographing of oxygen and pH in vivo using sensor films, Angew. Chem., Int. Ed. 50 (2011) 10893-10896.

[16] M.-S. Steiner, R.J. Meier, A. Duerkop, O.S. Wolfbeis, Chromogenic sensing of biogenic amines using a chameleon probe and the red-green-blue readout of digital camera images, Anal. Chem. 82 (2010) 8402-8405.

[17] C. Connolly, T. Fleiss, A study of efficiency and accuracy in the transformation from RGB to CIELAB color space, IEEE Trans. Image Process 6 (1997) 1046-1048.

[18] A.D. Broadbent, Colorimetry, Methods A2 - Lindon, John C, Encyclopedia of Spectroscopy and Spectrometry (2nd Ed.), Academic Press, Oxford, 2010, pp. 372-379.

[19] V. Sant'Anna, P.D. Gurak, L.D. Ferreira Marczak, I.C. Tessaro, Tracking bioactive compounds with colour changes in foods - A review, Dyes Pigm. 98 (2013) 601-608.

[20] T.S. Carpenter, S.M. Rosolina, Z.-L. Xue, Quantitative, colorimetric paper probe for hydrogen sulfide gas, Sens. Actuators B 253 (2017) 846-851.

[21] M.A. Bezerra, Q.O. dos Santos, A.G. Santos, C.G. Novaes, S.L.C. Ferreira, V.S. de Souza, Simplex optimization: A tutorial approach and recent applications in analytical chemistry, Microchem. J. 124 (2016) 45-54.

[22] A.G. Santos, Q.O. dos Santos, V.A. Lemos, C.G. Novaes, M.A. Bezerra, Application of simplex optimization in the development of an on-line preconcentration system for the determination of Cu in human hair samples using FAAS, Curr. Anal. Chem. 12 (2016) 573-579.

[23] Q.O. dos Santos, C.G. Novaes, M.A. Bezerra, V.A. Lemos, I. Moreno, D.G. da Silva, L. dos Santos, Application of simplex optimization in the development of an

automated online preconcentration system for manganese determination, J. Braz. Chem. Soc. 21 (2010) 2340-2346.

[24] Y. Kohno, T. Okubo, R. Matsushima, Visual color sensor for indole vapors, Chem. Lett. 36 (2007) 98-99.

[25] Y. Kohno, J. Kamiya, T. Okubo, R. Matsushima, Color sensors for indole vapors based on Ehrlich-type reactions, Anal. Sci. 25 (2009) 129-132.

[26] Variable. http://www.variableinc.com/ (accessed on Nov. 14th, 2017).

[27] J.F. MacFaddin, Biochemical Tests for Identification of Medical Bacteria, 3rd ed., Williams & Wilkins, Baltimore, MD, 2000. pp. 221–232.

[28] E.J. Baron, S.M. Findegold, Bailey & Scott's Diagnostic Microbiology, Mosby, St. Louis, MO, 2002. pp. 152–153.

[29] N.O. Bullock, J. Aslanzdeh, Biochemical profile-based microbial identification system, in: Y.-W. Tang, C.W. Stratton, Eds., Advanced Techniques in Diagnostic Microbiology, Springer Science + Business Media, New York, 2013, pp. 87–121.

[30] J.M. Miller, J.M. Wright, Spot indole test: evaluation of four reagents, J. Clin. Microbiol. 15 (1982) 589–592.

[31] J.Z. Kleeberg, Ehrlich's benzaldehyde reaction (with urobilinogen) 80 years later, Gastroenterology 20 (1982) 424–428.

[32] R.S. Alexander, A.R. Butler, Electrophilic substitution in pyrroles. Part I. Reaction with 4-dimethylaminobenzaldehyde (Ehrlich's reagent) in acid solution, J. Chem. Soc. Perkin Trans. 2 (1976) 696-701.

[33] Q. Jin, L. Shan, J. Yue, X. Wang, Spectrophotometric determination of total serotonin derivatives in the safflower seeds with Ehrlich's reagent and the

underlying color reaction mechanism, Food Chem., 108 (2008) 779-783.

[34] A.C. Lamb, R.A. Federico-Perez, Z.-L. Xue, Product in indole detection by Ehrlich's reagent, Anal. Biochem. 484 (2015) 21-23.

[35] Color Muse. https://colormuse.io/ (accessed on Nov. 14th, 2017).

[36] M.T. Jensen, R.P. Cox, B.B. Jensen, 3-Methylindole (skatole) and indole production by mixed populations of pig fecal bacteria. Appl. and Environ. Microbiol. 61 (1995) 3180-3184.

[37] J.-M Guo, Y.-Y Xin, X.-B., Yin, Selective dfferentiation of indoleacetic acid and indolebutyric acid using colorimetric recognition after Ehrlich reaction. J. Agric. Food Chem. 58 (2010) 6556-6561.

[38] D. Kupfer, Qualitative method for partial characterization of indole derivatives. Anal. Biochem. 8 (1963) 75-81.

[39] R.H. Hackman, M. Goldberg, Microchemical detection of melanins, Anal. Biochem. 41 (1971) 279-285.

[40] H.N. Chinivasagam, H. A. Bremner, R. Reeves, Can spoilage bacteria cause blackspot (melanosis) in stored prawns? Lett. Appl. Microbiol. 27 (1998) 5-8

[41] F. Solano, Melanins: Skin pigments and much more -types, structural models, biological functions, and formation routes. New J. Sci. 2014 (2014) 1-28.

[42] C. Darkoh, C. Chappell, C. Gonzales, P. Okhuysen, A rapid and specific method for the detection of indole in complex biological samples, Appl. Environ. Microbiol. 81 (2015) 8093-8097.

[43] K. Prameela, K. Venkatesh, S.B. Immandi, A.P.K. Kasturi, C. Rama Krishna, C. Murali Mohan, Next generation nutraceutical from shrimp waste: The

convergence of applications with extraction methods, Food Chem. 237 (2017) 121-132.

[44] D.T. Burns, K. Danzer, A. Townshend, Use of the term "recovery" and "apparent recovery" in analytical procedures, IUPAC Recommendations 2002, https://www.iupac.org/publications/ci/2003/2503/pac2_burns.html (accessed on Nov. 6th, 2017).

[45] QuantiChrom™ Indole Assay Kit. BioAssay Systems. https://www.bioassaysys.com/Indole-Assay-Kit.html. (accessed on June 1st, 2017).

[46] I. Azhar, F. Mazhar, Q.N. Manzar, I. Hussain, S. Shamim, Colorimetric determination of indolic drugs, Pak. J. Pharm. Sci. 18 (2005) 48-51.

Part 3

Simultaneous determination of aniline and indole in kerosene

Abstract

The optical probe described in Part 2 has been used for the simultaneous detection of aniline and indole in kerosene. Determination of these compounds in aviation fuels is of interest as these species reduce fuel stability when present in higher concentrations. We observe a larger sensitivity on response of the probe to aniline. The response to indole is observed when the probe is exposed to both analytes at the same time. Thus, we have explored the simultaneous determination of aniline and indole by the probe using a chemometric calibration with Classical Least Squares (CLS) and Principal Component Regression (PCR). Based on the fitness of the calibration model, an explanation of the non-linear behavior is presented.

3.1. Introduction

Jet fuel consumption has steadily increased in the past 20 years, reaching a world consumption of approximately 5.4 million barrels per year in 2012. This represents a 40% increase in consumption from 1990 [1]. Fuel supply for aviation requires control of parameters such as energy density and combustion quality. Large quantities of high-energy, stable fuels are needed for aircrafts. Great interest has been put into the development of fuel mixtures that provide optimal performance and easy handling. Current, widely used guidelines for quality standards in jet fuel are included in ASTM D1655 in the US [2] and DEF STAN 91/91 in the UK [3]. Jet fuel is traditionally manufactured by fractional distillation of crude oil. Other sources and methods, such as oil shale, oil sands and synthesis gas through the Fischer-Tropsch process [4], have been used as well.

Properties of fuel must be maintained within standards even after long periods of storage. In addition, the fuels need to give minimum accumulation of deposits during burning.

Specifications for composition state that jet fuel aromatic content should not exceed 25% v/v [5]. The presence of aromatic compounds in jet fuel has an impact on both its thermal stability and suitability for use in aviation. Several studies have focused on the effects of nitrogen-containing aromatic compounds on the quality of jet fuel, mostly indoles, anilines, pyrroles, quinolines, and carbazoles (Scheme 3.1) [6]. For instance, anilines and indoles represent 64% and 18% of nitrogen compounds in petroleum based fuels. The N-containing compounds destabilize fuel and lead to formation of resinous products that form deposits. As demonstrated by Dahlin et al.,

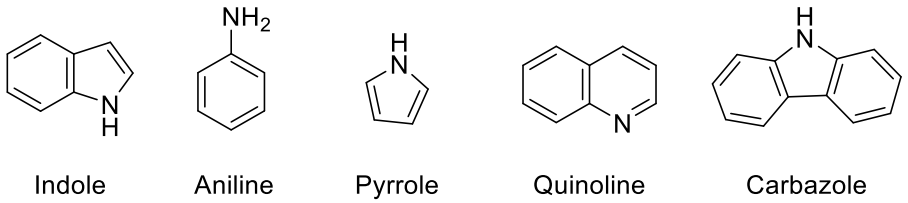

Scheme 3.1. Aromatic nitrogenated compounds present in aviation fuels.

nitrogen heterocyclic compounds in low concentrations in fuels cause the formation of (3.5-10.2) × 10^7 g/mm^2 gum deposits after just 6 days of storage [7]. Moreover, synergistic interaction of nitrogen compounds with other organic basis and acids found in fuel mixtures has shown to make the fuels less stable through the formation of deleterious compounds [8].

Jet fuel is used under high temperature conditions during flights. Polymerization of fuel components under heating may lead to the formation of deposits affecting the mechanical parts during flight. Methods for the characterization of jet fuel performance under such conditions include the fuel coker test (ASTM D-l660, IP 197) and the thermal oxidation stability test (ASTM D-3241, IP 323) [5]. The relationship between polar species concentration and deposit formation from fuels under thermal stress has been explored. Sobkowiak and coworkers have demonstrated an excellent correlation of mean carbon deposit developed after thermal treatment at 550 °C and indoles/carbazoles concentration in jet fuel [9].

Among traditional techniques utilized for the characterization of nitrogen-containing compounds in fuels are mass spectrometry, X-ray, IR, HPLC, gas chromatography and XANES [10-12]. Potential drawbacks by these methods are the need for specialized equipment and off-site analysis, requiring sample transportation

and handling. Optical sensors are a valuable tool to overcome these disadvantages. Potential use of the optic probe in Part 2 for simultaneous analysis of indole and aniline is the focus of this Part.

3.1.1. Chemometrics

Modern analytical chemistry often relies on the acquisition of multivariate data to characterize a sample. As opposed to univariate measurements, current instrumentation is capable of extracting multivariate data to explore the properties of a system. The increase in data complexity has resulted in the extensive use of chemometrics in analytical chemistry. Svante Wold first introduced the term chemometrics in 1971 [13]. Massart and collaborators define chemometrics as a discipline used to “provide maximum relevant chemical information by analyzing chemical data and to obtain knowledge about chemical systems” [13].

3.1.1.1. Classical Least Squares method

Classical Least Squares (CLS) method depends on the existence of a defined relationship between the measurement matrix and the component concentrations [14,15]. Beer’s law is the common illustration of this concept. Each wavelength exhibits an absorbance value that is directly proportional to the concentration of the analyte through a response factor (ε, molar absorptivity). This can be expressed in matrix notation as follows:

$$\mathbf{A} = \mathbf{CK} \qquad \text{Eq. 3.1}$$

where **A** (m×n) is the matrix of calibration spectra, **C** (m×l) is the matrix of concentrations and **K** (l×n) is the matrix of response factors (εb, molar absorptivity times pathlength).

In order to make predictions on concentrations based on known spectra, we calculate a solution on Eq. 3.2:

$$\mathbf{AK^{+}} = \hat{\mathbf{C}} \qquad \text{Eq. 3.2}$$

where **A** is the spectrum of the unknown, $\hat{\mathbf{C}}$ is the matrix of predicted concentrations, and $\mathbf{K^{+}}$ is the pseudoinverse matrix of **K**.

CLS is based on Beer's law and assumes linear additivity of the responses, i.e., the calculated spectra are expected to be linear combinations of the original calibration spectra. A feature of the linear additivity is that all variability is assumed to be explained by the spectral features of the sample. Thus, for a CLS model to make effective predictions, all components found in the unknown samples must be included in the calibration set. When all components on a system are known and samples of the components can be easily obtained, CLS presents a straightforward interpretation of the calibration model used to make quantitative predictions on unknown samples.

3.1.1.2. Principal Component Regression method

Another general chemometric technique is Principal Component Regression (PCR). Unlike CLS, it is not necessary to know all analytes and their concentrations to establish a PCR calibration. Rather than relying on a direct relationship between the concentration of an analyte and a measurable variable, PCR consists on regressing a subset of variables from the response matrix (i.e., spectra) to make predictions on the concentrations (Eq. 3.3).

$$\mathbf{C} = \mathbf{AK} \qquad \text{Eq. 3.3}$$

Where matrix **C** contains the concentrations**, A** is the response matrix (measurements) and **K** includes the coefficients that correlate the concentrations of each component to the intensity of their spectrum [15].

Finding this subset of variables from the original matrix implies the use of Principal Component Analysis (PCA) as a first step. PCA allows us to reduce the original variables to a lower number. These new variables explain most of the variability observed in the initial dataset, and they are denominated *Principal Components* (PCs) [16]. PCs often do not have a chemical interpretation. In order to determine principal components, Singular Value Decomposition is commonly used. The SVD algorithm decomposes the response matrix **A** in the following manner (Eq. 3.4):

$$\mathbf{A} = \mathbf{USV}^{T} \qquad \text{Eq. 3.4}$$

where **U** is the loadings, $\mathbf{V}^T$ is a matrix containing the scores, and **S** is a diagonal matrix of singular values.

The **U** matrix contains the coordinates of the samples along the PC axes. The **V** matrix contains the information about how the original measurements are related to the PCs. **S** is a diagonal matrix that explains the amount of variance each principal component describes (i.e., singular values). The columns in the **U** matrix contain the PCs, while the product of **S** and **V** matrices describe their "scores". However, not all of them are retained in the final model. A fundamental step in PCR is choosing the adequate number of PCs, which is typically based on the percentage of variance in the experimental data they explain. This characteristic of PCR allows for the regression on relevant chemical information while discarding irrelevant variability (e.g., noise) that do not describe chemical changes occurring in it.

3.2. Materials and methods

3.2.1. Initial aniline and indole analyses

Individual analyses of aniline and indole in kerosene were conducted to understand the response of the probe to each chemical alone. In the preliminary tests, probes were prepared as described previously in Part 2. The probe formulation for initial tests of indole and aniline in kerosene was one prior to the simplex optimization described in Part 2, Table 2.2, Experiment 1. Indole and aniline were added to kerosene (98%, Ricca Chemical) to make solutions with indole and aniline concentrations of 0.1-1.0 mg L^{-1} to simulate the matrix of a typical fuel sample.

Preliminary tests were also conducted with solutions containing both indole and aniline to determine the response of the probe after simultaneous exposure to the two analytes for 30 min. In the test solutions, aniline concentration was kept constant at 0.2 mg L^{-1} and indole concentrations ranged from 0.1 to 1.0 mg L^{-1}.

3.2.2. CLS analysis

In the tests for the CLS analysis, the probes optimized by the simplex method were used. Aniline and indole mixtures of known concentrations were used as validation. Each sample was run in duplicates. The calibration dataset consisted of the visible spectra of single-component solutions of 0.5 mg L^{-1} aniline and 0.5 mg L^{-1} indole. Duplicates for calibration spectra were averaged. The composition of validation samples is described in Table 3.1.

The calibration and validation samples were exposed under different time and volume conditions to investigate the effect of the probe saturation on the predictive power by CLS analysis. Table 3.2 summarizes the exposure conditions on screening calibration sets. For each set of conditions, a calibration and a validation dataset were run. In addition to performing the baseline subtraction and smoothing as described in Part 2, spectra were normalized to unity. In order to apply CLS, we retained only the absorbance data at 380-700 nm. A pseudoinverse matrix for each analyte ($\mathbf{K^+}$) was calculated in Excel. Concentrations were calculated by multiplying this matrix by the absorption spectrum (response matrix **A**).

Table 3.1. Concentration of each analyte in CLS validation samples

Sample	Concentration (mg L^{-1})	
	Aniline	Indole
1	0.25	0.75
2	0.50	0.50
3	0.75	0.25

Table 3.2. Exposure conditions on screening calibration sets

Set number	Time (min)	Volume (mL)
1	15	5
2		10
3	30	5
4		10

3.2.3. PCR analysis

A set of volume and exposure time conditions based on the previous CLS treatment were chosen for further studies. Concentrations of the solution mixtures are described in Table 3.3. From the 33 solutions, two subsets were designated as calibration (15) and validation (17) datasets. These samples encompass aniline and indole concentrations between 0 and 1.0 mg L^{-1} at different ratios, in order to account for variability on the response at different concentration levels. After the model was built with the calibration dataset, predictions were performed on the validation samples to assess the fitness of the calibration. Sample volume of 5 mL and time of 30 min were used as exposure conditions.

A software developed in-house with C++ was utilized to perform PCR analysis. Visible spectra were used without modification. To correct for baseline variation among different spectra, a drift correction was applied based on modeling pseudo-Principal Components (pseudo-PCs). On this drift-correction approach, pseudo-PCs were modeled simultaneously with the PCs of the system. While the PCs describe the chemical signature of the analytes, the artificial pseudo PCs were of polynomial shape and modeled spectroscopically broad drift features. By concurrently modeling real spectroscopic signatures and baseline drift artifacts, an accurate description of real chemical features and instrumental artifacts was accomplished [17,18]. SVD was performed to calculate principal components. A predicted vs. known concentrations graph for each individual component was constructed.

Table 3.3. Concentrations used for PCR analysis

Calibration set			Validation set	
Concentration (mg L^{-1})			Concentration (mg L^{-1})	
Aniline	Indole		Aniline	Indole
0.10	0.75		0.0	0.50
0.10	1.0		0.10	0.50
0.20	0.70		0.10	0.25
0.25	0.75		0.20	0.30
0.25	1.0		0.30	0.20
0.40	0.60		0.50	0.0
0.50	0.10		0.50	0.50
0.50	0.75		0.50	0.25
0.50	1.0		0.60	0.40
0.60	0.80		0.70	0.20
0.75	0.25		1.0	0.10
0.75	0.50		1.0	1.0
0.80	0.60		1.0	0.75
1.0	0.25		0.25	0.50
1.0	0.50		0.75	0.10
			0.75	1.0
			0.75	0.75

3.3. Results and discussion

3.3.1. Individual analysis of aniline and indole

The response of probe to indole has been discussed in Part 2. In this case, exposure to indole solutions in kerosene showed the same red color development with a linear correlation (R^2 = 0.988, slope = 0.031), as shown in Figure 3.1.

When exposed to a solution of aniline, a yellow color appeared immediately in the probe. The characteristic yellow color can be explained by the formation of N,N-dimethyl-4-[(phenylimino)methyl]aniline, a Schiff base. The reaction in Scheme 3.2 has been reported, obtaining a yellow-greenish powder that is commonly used as a dye [19]. A notable difference between the response of aniline and indole is the yellow color with aniline developed much faster.

A linear correlation (R^2 = 0.990; slope = 0.518) was found between the absorbance of the product at 432 nm and the concentration of aniline in the 0.05-1.0 mg L^{-1} range for a 30 min exposure time (Figure 3.2). Thus, the probe showed a higher sensitivity towards aniline than to indole as evidence by their calibration slopes.

3.3.2. Simultaneous analysis of aniline and indole

Due to the ability of the probe to sense both analytes individually, how the probe responds to one analyte in the presence of the other was investigated.

The signal of the indole product at 537 nm in mixture solutions showed a comparable response as that of the indole alone, as evidenced by similar slopes. However, when analyzing the product of aniline in the presence of indole, a more scattered response was observed (Figure 3.3-a). No significant overlapping between

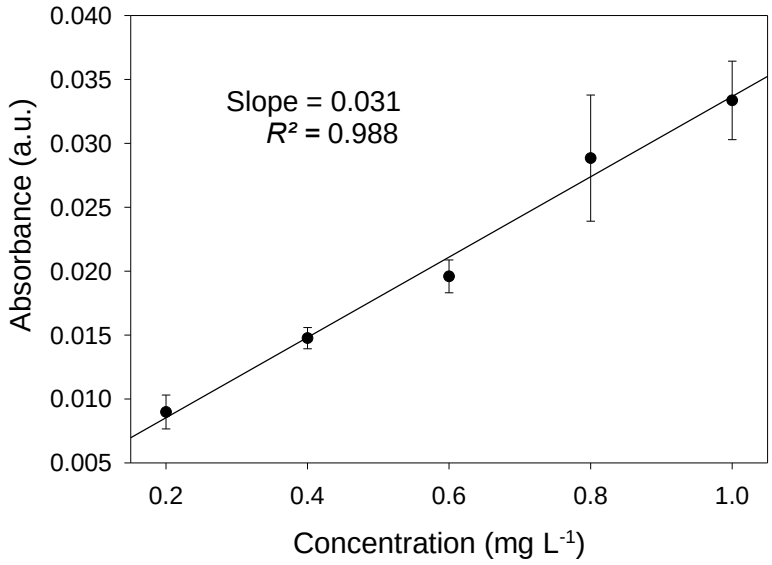

Figure 3.1. Calibration plot for determination of indole in kerosene with probe.

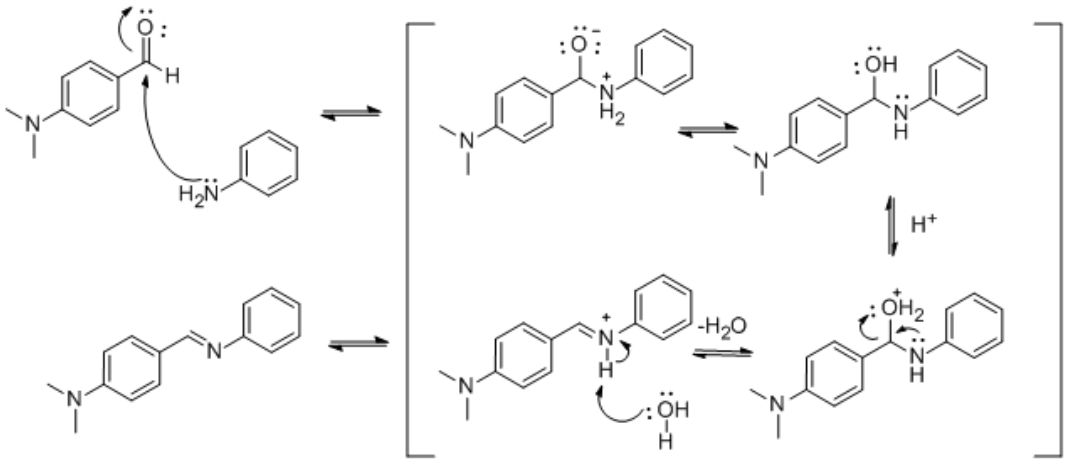

Scheme 3.2. Reaction in the synthesis of yellow azo-compound from aniline.

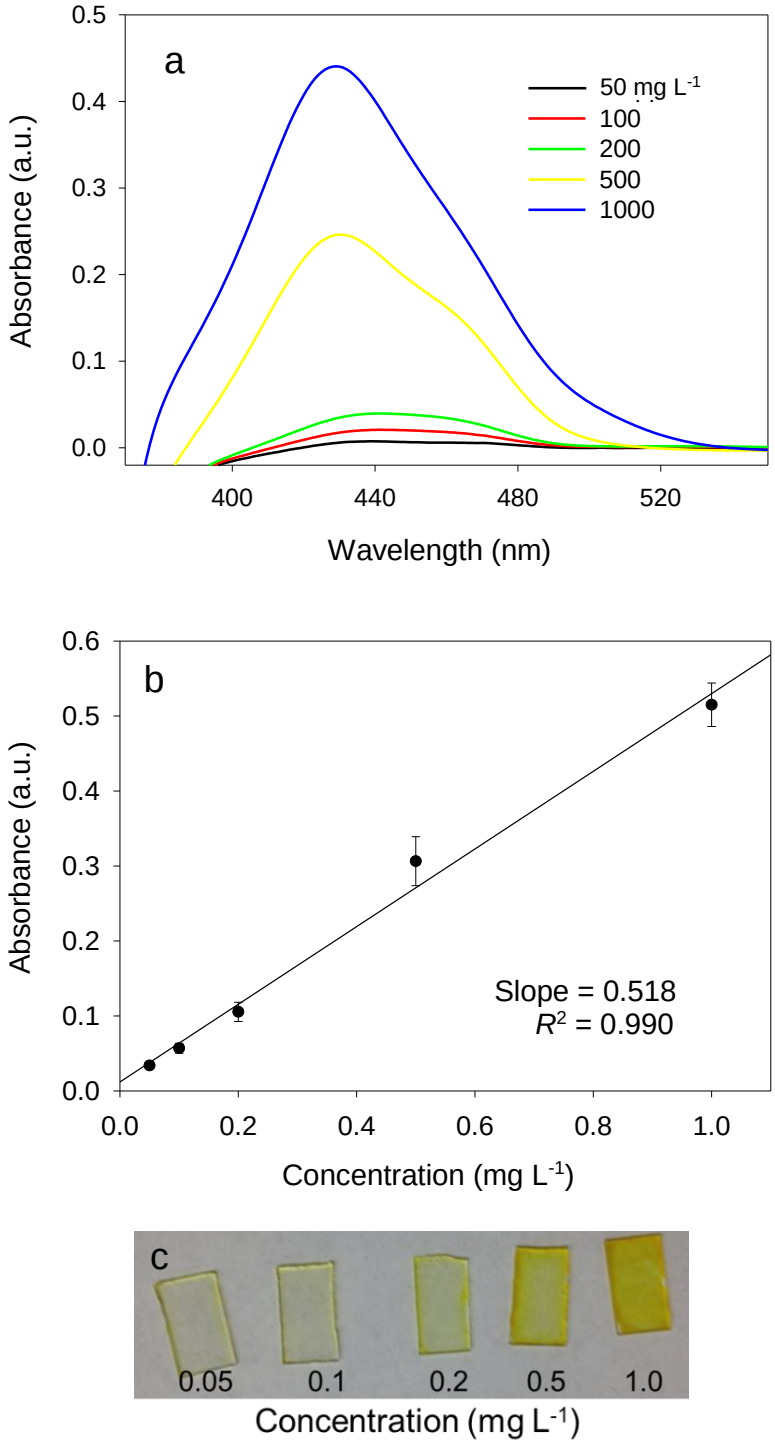

Figure 3.2. (a) Visible spectra of probe exposed to aniline. (b) Calibration plot for aniline concentrations. (c) Probe response to different aniline concentrations.

the peaks of the two products was observed (Figure 3.3-b). Thus, we initially conducted the simultaneous determination of both analytes by CLS.

3.3.2. CLS analysis

CLS analysis allowed for an initial assessment of the best set of conditions for the simultaneous analysis of the two analytes by the probe. Since saturation for aniline is reached in 30 min, we speculated that reducing the volume and/or exposure time may reduce the saturation. Table 3.4 shows the equation and R^2 for the predicted vs actual concentration plot. The corresponding plots can be found in Appendix B.

Table 3.4. Equations for the linear fit of the CLS predictions

Time (min)	Volume (mL)	Analyte	Equation	R^2
15	5	Aniline	$y = 1.4021x + 0.034$	0.8209
		Indole	$y = 0.4962x + 0.2647$	0.7592
	10	Aniline	$y = 1.8793x - 0.1667$	0.9136
		Indole	$y = 0.3285x + 0.3260$	0.8547
30	5	Aniline	$y = 0.8786x - 0.0226$	0.927
		Indole	$y = 0.4345x + 0.2278$	0.630
	10	Aniline	$y = 1.1016x + 0.0105$	0.9502
		Indole	$y = 0.6784x + 0.0356$	0.9012

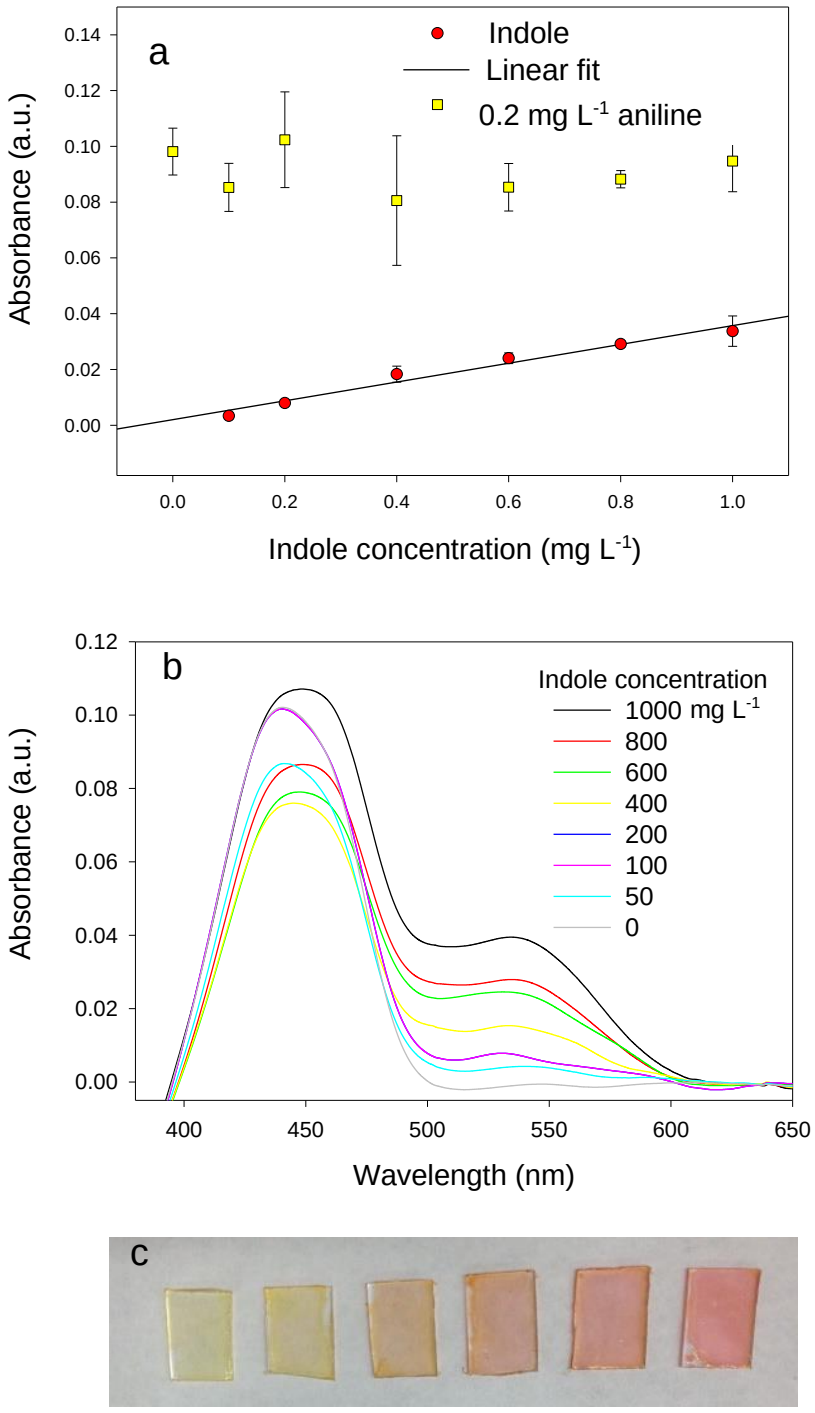

Figure 3.3. (a) Calibration plot of indole with aniline concentration held at 0.2 mg L^{-1}. (b) Corresponding visible spectra. (c) Color development of the probe.

In general, we obtain lower R^2 values for a 15 min exposure time. Better slopes, closer to 1, are obtained by exposing the samples for 30 min. This is mainly because indole reacts with the probe more slowly. Thus, a longer exposure (i.e., 30 min) favors a more noticeable development of its colored product. However, the reaction of aniline with the probe reaches saturation in 30 min. From the results of CLS assessment, we have determined that linear additivity of the pure component spectra would not hold throughout the entire concentration range. This is a common assumption made on CLS calibration models [14]. Therefore, we subsequently explored PCR in order to model additional variability. The set of conditions used for further analysis was a 30 min exposure with 5 mL samples.

3.3.3. PCR analysis

Two wavelength ranges were tested to determine the optimal calibration range. The 375-600 nm range provided the best fit for the determination of both analytes. Five principal components were retained to explain maximum variance. The number of principal components selected was larger than the two analytes in order to model additional non-linear behavior in the system. Figure 3.4 shows a predicted vs. actual plot for this PCR calibration model. For aniline determination, the equation of the linear fit for this plot is $y = 0.073x + 0.0005$ ($R^2 = 0.773$). For indole, the equation is $y = 0.621x + 0.2282$ ($R^2 = 0.663$). As shown in the graph, most predictions on validation samples for aniline result in an underestimation of the actual concentration. On the other hand, indole predictions result in an overestimation.

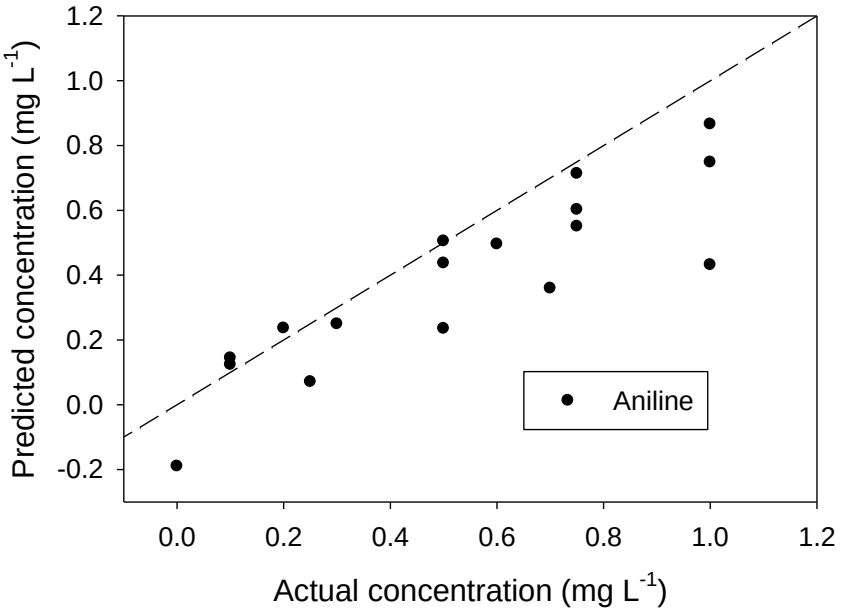

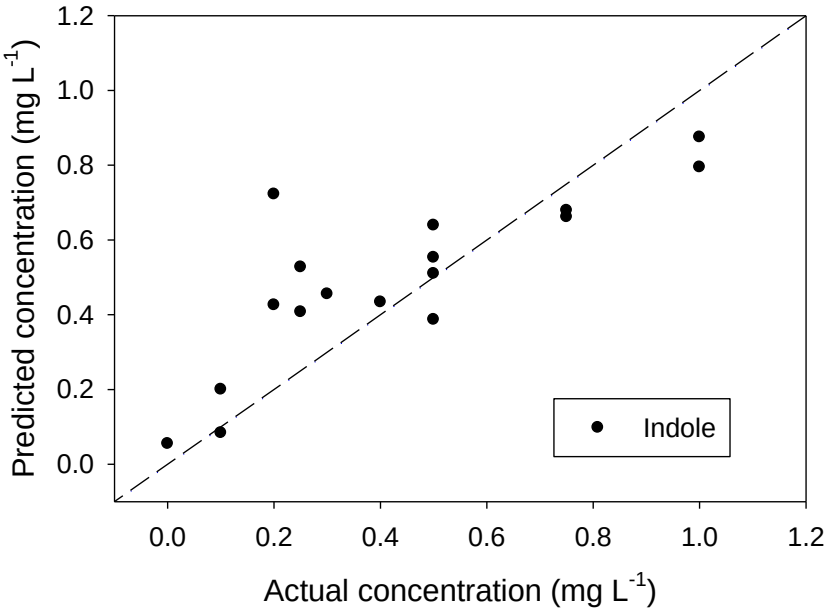

Figure 3.4. Predictions of the validation dataset with PCR calibration for aniline (top) and indole (bottom). Note that the dashed line is a 45° diagonal added as a reference for an ideal fit.

The reaction of either aniline or indole with *p*-dimethylaminobenzaldehyde (DMAB) is second order in nature [20]. We think that the non-linear kinetics of both reactions are responsible for the errors in the prediction samples. Faster color development of aniline is an indication of preferential reaction between DMAB and aniline. The limited amount of DMAB in the probe likely makes the nonlinearity of the probe more prominent. Based on the mass of the polymer film and the formulation of the original ethyl cellulose solution used to make the probes, DMAB content in the probe was expected to be 2.5×10^{-8} mol in each film. Assuming a quantitative reaction, complete saturation of the probe would be achieved with 5.0×10^{-8} mol of indole or 2.5×10^{-8} mol of aniline. For 5 mL of analyte solutions, saturation is expected to be with 1.20 mg L^{-1} indole or 0.46 mg L^{-1} aniline.

Other factors may also lead to the different behavior observed for simultaneous analyses in comparison to the behaviors in their individual determination. Molecules with larger masses are known to give smaller diffusion coefficients [21]. Aniline (93.13 g mol^{-1}) is slightly smaller than indole (117.15 g mol^{-1}), which may affect their diffusion into the probe film prior to their reaction with DMAB.

We have tested adding more DMAB to the probe. However, the approach resulted in more opaque films that were not appropriate as probes. Thus, this approach was not used. The current content in the probe was determined based on simplex optimization (Part 2, Section 2.3.2).

3.4. Conclusion

We have demonstrated that our probe can develop a sensitive response to both amines individually. Response to aniline is kinetically favored and shows a higher sensitivity than the response of the probe to indole. Although the presence of low aniline concentrations does not significantly affect indole determination, we have observed that increasing the amount of aniline in the system did compromise the accuracy of the predictions made by PCR calibration.

References

[1] IndexMundi, World Jet Fuel Consumption by Year (2017) www.indexmundi.com/energy.aspx?product=jet-fuel (accessed on July 14th, 2018).

[2] A. International, ASTM D1655-14a, Standard Specification for Aviation Turbine Fuels, 2014. https://compass.astm.org/download/D1655-14A.15563.pdf (accessed on July 16th, 2018).

[3] Ministry of Defence, Defence Standard 91/91 Turbine Fuel, Kerosine Type, Jet A-1. Glasgow, UK, 2012) ftp://ftp.iks-jena.de/mitarb/lutz/standards/dstan/91/091/00000400.pdf (accessed on July 16th, 2018).

[4] G. Liu, B. Yan, G. Chen, Technical review on jet fuel production, Renew. Sust. Energ. Rev. 25 (2013) 59-70.

[5] J.C. Speight, Handbook of Petroleum Product Analysis, John Wiley & Sons, 2002.

[6] G.W. Mushrush, E.J. Beal, D.R. Hardy, J.M. Hughes, Nitrogen compound distribution in middle distillate fuels derived from petroleum, oil shale, and tar sand sources, Fuel Process. Technol. 61 (1999) 197-210.

[7] K.E. Dahlin, S.R. Daniel, J.H. Worstell, Deposit formation in liquid fuels. 1. Effect of coal-derived Lewis bases on storage stability of Jet A turbine fuel, Fuel 60 (1981) 477-480.

[8] G.W. Mushrush, E.J. Beal, R.N. Hazlett, D.R. Hardy, Chemical basis of middle-distillate fuel instability - Interactive effects of selected nitrogen heterocycles with organic acids and bases in a shale-derived diesel fuel, Fuel Sci. Technol. Int. 11 (1993) 429-433.

[9] M. Sobkowiak, J.M. Griffith, B. Wang, B. Beaver, Insight into the mechanisms of middle distillate fuel oxidative degradation. Part 1: On the role of phenol, indole, and carbazole derivatives in the thermal oxidative stability of Fischer−Tropsch/petroleum jet fuel blends, Energy Fuels 23 (2009) 2041.

[10] S. Mitra-Kirtley, O.C. Mullins, J.F. Branthaver, S.P. Cramer, Nitrogen chemistry of kerogens and bitumens from X-ray absorption near-edge structure spectroscopy, Energy Fuels 7 (1993) 1128.

[11] M.M. Boduszynski, Composition of heavy petroleums. 2. Molecular characterization, Energy Fuels 2 (1988) 597.

[12] R.C. Striebich, J. Contreras, L.M. Balster, Z. West, L.M. Shafer, S. Zabarnick, Identification of polar species in aviation fuels using multidimensional gas chromatography-time of flight mass spectrometry, Energy Fuels 23 (2009) 5474.

[13] D.L. Massart, Handbook of Chemometrics and Qualimetrics, Amsterdam New York: Elsevier, Amsterdam, New York, 1997.

[14] K.R. Beebe, Multivariate Calibration and Prediction, Chemometrics: A Practical Guide, R.J. Pell, M.B. Seasholtz, Eds., New York: Wiley, New York, 1998.

[15] D.M. Haaland, E.V. Thomas, Partial least-squares methods for spectral analyses. 1. Relation to other quantitative calibration methods and the extraction of qualitative information, Anal. Chem. 60 (1988) 1193.

[16] N. Kumar, A. Bansal, G.S. Sarma, R.K. Rawal, Chemometrics tools used in analytical chemistry: An overview, Talanta 123 (2014) 186.

[17] F. Vogt, K. Rebstock, M. Tacke, Correction of background drifts in optical spectra by means of "pseudo principal components", Chemom. Intell. Lab. Syst. 50 (2000) 175.

[18] F. Vogt, H. Steiner, K. Booksh, B. Mizaikoff, Chemometric correction of drift effects in optical spectra, Appl. Spectrosc. 58 (2004) 683.

[19] A.K. Kaura, M. Kaura, Synthesis, spectral and comparative antimicrobial study of Schiff bases, Int. J. Chem. Pharm. Sci. 3 (2012) 24.

[20] S.A. Al-tamrah, Kinetic studies on the determination of pyrroles and tryptophan by Ehrlich reaction, Anal. Lett. 22 (1989) 387.

[21] D.P. Valencia, F.J. González, Understanding the linear correlation between diffusion coefficient and molecular weight. A model to estimate diffusion coefficients in acetonitrile solutions, Electrochem. Commun. 13 (2011) 129.

Part 4

Product in indole detection by Ehrlich’s reagent

A version of this part was originally published in the following paper. Minor changed were made.

A.C. Lamb, R.A. Federico-Perez, Z.-L. Xue, Product in indole detection by Ehrlich's reagent, Anal. Biochem. 484 (2015) 21-23.

R. A. Federico-Perez conducted the literature review, identified the discrepancy regarding the nature of the indole reaction with Ehrlich's reagent in the literature, and proposed the current study. He conducted the earlier studies of the reaction, made the product in small scale, and characterized the product β-bis(indolyl)methane. Dr. A.C. Lamb conducted the subsequent synthesis of the product in large scale, characterized it by NMR, and solved the crystal structure of the product. Dr. Z.-L Xue supervised the work. R. A. Federico-Perez and Dr. A.C. Lamb wrote the manuscript together.

Abstract

Ehrlich's reagent [*p*-dimethylaminobenzaldhyde (DMAB) in 95% EtOH with HCl as catalyst] is employed in spot tests of indoles, providing a diagnosis of, e.g., liver diseases, hemolytic processes, occlusion of the common bile duct, and carcinoid syndrome. Although the reagent has been widely used for over a century, it is not clear how many indole molecules react with a DMAB molecule and whether the reaction takes place at the α- or β-position of the indole molecule. Studies here show that the reaction of DMAB with indole in a 1:2 ratio gives β-bis(indolyl)methane. The reaction occurs at the β-position of indole under the conditions of the Ehrlich test, as confirmed by the crystal structure of β-bis(indolyl)methane.

3.1. Introduction

For over 100 years, Ehrlich's reagent has been employed in spot tests of indoles produced from tryptophan by bacteria or intracellular enzymes [1-4]. In these tests, if indole is present, a color reaction of *p*-dimethylaminobenzaldhyde (DMAB) with metabolites in urine provides a diagnosis of, e.g., liver diseases, hemolytic processes, occlusion of the common bile duct, and carcinoid syndrome [5]. Certain bacteria oxidize tryptophan, an amino acid, into several indolic metabolites, including indole itself [1-4], Ehrlich's indole test determines which bacteria are present through the formation of a distinctive red product. Ehrlich's reagent has also been used in spot tests of other compounds such as α-ketoglutaramate [6], guanidine compounds [7], urea [7] and pyrroles [8]. Two fundamental questions that have not been resolved in the use of Ehrlich's reagent to detect indole are: (1) How many indole molecules react with a DMAB molecule; (2) Does the reaction take place at the α- or β-position of the indole molecule?

A recent paper reported the spectroscopic determination of serotonin derivatives in safflower seeds. The detection is based on the reaction of Ehrlich's reagent with indole, and it was suggested that this is a 1:1 reaction at the α-position of indole (Scheme 4.1) [9]. The reaction was carried out under the conditions of the Ehrlich test, i.e., 95% ethanol as solvent and HCl as catalyst. A handbook on the indole test [1] and other papers [10-12] suggested that the same 1:1 reaction occurs at the β-position of indole. Kohno and coworkers have used Ehrlich's reaction of indole with DMAB as a color sensor for indole vapor [10].

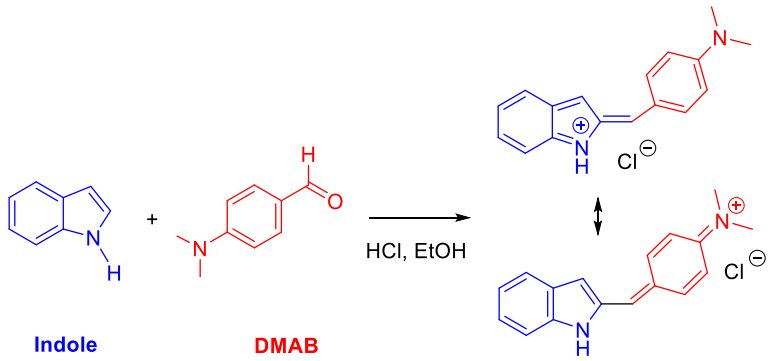

Scheme 4.1. One product indicated for the Ehrlich reagent [9].

A recent paper reported a solvent-free, 1:2 reaction of DMAB with indole at 100 °C, using a cobalt manganese oxide nano catalyst, and indicated that the α-H atom of indole was removed (Scheme 4.2) [13]. No characterization of the product was provided.

There have been studies of the reactions of indole and several indole derivatives with different aldehydes [14-17] under conditions *different* from those of Ehrlich's reagent [1-5, 9-12]. For example, Bandgar and Shaikh reacted DMAB with indole in acetonitrile with 20% of I_2, giving β-bis(indolyl)methane [14]. An and coworkers used a solvent-free, 1:2 reaction of DMAB with indole, with sulfamic acid as catalyst, to yield β-bis(indolyl)methane [15]. ^{1}H NMR spectrum of β-bis(indolyl)methane and its melting point are reported in this work [15]. Yang and coworkers have also reported the formation of β-bis(indolyl)methane from DMAB and indole in acetonitrile using $CrCl_3$•$6H_2O$/hydrogenated bis-Schiff base as catalyst [16]. β-bis(indolyl)methane was characterized by its ^{1}H NMR and IR spectra and elemental analysis [16].

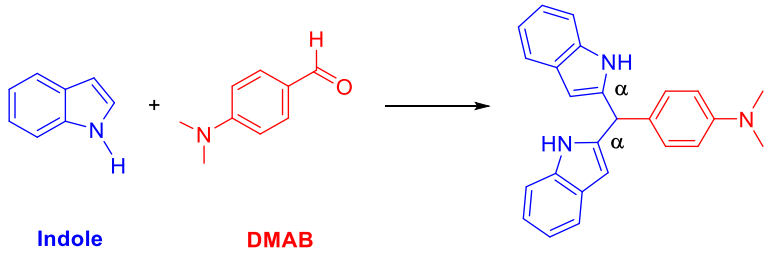

Scheme 4.2. Solvent-free, 1:2 reaction of DMAB with indole at the α-position with a cobalt manganese oxide nano catalyst [13].

Handy and Westbrook have used a deep eutectic solvent (a combination of urea and choline chloride) for the reaction of DMAB with indole, forming β-bis(indolyl)methane [17].

Since there is confusion regarding the structure of the product in the reaction of Ehrlich's reagent with indole [1-5, 9-12], and the crystal structure of β-bis(indolyl)methane has not been reported, we have studied the reaction of DMAB with indole under the conditions of the Ehrlich's test (95% EtOH as solvent and HCl as catalyst). The studies show that *p*-dimethylaminobenzaldhyde (DMAB) reacts with two indole molecules at the β-position, yielding β-bis(indolyl)methane (Scheme 4.3). These features have been confirmed by single-crystal structure determination of β-bis(indolyl)methane.

Part 2 of this dissertation reported the development of a thin-film probe for the detection of indole. The present studies elaborate on the nature of the sensing mechanism previously discussed.

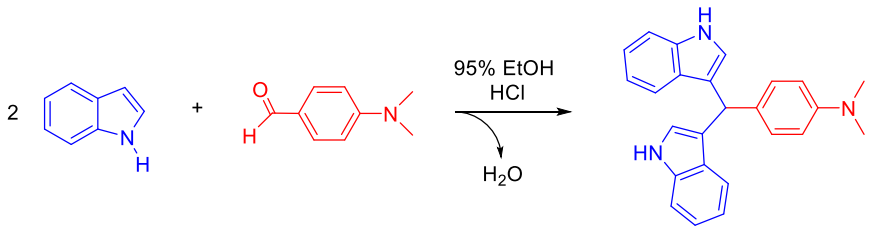

Scheme 4.3. Reaction of DMAB with indole by the Ehrlich test, yielding β-bis(indolyl)methane.

3.2 Materials and methods

All reagents were used as received. *p*-dimethylaminobenzaldehyde (Certified ACS) and hydrochloric acid (Certified ACS Plus, 12.1 N) were purchased from Fischer Scientific. Indole (99+%) was purchased from Acros. Ethanol (95% in water and 100%) was purchased from Decon Labs, Inc. $CDCl_3$ (Cambridge Isotopes) was stored over 5 Å molecular sieves. All NMR spectra were recorded on a Varian VNMRS-500 MHz spectrometer. UV-vis spectra were recorded on a Thermo Scientific Evolution 600 spectrometer. Mass spectrum was recorded on a JOEL AccuTOFTM DART (Direct Analysis in Real Time) Mass Spectrometer.

3.2.1. Synthesis of β-bis(indolyl)methane under the conditions of the Ehrlich test

DMAB (1.040 g, 6.97 mmol) was dissolved in 95% ethanol (10 mL) at room temperature. HCl (0.7 mL, 0.5 M) was added dropwise to the ethanol solution of DMAB and stirred for 15 min. Indole (1.63 g, 13.9 mmol) was dissolved in 95% ethanol (10 mL) at room temperature. The ethanol solution of indole was added dropwise to the ethanol solution of DMAB. The reaction mixture was stirred for 18 h to ensure the completion of the reaction. Ethanol and water were removed by a rotary evaporator. After the removal

of ethanol by a rotary evaporator, it was found that water was hard to remove. ^{1}H and $^{13}C\{^{1}H\}$ NMR spectra of the product show that it is β-bis(indolyl)methane, and it is identical to the product obtained from the reaction in 100% ethanol described below. These observations prompted us to use 100% ethanol instead of 95% ethanol for subsequent studies.

3.2.2. Synthesis of β-bis(indolyl)methane in 100% ethanol with HCl as catalyst

HCl (6.7 mL, 0.5 M) was added dropwise to a solution of DMAB (10.03 g, 67.2 mmol) in 100% ethanol (100 mL) at room temperature and stirred for 15 min. An ethanol solution of indole (15.79 g, 135 mmol) in 100% ethanol (100 mL) was added dropwise to the ethanol solution of DMAB at room temperature. The reaction mixture was stirred for 18 h. Slow evaporation of ethanol at room temperature over three days gave X-ray quality crystals of β-bis(indolyl)methane. The reaction mixture was filtered and concentrated to afford more crystals. The pink crystals were washed with warm hexanes and dried to give β-bis(indolyl)methane (20.37 g, 55.7 mmol, 83% yield). ^{1}H NMR (chloroform-d_1, 499.73 MHz, 23 °C) of β-bis(indolyl)methane: δ 2.90 (s, 6H), 5.79 (s, 1H), 6.66 (m, 4H), 6.98 (t, 2H), 7.14 (t, 2H), 7.20 (d, 2H), 7.32 (d, 2H), 7.39 (d, 2H), 7.85 (br s, 2H); $^{13}C\{^{1}H\}$ NMR (chloroform-d_1, 125.67 MHz, 23 °C) of **3**: δ 39.16 (CH_3), 40.81 (NMe_2), 110.90 (Ar-H), 112.67 (Ar-H), 119.09 (Ar-H), 120.09 (Ar-H), 120.48 (C), 121.76 (Ar-H), 123.46 (Ar-H), 127.20 (C), 129.24 (Ar-H), 132.33 (C), 136.71 (C), 149.06 (C). ^{1}H and ^{13}C NMR assignments were confirmed by an HSQC (Heteronuclear Single Quantum Coherence) experiment. DART-MS: Calculated *m*/*z* = 366.1970 [β-bis(indolyl)methane+H^+]; Found *m*/*z* = 366.1956 [β-bis(indolyl)methane+H^+].

3.2.3. Synthesis of β-bis(indolyl)methane with a 2:1 ratio of DMAB and indole

HCl (1.3 mL, 0.5 M) was added dropwise to a solution of DMAB (2.00 g, 13.4 mmol) in 100% ethanol (25 mL) at room temperature and stirred for 15 min. An ethanol solution of indole (0.78 g, 6.65 mmol) in 100% ethanol (15 mL) was added dropwise to the ethanol solution of DMAB at room temperature. The reaction mixture was stirred for 18 h. ^{1}H and $^{13}C\{^{1}H\}$ NMR spectra confirmed that β-bis(indolyl)methane was formed along with unreacted starting materials.

3.3. Results and discussion

Reaction of DMAB with indole by the Ehrlich test has been found to give a pink solid product. ^{1}H, $^{13}C\{^{1}H\}$ and HSQC NMR spectra of the product are consistent with β-bis(indolyl)methane. The ^{1}H NMR spectrum is the same as those reported for β-bis(indolyl)methane [15,16]. Reaction of excess DMAB with indole in a 2:1 ratio was also studied. ^{1}H and $^{13}C\{^{1}H\}$ NMR spectra showed that β-bis(indolyl)methane was the only product. We were not able to identify any intermediate in the reaction of DMAB with indole in either 1:2 or 2:1 ratio.

The product β-bis(indolyl)methane has also been characterized by UV-visible spectroscopy and the spectra in 95% ethanol are given in Figure 4.1. In the visible range, the maximum wavelength of the pink β-bis(indolyl)methane is 536 nm. In 0.10-5.0 mM, β-bis(indolyl)methane obeys the Lambert-Beer's law with a molar extinction coefficient/absorptivity constant $\varepsilon = 1.0 \times 10^{2}\ M^{-1}\ cm^{-1}$. We also found that using 100% ethanol instead of 95% ethanol as solvent improved the yield of β-bis(indolyl)methane.

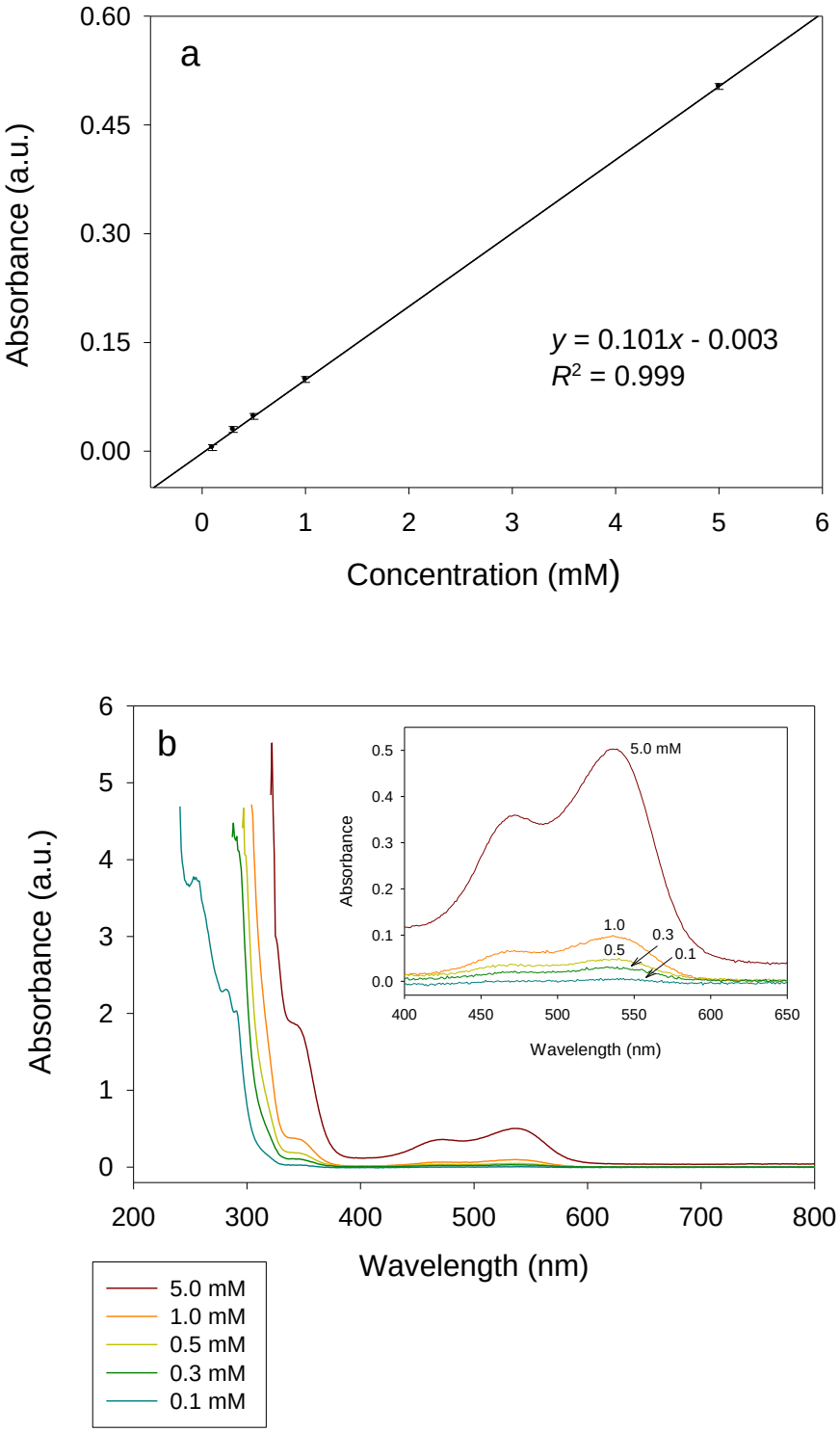

Figure 4.1. (a) Calibration plot of β-bis(indolyl)methane. (b) UV-visible spectra of β-bis(indolyl)methane in 95% ethanol.

The ORTEP of β-bis(indolyl)methane is shown in Figure 4.2. Crystal data and structure refinement are given in Table C1 (Appendix C). CCDC No. for the structure is 1856927 (https://www.ccdc.cam.ac.uk/). To our knowledge, this is the first characterization of β-bis(indolyl)methane by single crystal diffraction. The crystal structure of β-bis(indolyl)methane confirms that two indole molecules react one molecule of DMAB. In the reaction, β C-H activation on indole leads to dehydration, yielding β-bis(indolyl)methane.

The molecular structure of β-bis(indolyl)methane reveals that, since C(17) is an sp^3 hybridized atom, there is no conjugation among the three aromatic components in β-bis(indolyl)methane. This is evident in the angles around C(17). As expected, the NMe_2 group is conjugated with the phenyl ring it is attached to, as the NMe_2 group is nearly co-planar with the phenyl group. Other bond lengths and angles are within the expected values.

Confirmation of the features described above complement the characterization of of the indole probe described in Part 2. By elucidating the stoichiometry of the reaction, it is possible to estimate the amount of indole required to saturate the probe. In addition, the reaction on the β-position offers an explanation for the minor effect of other β-substituted analogs in the sensing of indole.

Proposed mechanism in the reaction of DMAB with indole is given in Scheme 4.4. The β C atom in indole may be more electron rich than the α C atom (Appendix C, Scheme C.1) to initiate the nucleophilic attack on the carbonyl C atom in DMAB to give **A**. Subsequent break of the β C-H bond leads to the formation of **B**. Similar nucleophilic attack by the second indole molecule with OH^- elimination yields

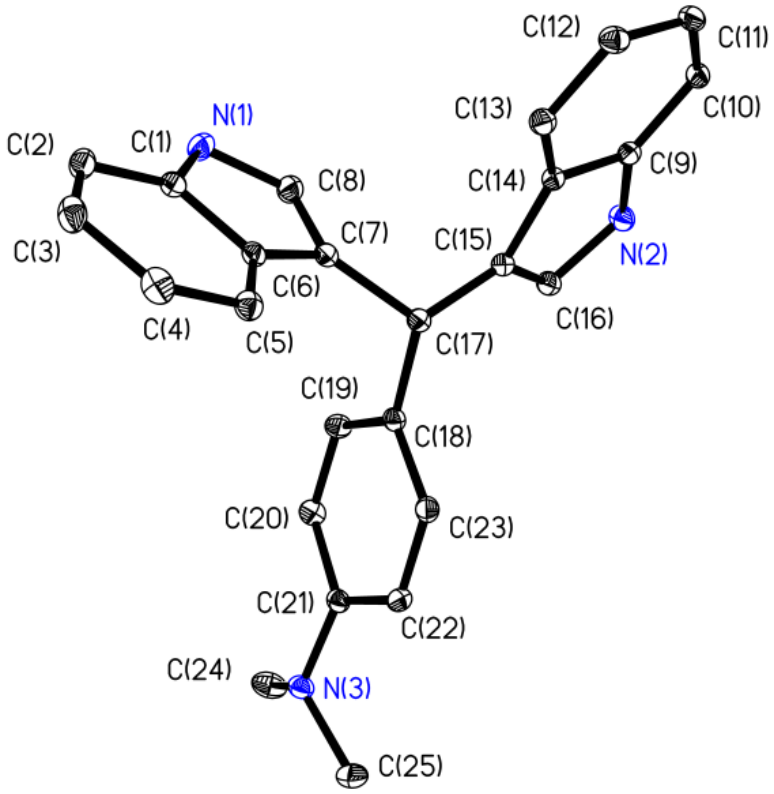

Figure 4.2. ORTEP view of β-bis(indolyl)methane. Selected bond lengths (Å) and angles (°): N1-C1 1.3700(13), N1-C8 1.3787(13), N2-C9 1.3766(13), N2-C15 1.3875(13), N3-C21 1.4122(13), N3-C24 1.4545(14), N3-C25 1.4623(14), C7-C8 1.3678(14), C7-C6 1.4360(13), C7-C17 1.5114(13), C17-C18 1.5248(13), C15-C16 1.3677(14). C1-N1-C8 109.05(8), N1-C1-C2 130.38(9), C7-C8-N1 110.09(9), N1-C1-C6 107.41(8), N2-C9-C10 130.64(9), N2-C9-C14 107.50(8), C16-C15-N2 110.17(9), C21-N3-C24 117.84(9), C21-N3-C25 116.66(8), C24-N3-C25 112.68(9), C22-C21-N3 120.76(9), C20-C21-N3 121.88(9), C6-C7-C8 106.45(9), C8-C7-C17 127.81(9), C6-C7-C17 125.71(8), C16-C17-C7 112.09(8), C16-C17-C18 115.08(8), C7-C17-C18 111.87(8), C14-C16-C17 122.57(9).

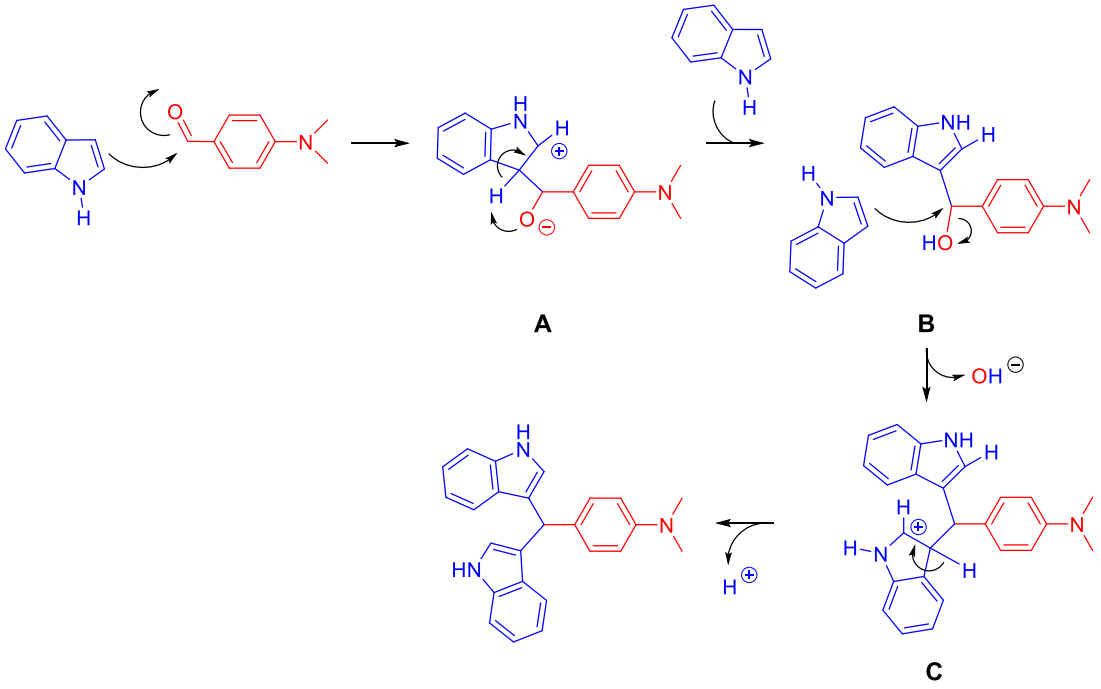

Scheme 4.4. Proposed mechanism in the reaction of DMAB with indole, yielding β-bis(indolyl)methane.

C. Break of the β C-H bond from the second indole moiety in **C** gives the product bis(indolyl)methane and H^+. Given the C-H bond activation and the likely sequential reaction with two indole molecules here, it is not surprising that this reaction is slower than the reaction of aniline with DMAB which involves a more nucleophilic N atom.

3.4. Conclusion

The current work has resolved two long-standing important questions. Indole reacts with DMAB in a 2:1 ratio in the Ehrlich test. The reaction occurs at the β-position of indole, yielding β-bis(indolyl)methane.

References

[1] J.F. MacFaddin, Biochemical Tests for Identification of Medical Bacteria, 3rd Ed., Williams & Wilkins, 2000, pp. 221-232.

[2] E.J. Baron, S.M. Findegold, Bailey & Scott's Diagnostic Microbiology, 2002, pp. 152-153.

[3] N.O. Bullock, J. Aslanzdeh, Biochemical profile-based microbial identification system, in: Y.-W. Tang, C.W. Stratton, Eds., Advanced Techniques in Diagnostic Microbiology, C. W. Springer Science+Business Media, New York, 2013, pp. 87-121.

[4] J.M. Miller, J.M. Wright, Spot indole test: Evaluation of four reagents, J. Clin. Microbiol. 15 (1982) 589.

[5] J.Z. Kleeberg, Ehrlich's benzaldehyde reaction (with uribilinogen) 80 years later, Gastroenterol. 20 (1982) 424.

[6] A.J.L. Cooper, Spot test for the detection of α-ketoglutaramic acid in human cerebrospinal fluid, Anal. Biochem. 90 (1978) 444-446.

[7] M.M. Hollander, A. J. Reiter, W. H. Horner, A. J. L. Cooper, Conversion of canavanine to α-keto-γ-guanidinooxybutyrate and to vinylglyoxylate and 2-hydroxyguanidine, Ach. Biochem. Biophys. 270 (1989) 698-713.

[8] F.M. Campbell, G.J. Rucklidge, M.D. Reid, L. Cantlay, S.P. Robins, Identification of damaged proteins in human serum using modified Ehrlich's reagent to target protein-bound pyrroles, Anal. Biochem. 398 (2010) 76-82.

[9] Q. Jin, L. Shan, J. Yuw, X. Wang, Spectrophotometric determination of total serotonin derivatives in the safflower seeds with Ehrlich's reagent and the underlying color detection mechanism, Food Chem. 108 (2008) 779-783.

[10] Y. Kohno, J. Kamiya; T. Okubo, R. Matsushima, Color sensors for indole vapors based on Ehrlich-type reactions, Anal. Sci. 25 (2009) 129-132.

[11] R.S. Alexander, A.R. Butler, Electrophilic substitution in pyrroles 1. Reaction with 4-dimethylaminobenzaldehyde (Ehrlich's reagent) in acid solution, Chem. Soc. Perkin II (1976) 696-701.

[12] H. Fischer, H. Orth, Die Chemie des Pyrrols, Akademische Verlagsgesellschaft mbH, Leipzig, 1937, vol. 2.

[13] C. Karami, H. Ahmadian, M. Nouri, F. Jamshidi, H. Mohammadi, K. Ghodrati, A. Farrokhi, Z. Hamidi, A novel method for synthesis of cobalt manganese oxide nanocataysts as a recyclable catalyst for the synthesis of some bis(indolyl) methane derivatives, Catal. Commun. 27 (2012) 92-96.

[14] B.P. Bandgar, K.A. Shaikh, Molecular iodine-catalyzed efficient and highly rapid synthesis of bis(indolyl) methanes under mild conditions, Tetrahedron Lett. 44 (2003) 1959-1961.

[15] L.T. An, F.Q. Ding, J.P. Zou, X.H. Lu, L.L. Zhang, An efficient and solvent-free reaction for synthesis of bis(indol-3-yl)methanes catalyzed by sulfamic acid, Chin. J. Chem. 25 (2007) 822-827.

[16] Y. Yang, Z. Xie, J. Wang, $CrCl_3 \cdot 6H_2O$-hydrogenated bis-Schiff base as a new efficient catalyst system for synthesis of bis(indolyl) methane, Chin. J. Chem. 29 (2011) 2091-2096.

[17] S. Handy, N.M. Westbrook. A mild synthesis of bis(indolyl) methanes using a deep eutectic solvent, Tetrahedron Lett. 55 (2014) 4969-4971.

Part 5

Control release of persulfate for *in-situ* chemical oxidation

Abstract

A system for the controlled release of potassium persulfate has been developed from pellets of diatomaceous earth for the oxidation of an organic contaminant. Fabrication of pellets containing potassium persulfate and their release profile have been studied. Sol-gel coatings on the pellets have been investigated to explore their effect on release rate of potassium persulfate. In addition, using sol-gel within the diatomaceous earth pellets and larger pellets, persulfate release for up to 21 h from the pellets has been obtained. We have also developed Fe^{2+}-containing pellets to release Fe^{2+} ions for *in-situ* activation of the oxidant persulfate. Controlled-released persulfate and Fe^{2+} ions from the pellets have been used for the batch treatment of 15 mg L^{-1} trichloroethylene (TCE) aqueous solution, giving residual TCE concentration of <0.06 mg L^{-1} after 6 h and degradation of 93% TCE after 2 h. The approach herein may be used in the remediation of contaminated groundwater.

5.1. Introduction

Groundwater contamination significantly affects the drinking water supply. Water pollution is largely originated from anthropogenic sources due to residential, commercial, industrial, and agricultural activities. The transport of pollutants in groundwater generally involves an area of higher concentration denominated plume, which flows along the same path [1].

Due to the presence of a wide variety of organic pollutants in groundwater, non-selective advance oxidation processes (AOPs) based on highly reactive intermediates have been applied for the remediation of the groundwater [2]. In general, AOPs aim at the generation of OH· radicals, which attack a wide range of organic molecules [3]. Several methods are possible to form these radicals, including Fenton and Fenton-like processes, photocatalysis, and use of H_2O_2 and O_3 [3].

In-situ chemical oxidation (ISCO) is a form of AOPs that offers the advantage of rapidly targeting environmental contaminants by introducing oxidative species directly into the plume or contaminated site. Persulfate has been widely used as an ISCO agent for several applications [4, 5]. The persulfate ion ($S_2O_8^{2-}$) is an oxidant that produces free radical $SO_4^{\bullet-}$ with an oxidation potential ($E°$ = 2.6 V) comparable to hydroxide radicals ($E°$ = 2.7 V). The process where persulfate radical is generated is called activation, and it can be thermally initiated or as a result of UV radiation or reaction with metal ions as shown in Scheme 5.1 [4].

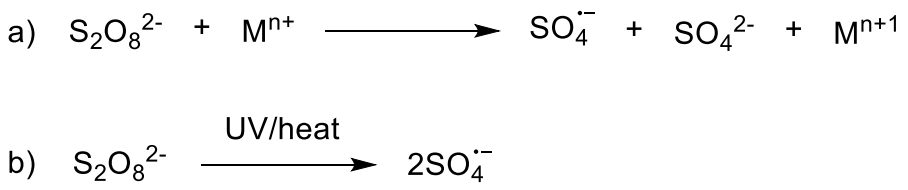

Scheme 5.1. Activation of persulfate by (a) a transition metal M and (b) UV/heat.

A limitation on the efficacy of ISCO oxidant species is their very short lifetime, usually of less than one second [6]. Therefore, an important factor on their applications is the assurance that they reach contaminants with a sustained delivery. For instance, systems based on paraffin wax have been reported for the controlled release of persulfate [7-9]. However, this organic matrix is not desirable, as it consumes persulfate itself prior to reaching target compounds.

Organohalides are a class of toxic compounds, mainly from their halogen atoms [10]. Trichloroethylene (TCE) is notorious for its prevalence and toxicological effects. TCE has had a widespread use since the early 20th century as a solvent for degreasing and dry cleaning, and as a chemical for paints and inks [11]. The Agency for Toxic substances and Disease Registry (ATDSR) ranks TCE the 16th among 275 compounds in the 2017 Substance Priority List (SPL). The SPL prioritizes compounds based on their toxicity, frequency, and likelihood of exposure at national priority sites [12]. In addition to acute effects such as headaches, dizziness, and skin sensitization, TCE has been regarded as a potential carcinogen [13]. Liang and collaborators have studied the oxidation of TCE by direct addition of persulfate and its activator to batch systems using thermal [14] and Fe^{2+} [15] activation.

This Part investigates the delivery of persulfate and its activator Fe^{2+} ions from

their respective diatomaceous earth pellets for the degradation of TCE in water. Diatomaceous earth is a highly porous and amorphous solid material. It is predominantly composed of silica and it originates from fossil remains of unicellular microorganisms [16]. Its availability and low cost make it an attractive material as the support in the pellets. In contrast to reported methods that employ organic paraffin wax, our approach relies on the use of an inorganic material that does not consume oxidant.

5.2. Materials and methods

Diatomaceous earth (gift of Prof. Angel Palomino, Department of Civil and Environmental Engineering, University of Tennessee, Knoxville), sodium silicate (41° Baume, J.T. Baker), concentrated HCl and H_2SO_4 (Certified ACS Plus, Fisher), $K_2S_2O_8$ (Certified ACS, Fisher), and $FeSO_4 \cdot 7H_2O$ (Baker's Analyzed) were used for pellet fabrication. KI (Alfa Aesar, 99%) and $NaHCO_3$ (Fisher, Certified ACS) were used as received on the determination of persulfate. $(NH_4)_2Fe(SO_4)_2 \cdot 6H_2O$ (iron(II) ammonium sulfate hexahydrate, Merck), hydroxylamine hydrochloride (Alfa Aesar, 99%), sodium acetate (ACS, >99%), glacial acetic acid (Fisher, Certified ACS), and 1,10-phenantroline (Alfa Aesar, 99+%) were used for Fe^{2+} determination. TCE (Acros Organics, 99+% extra pure) and 2-bromofluorobenzene (BFB, Acros Organics 99%, as GC internal standard), NaCl (Certified ACS, Fisher), acetone (Certified ACS, Fisher) and pentane (Certified ACS, Fisher) were used for TCE determination. Chloride measurements were made with a Cole-Parmer chloride ion-selective electrode, using sodium nitrate (Certified ACS) for the preparation of an ionic strength adjuster solution.

5.2.1. General procedure for the preparation of diatomaceous earth pellets

A portion of diatomaceous earth was mixed with $K_2S_2O_8$ that had been previously ground to reduce particle size. The mixture was added into a 13-mm pellet die and pressed under 5-7 tons of pressure for 1 min in a manual bench top pellet press. Pellets were retrieved from the die for subsequent processing.

5.2.2. Organic sol-gel coating

$Si(OMe)_4$ (tetramethyl orthosilicate or TMOS, Acros Organics 99%) was used as a precursor for the synthesis of the sol-gel. The molar ratio of water/TMOS/MeOH was 4:1:4. For acid-catalyzed sol-gel coating A, the HCl molar ratio was kept at 0.05. For the base-catalyzed sol-gel coating B, a 0.02 molar ratio of NH_4OH was used. Coating A was allowed to react overnight, whereas coating B was applied within 10 min of the reaction. A 0.4 g pellet with 15% potassium persulfate pressed under 7 ton was used. 50 µL of coating was directly added and distributed with a pipet tip on each face and the edge of the pellet.

5.2.3. Inorganic sol-gel coating

A solution of 0.4 M HCl (4 mL) was added dropwise to 1.25 g of sodium silicate under stirring. Diatomaceous earth (0.4 g) was mixed with it and the suspension was allowed to cure for 1 h at room temperature, followed by drying for 2 h at 100 °C. The mixture was ground and dried again for an additional hour. After grinding a second time, the modified diatomaceous earth was ready for further processing.

A portion of $K_2S_2O_8$ (15% w/w) was mixed with diatomaceous earth prepared as

described above, for a total nominal mass of 0.2 g. $FeSO_4 \cdot 7H_2O$ (20% w/w) pellets were prepared in a similar manner with a total mass of 0.2 and 0.3 g. Each mixture was pressed (5-ton) on a cylindrical press die and stored prior to use.

In order to study the persulfate release profile under different conditions, a sol-gel coating was applied to the 15% persulfate pellets. Sol-gel was prepared as described before and 50 µL was applied to one side of the pellet. Spin-coating was applied at 1,500 rpm to eliminate the excess coating. After drying, the same procedure was applied to the other side. This treatment is designated as Coating 1. Another treatment was performed by applying 100 µL sol-gel on each side without spin coating (Coating 2).

5.2.4. Persulfate and Fe^{2+} release profiles

We have characterized the release of persulfate and Fe^{2+} ions into water by measuring their respective concentrations in the water solutions over time. A pellet was immersed in 500 mL DI water (18.1 MΩ-cm) in an Erlenmeyer flask under magnetic stirring at 700 rpm. Aliquots (2 mL) were taken at different time intervals. Samples were frozen prior to analysis.

Persulfate was determined by using a modification of the spectroscopic I^-/I_2 method described by Liang [17]. Aqueous indicator 1.0 M KI/0.15 $NaHCO_3$ solution and a 25 mM $K_2S_2O_8$ stock solution were prepared. Five persulfate calibrations standards in the concentration range of 5-120 µM were made by delivering the corresponding volume of stock solution in a 25-mL volumetric flask, followed by adding 2.5 mL of indicator solution. The solution was allowed to equilibrate for 20 min before diluting to

the mark. A yellow-brown color developed, indicating formation of I_2. Similarly 1 mL of indicator solution was added to 1 mL of sample and absorbance measurements were taken after 20 min. Indicator solution was diluted in half and used as an analytical blank. The absorbance at 352 nm was measured on an Agilent 8453 UV-visible spectrophotometer. Sample volume was adjusted for out of range measurements.

Fe^{2+} was determined by the iron-phenantroline method, monitoring the color development at 511 nm [18]. We made 250 mL of 20 mg L^{-1} Fe^{2+} stock solution, acidifying it with 1 mL of concentrated H_2SO_4 before diluting to the mark. Seven calibration standards between 0.08 and 12 mg L^{-1} Fe^{2+} were prepared by adding the appropriate volume of stock solution, 1.0 mL of hydroxilamine hydrochloride (10 g L^{-1}, solution A), 5 mL of acetate buffer (pH 4, solution B), and 2.5 mL of 1,10-phenanthroline (2 g L^{-1}, solution C), diluted to a final volume of 50 mL. Samples were prepared by adding 0.1 mL of A, 0.5 mL of B, and 0.25 mL of C, to 1.0 mL of original sample, and diluting to a final volume of 5.0 mL.

5.2.5. TCE determination

GC-MS determination was carried out by following a modification of the EPA method 551.1 [19]. A 10,000 mg L^{-1} stock solution of trichloroethylene (TCE) in acetone was prepared and labeled as Stock 1. Primary dilution standards of Stock 1 were prepared such that when 10 µL of each one was added to 10 mL of water, the new aqueous standards concentrations encompassed the working range of the calibration (0-5 mg L^{-1}). Stock 1 and primary dilution standards were stored in 5-mL capped vials at -30 °C using a secondary container.

GC-MS measurements were performed on a Hewlett-Packard HP 6890 Series GC system with a HP 5973 mass spectrometer detector, equipped with a HP-5ms Ultra inert column (30.0 m × 0.25 mm i.d. × 0.25 µm film thickness). A 2-µL injection volume was used. Temperature programming was set at 4 min @ 27 °C, 5 °C/min to 61 °C, and 3 min @ 27 °C. Column flow rate was 1.5 mL/min. Selected-ion monitoring mode was used to scan two characteristic ions for TCE (110 and 130 m/z) and BFB (174 and 176 m/z).

5.2.6. TCE extraction

Procedural aqueous calibration standards were prepared on the same day of analysis. A 10-µL volume of primary dilution standard was delivered directly into 10 mL of DI water to avoid loss from evaporation. Bromofluorobenzene (BFB) was used as an internal standard. An initial 10,000 mg L^{-1} stock solution was prepared as described above and designated as BFB Stock 1. A secondary 500 mg L^{-1} BFB stock was made by diluting 0.5 mL up to 10 mL in acetone.

A solution of pentane with BFB was prepared by dissolving 50 µL of BFB Stock 2 up to 50 mL with pentane for a final BFB concentration of 0.5 mg L^{-1}. Aqueous standards (10 mL), including a blank, are extracted with 3-mL of pentane and BFB solution in a 25 mL vial. Addition of pentane was performed using a 3-mL volumetric pipet, followed by addition of 5 g of NaCl. After securing the cap, the solution is inverted a few times and left 15 min in a waving shaker on the lowest setting. The solution was allowed to stand before the organic layer was extracted. The same procedure was applied for both standards and samples.

5.3. Results and discussion

In order to characterize the performance of our pellets, the release kinetics was fitted using the Higuchi equation. This model based on the square-root of time:

$$Q_t = K\, t^{0.5} \qquad \text{Eq. 5.1}$$

where Q_t is the cumulative percent release at time t and K is the release rate constant. K is dependent of the diffusion coefficient of the substance, the tortuosity of the medium and the total amount of substance present [20]. This model has been used to describe the release of solid substances from porous matrices. Although the derivation of Higuchi's model includes built-in assumptions such as a planar system geometry and the absence of swelling from the matrix [21], we utilize it herein for the comparison of release between our proposed systems due to its simplicity. Other applications of Higuchi's release model for systems involving sol-gel can be found in the literature [22-24].

5.3.1. Preliminary studies with organic sol-gel coatings

We initially explored the effect of sol-gel coatings on the release of persulfate. Given that structural differences are observed between acid- and base-catalyzed sol-gels, an initial test was conducted to determine notable differences between release profiles of the pellets containing the acid- and base-catalyzed sol-gels.

The weight of Coatings A and B were 34.6 mg and 19.5 mg, respectively. A Higuchi release constant of 55.7 was calculated for the persulfate release from the

pellet with Coating A, while Coating B showed a constant of 45.1. Although a slower release would be theoretically expected with a heavier coating, we have observed that Coating B shows a slower rate as evidenced by the value of *K*. Moreover, a maximum cumulative release around 8 h for B is obtained, whereas A plateaus around 4 h (Figure 5.1). Structural differences in the sol-gel due to the catalysis method can explain these observations. Base catalysis generates gels with a globular conformation and larger particle size [25]. In addition, the condensation occurs faster resulting in a tighter network. On the other hand, acid catalysis generates linear chains with less crosslinking at a slower rate. Since cracking of the pellet surface was often observed by this approach, we have focused on a different approach to improve the structural integrity of the pellets by incorporating sol-gel *inside* the matrix rather than just for coating on the pellet surface.

5.3.2. Inorganic sol-gel as binder

Based on our preliminary studies, we modified the material by mixing inorganic sol-gel with diatomaceous earth prior to pelletization as described in Section 5.2.3. The use of sol-gel as a binder, in addition to a size reduction, resulted in a better pellet integrity as evidenced by the absence of cracking before and during immersion in water. Figure 5.2 shows the persulfate release profile for the three different diatomaceous earth pellet coatings. Inorganic sol-gel based on sodium metasilicate was utilized as opposed to organic precursors because the former does not generate methanol as a hydrolysis product. The mass gain for each coating treatment when compared to an uncoated pellet is presented in Table 5.1, along with the Higuchi fitting parameters.

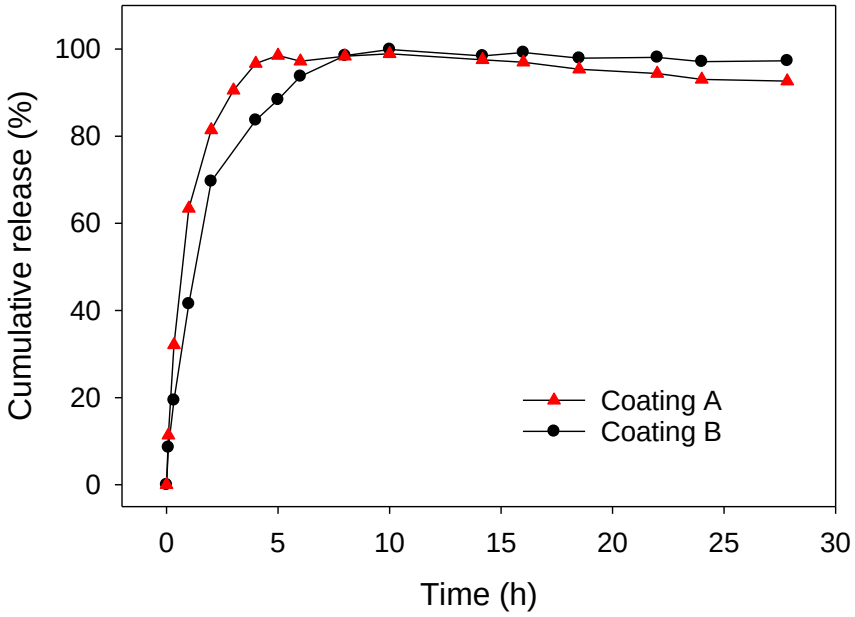

Figure 5.1. Persulfate release profile for pellets with coatings A and B (organic). for the initial values prior to each plateau on each case.

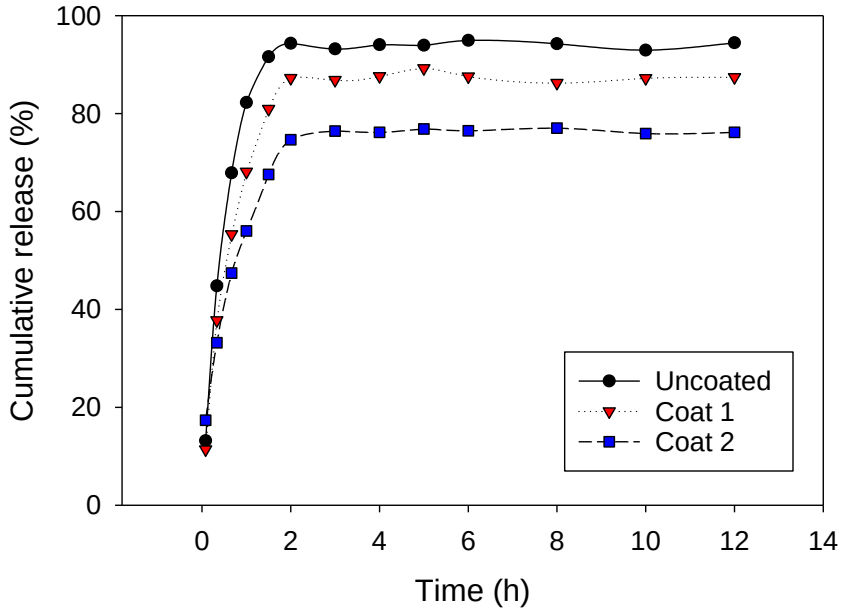

Figure 5.2. Persulfate release profile for pellets with coatings 1 and 2 (inorganic). Each point represents the mean value for three pellets.

A slower release is observed as a consequence of a thicker coating as evidenced by a smaller slope. However, the maximum amount of persulfate released also decreases with a heavier sol-gel coat. Figure 5.3 shows images of the pellets described here.

5.3.3. Fe^{2+} release profile

An analogous release profile was obtained to characterize the presence of Fe^{2+} in solution. $FeSO_4 \cdot 7H_2O$ was used as a source of Fe^{2+}. The load of $FeSO_4 \cdot 7H_2O$ was kept at 20%, using two different masses (0.2 and 0.3 g) to explore differences on their iron(II) delivery. Figure 5.4 shows that in either case, complete release of the original $FeSO_4$ is not achieved after several hours. This is due to the formation of an Fe^{2+} coating (Fe^{2+}-O-Si≡) on the pellet surface, which restricts the availability of Fe^{2+} ions released into the solution.

Table 5.1. Mass gain and fitting parameters for each coating treatment

Treatment	Coat mass (n = 3)	Maximum release	Higuchi slope	R^2
Uncoated	N/A	94%	97.77	0.995
Coating 1	50.6 ± 5.2 mg	87%	74.32	0.992
Coating 2	67.0 ± 5.6 mg	77%	51.57	0.996

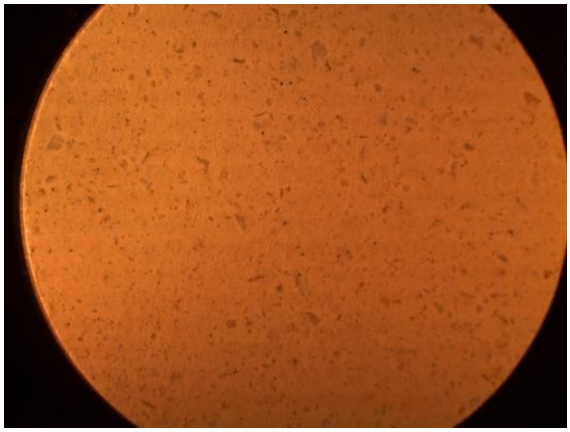

a

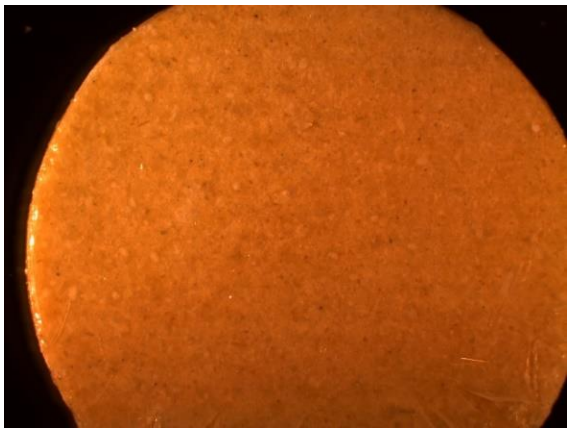

b

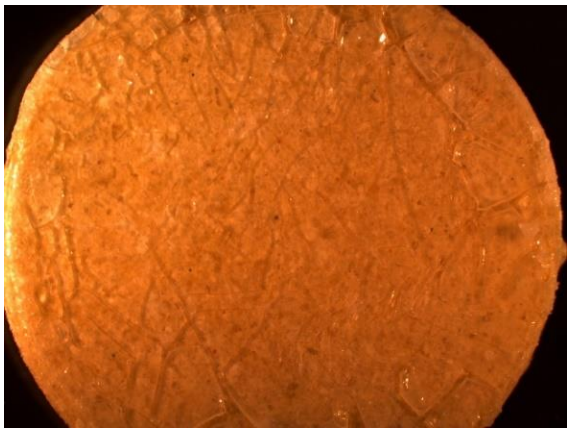

c

Figure 5.3. Photos of diatomaceous earth pellets: (a) Uncoated; (b) Coating 1; (c) Coating 2.

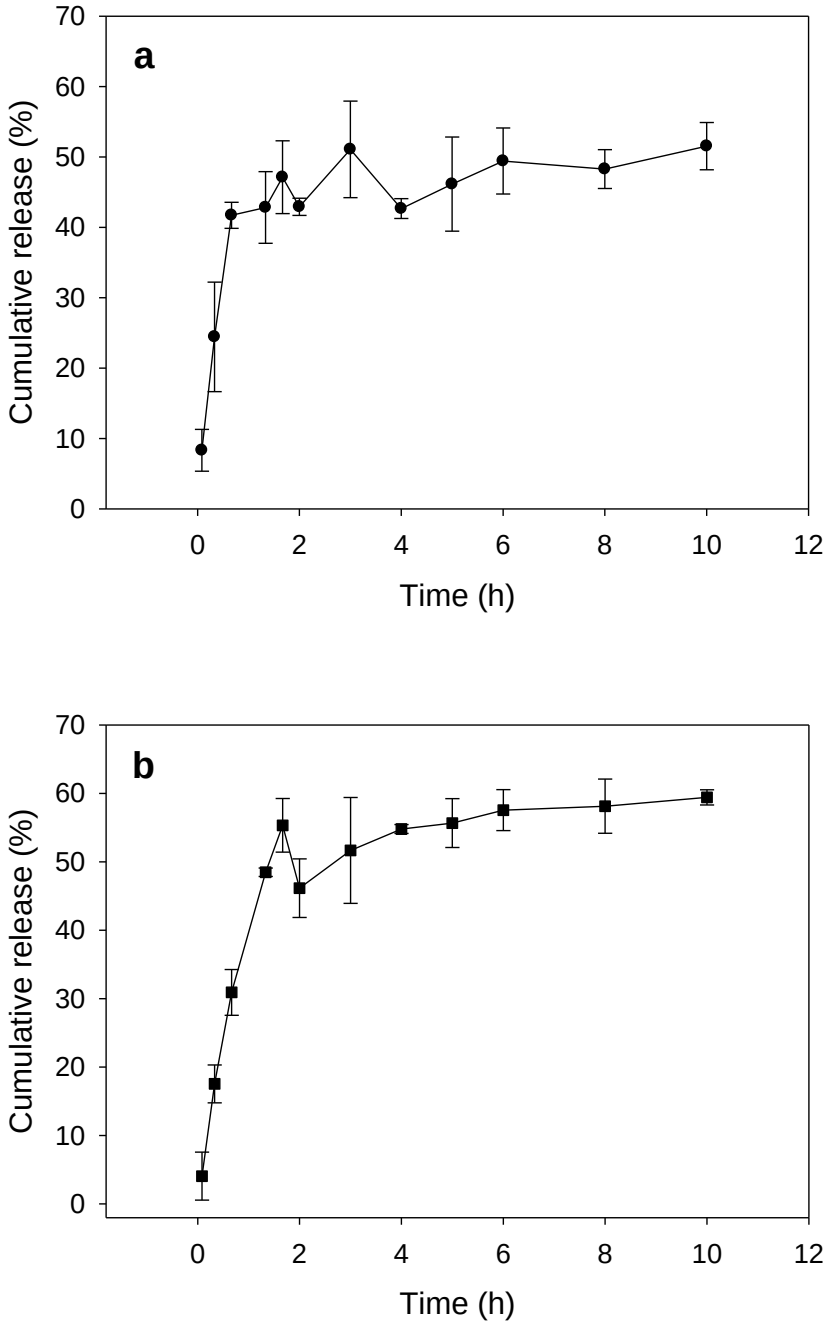

Figure 5.4. Release profile for 20% $FeSO_4$ pellets. Nominal masses are (a) 0.2 g and (b) 0.3 g.

For a pellet with a nominal mass of 0.2 g, 51% of original $FeSO_4$ is released, whereas 59% is obtained for a pellet of 0.3 g nominal mass. Further experiments were conducted using the latter to activate persulfate.

Given the reaction leading to the formation of persulfate radical (Scheme 5.1), a competitive reaction for persulfate radical can occur when there is a stoichiometric excess of Fe^{2+} (Eq. 5.2), resulting in the formation of sulfate ion and restricting the oxidation capability of the system [15]:

$$SO_4^{\bullet-} + Fe^{2+} \rightarrow SO_4^{2-} + Fe^{3+} \qquad \text{Eq. 5.2}$$

Maximum efficiency of persulfate activation will be achieved by ensuring that the $S_2O_8^{2-}/Fe^{2+}$ ratio is approximates 1 at a given time when released into solution. We see that at approximately 1 h, the proportion between both compounds are close to 1, further decreasing as release progresses and Fe^{2+} becomes more prevalent (Figure 5.5).

Calculations for this ratio were based on the cumulative release for each species in their individual experiments. The reaction between persulfate and Fe^{2+} could affect their individual release profiles, causing actual ratios to vary from the ones calculated.

5.3.4. TCE studies

The limit of detection (3σ) for our TCE method was estimated to be 0.057 mg/L. A single sample of treated TCE was spiked with the 0.5 mg L^{-1} standard solution, showing a recovery of 109% and discarding analyte loss due to matrix effects during

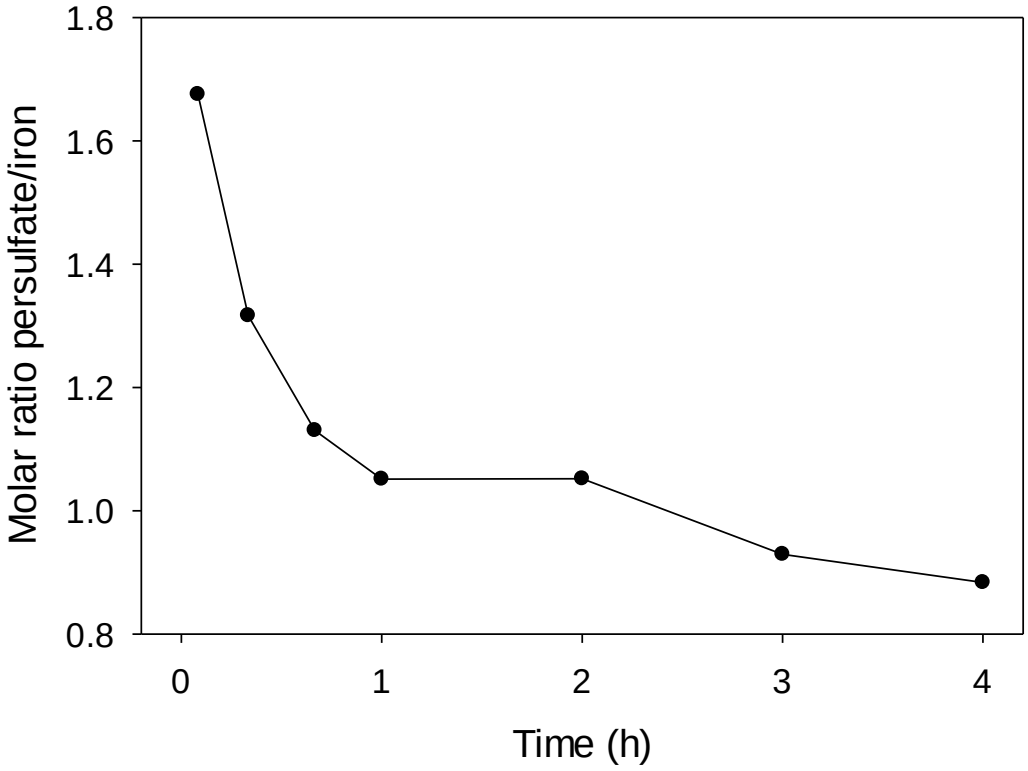

Figure 5.5. Molar ratio of persulfate to Fe^{2+} vs. time.

analysis after treatment. We conducted two independent preliminary studies to show the effect of persulfate treatment after 3 and 6 h. For this, TCE solution (100 mL) was exposed to a 0.2 g, uncoated persulfate pellet and a 0.3 g, Fe^{2+} pellet in a 240-mL French square glass bottle sealed with a rubber stopper. After 3 h, a 0.70 ± 0.19 mg/L TCE concentration was observed (n = 3). After 6, the concentration was below the limit of detection. A parallel control experiment was performed by treating TCE with pellets that contained no persulfate or iron sulfate. A 50% drop in TCE concentration was observed after 3 h. In order to whether TCE adsorbed onto the pellet, a second control experiment was performed with no pellets. A similar value was obtained showing that loss was not attributed to retention of TCE by the pellet.

We have compared the effect of controlled-released persulfate versus direct use of persulfate and Fe^{2+} that are not controlled-released. An equivalent amount of $K_2S_2O_8$ and $FeSO_4 \cdot 7H_2O$ were added (30 and 60 mg, respectively) the TCE solution and the mixture was allowed to react under the same conditions. TCE concentration of 3.32 ± 0.52 mg/L was found after 6 h. We attribute this to the stoichiometric excess of Fe^{2+} ions early in the treatment, which drives the activation of persulfate to form stable SO_4^{2-} ions as a primary product instead of the more active sulfate radicals $SO_4^{\bullet-}$ as discussed earlier (Section 5.3.3). In comparison, using controlled-release persulfate and Fe^{2+}, the concentration was below the limit of detection after 6 h, demonstrating the advantage of our controlled-release approach.

For subsequent experiments, a custom-made glass container consisting of a 125-mL Erlenmeyer flask with a ground glass joint was utilized. Reduction of headspace and use of a glass stopper decreased TCE loss to 18% after a 6-h exposure.

In order to characterize the degradation profile of TCE, we determined the concentrations of TCE at time intervals of 1 h after the start of the initiating treatment. The effect of modified diatomite pellets with a persulfate load (w/w) of 15 and 30%, both with an iron(II) pellet at 20% load as an activator, was compared. Figure 5.6 shows the progress of both treatments in 5 h.

We observed that most of the oxidative effect of persulfate occurs in the first two hours. For a 15% persulfate pellet, 71% and 83% of TCE are consumed within 1 and 2 h, respectively. A 30% persulfate pellet depletes TCE more effectively, showing 88% consumption after 1 h and 93% at 2 h. Using the release profile of persulfate from a 15% load pellet as a reference, this timeframe approximately coincides with the time required to reach maximum release from the diatomaceous earth matrix. A parallel control test shows a 30% loss during the treatment, which can be explained by the exposure of the container to open air during sampling. Given the short half-life of the persulfate radical in solution, we regard the persulfate delivery into the solution as the limiting step on the treatment process as opposed to the oxidative TCE dechlorination. An additional study was conducted to determine the amount of chloride present in the TCE solution after a 6 h treatment with our approach. For this test, pellets were made using sulfuric acid as previously described in the general method in order to avoid the contribution of chloride ions from HCl. Ionic strength adjuster solution (0.1 M, 0.5 mL) was added to the TCE solution for a final volume of 50 mL. The Cl^- concentration was 14.25 mg L^{-1}. Based on the initial 15 mg L^{-1} TCE concentration, a theoretical concentration of 12.14 mg L^{-1} would be indicative of cleavage of all C-Cl bonds from TCE. Although a larger value is observed due to the error, this test can be used as

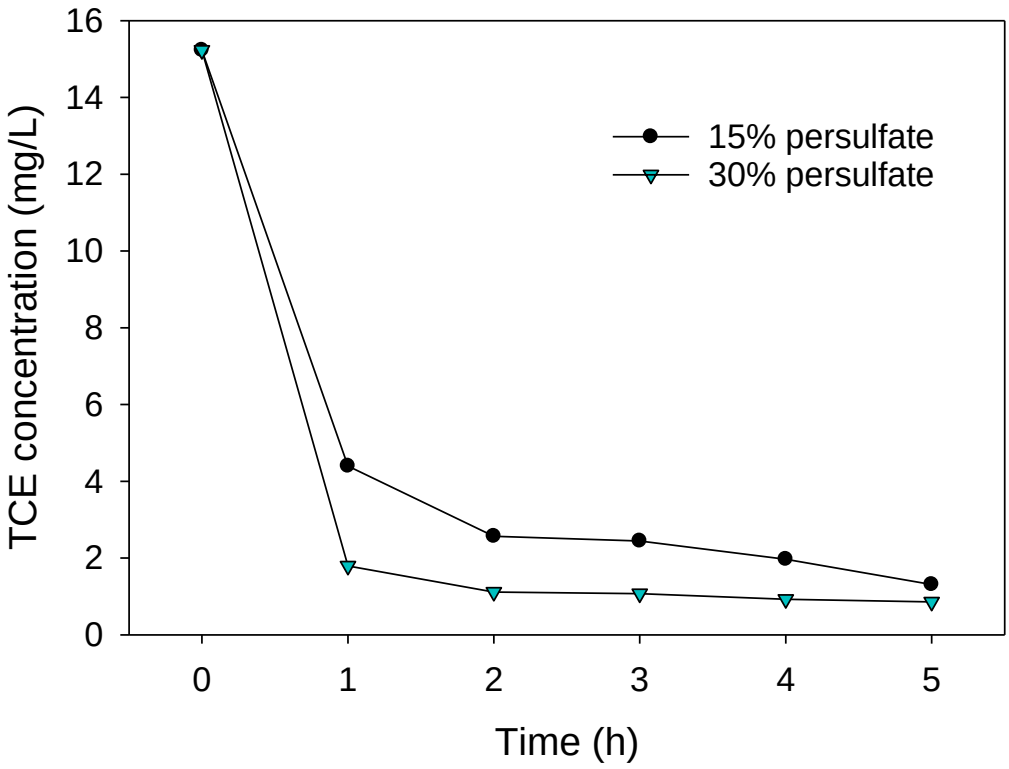

Figure 5.6. TCE degradation profile.

supporting evidence for the effectiveness of our treatment.

5.3.5. Sol-gel/diatomaceous earth matrix

As observed in prior experiments (Figures 5.1 and 5.2), the modification of the pellet size impacts the time required for maximum release. Our experiments showed a maximum cumulative release of no more than 8 h. In order to enhance the release time, we modified the procedure described in Section 5.2.3. Besides increasing the pellet size, we also tested the addition of persulfate at an earlier stage.

Following the general diatomaceous earth modification procedure, 8 mL of 0.2 M H_2SO_4 were added dropwise with a buret under constant stirring to sodium silicate solution (2.5 g). The solution was stirred for two additional minutes until an increase in viscosity was observed. A dry mixture of 0.5 g of diatomaceous earth and 0.5 g pf persulfate was added. After the sol-gel solution was kept at room temperature for 1 h, the solution was placed in an oven at 40 °C for one week for drying. The dry mixture was ground and weighed, obtaining a mass of 2.1739 g. Portions of 0.5 and 1.0 g were taken and pressed into pellets and persulfate release profiles were characterized (Appendix D, Figure D.1).

The maximum cumulative release for the 1.0 g pellet occurred at 21 h. In contrast, 7 h were required for the 0.5 g pellet to reach this level. On this approach, persulfate is not added to diatomaceous earth immediately before pelletization as performed earlier. Since loss of persulfate was suspected to occur during drying, the release of persulfate is given in terms of concentration rather than cumulative release. However, both pellets have the same weight percent of persulfate, since they were

made with the same diatomaceous earth/sol-gel batch.

In addition to having a larger total persulfate content, the pellet with a 1.0 g nominal mass has a lower surface area to volume ratio (A/V) compared to the 0.5 g pellet. Larger A/V ratios were shown to correlate with faster release [26, 27]. Thus, longer release profiles were achieved by modifying the structure and loading of the pellets. Triplicates for the 1.0 g pellets were conducted on a separate experiment, showing a fair reproducibility between tests. Based on the original loading of persulfate and the dry mass of the final diatomaceous earth/sol-gel mixture, the maximum concentration of persulfate corresponds to approximately 100% release of the original loading (Figure 5.7), discarding loss of the oxidant during sol-gel formation and drying.

5.4. Conclusion

Development and characterization of persulfate- and Fe^{2+}-containing pellets for remediation of contaminated water are reported here. The low cost of diatomaceous earth makes the approach particularly attractive. We demonstrate that treatment of TCE-contaminated water with our approach is feasible by reducing the TCE concentration to <0.06 mg L^{-1} in 6 h. Moreover, the longest release time is achieved by modifying the pellet size and by loading persulfate into a diatomaceous earth/sol-gel matrix prior to gel formation. Additional studies to extend the release and sustain the activation of persulfate could be conducted for a potential application of this method in groundwater remediation.

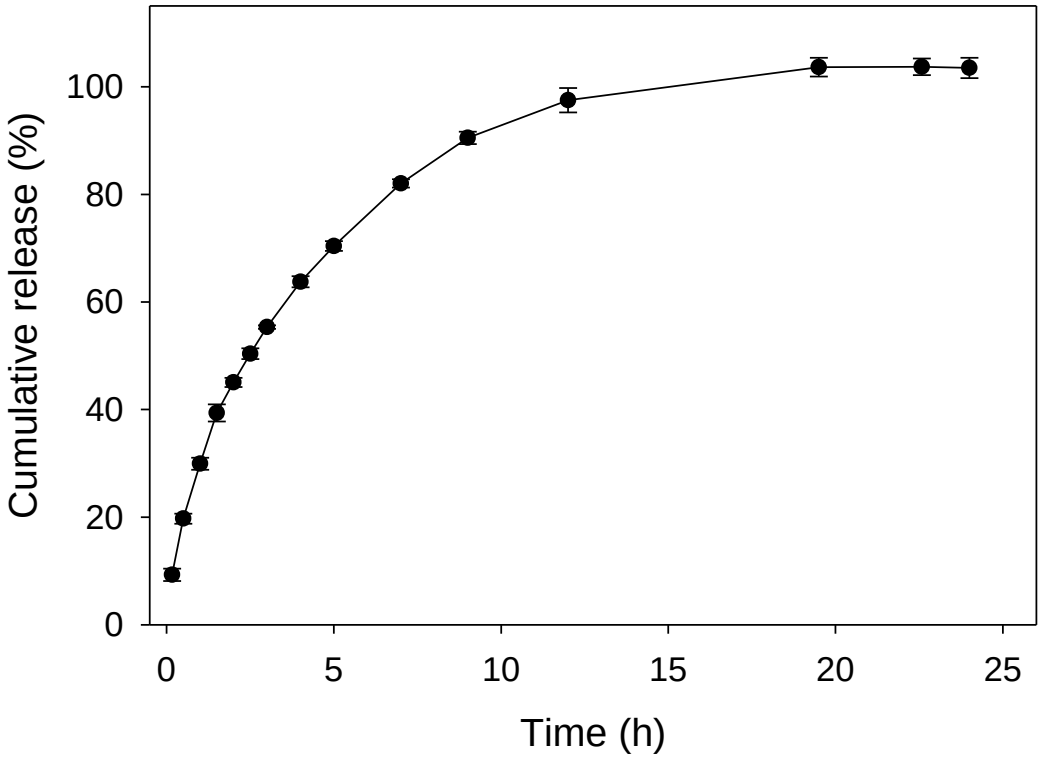

Figure 5.7. Release profile for 1.0 g pellets with pre-mixed persulfate (*n* = 3).

References

[1] US Environmental Protection Agency, Groundwater Contamination: Magnificent Groundwater Connection. https://www.epa.gov/sites/production/files/2015-08/documents/mgwc-gwc1.pdf (accessed on July 1st, 2018).

[2] P.D. Swaim, R. Morgan, L. Foster, P. Mueller, M. Vorissis, W. Carter, Implementing an effective UV advanced oxidation process, Proc.-Water Qual. Technol. Conf. Expo. 11 (2008) 678-688.

[3] R. Andreozzi, V. Caprio, A. Insola, R. Marotta, Advanced oxidation processes (AOP) for water purification and recovery, Catal. Today 53 (1999) 51-59.

[4] A. Tsitonaki, B. Petri, M. Crimi, H. Mosbaek, R.L. Siegrist, P.L. Bjerg, In situ chemical oxidation of contaminated soil and groundwater using persulfate: A Review, Crit. Rev. Environ. Sci. Technol. 40 (2010) 55-91.

[5] L.W. Matzek, K.E. Carter, Activated persulfate for organic chemical degradation: A review, Chemosphere 151 (2016) 178-188.

[6] S.G. Huling, Pivetz, Bruce E., In-Situ Chemical Oxidation. US Environmental Protection Agency. https://archive.epa.gov/ada/web/pdf/insituchemicaloxidation_engineering_issue.pdf (accessed on July 2nd, 2018).

[7] C. Liang, C.-Y. Chen, Characterization of a sodium persulfate sustained release rod for in situ chemical oxidation groundwater remediation, Ind. Eng. Chem. Res. 56 (2017) 5271-5276.

[8] C. Chokejaroenrat, C. Sakulthaew, T. Satapanajaru, T. Tikhamram, A. Pho-Ong, T. Mulseesuk, Treating methyl orange in a two-dimensional flow tank by in situ chemical oxidation using slow-release persulfate activated with zero-valent iron,

Environ. Eng. Sci. 32 (2015) 1007-1015.

[9] A. Kambhu, S. Comfort, C. Chokejaroenrat, C. Sakulthaew, Developing slow-release persulfate candles to treat BTEX contaminated groundwater, Chemosphere 89 (2012) 656-664.

[10] S.E. Manahan, Environmental chemistry, Boca Raton: Lewis, Boca Raton, 1994.

[11] B. Bakke, P.A. Stewart, M.A. Waters, Uses of and exposure to trichloroethylene in U.S. industry: A systematic literature review, J. Occup. Environ. Hyg. 4 (2007) 375-390.

[12] Agency for Toxic Substances and Disease Registry, ATSDR's Substance Priority List, 2017. https://www.atsdr.cdc.gov/spl/index.html (accessed on June 28th, 2018).

[13] US Environmental Protection Agency. Risk Management for Trichloroethylene (TCE). https://www.epa.gov/assessing-and-managing-chemicals-under-tsca/risk-management-trichloroethylene-tce (accesed on July 1st, 2018).

[14] C.J. Liang, C.J. Bruell, M.C. Marley, K.L. Sperry, Thermally activated persulfate oxidation of trichloroethylene (TCE) and 1,1,1-trichloroethane (TCA) in aqueous systems and soil slurries, Soil Sedim. Contam. 12 (2003) 207-228.

[15] C. Liang, C.J. Bruell, M.C. Marley, K.L. Sperry, Persulfate oxidation for in situ remediation of TCE. I. Activated by ferrous ion with and without a persulfate–thiosulfate redox couple, Chemosphere 55 (2004) 1213-1223.

[16] R. Calvert, Diatomaceous earth, J. Chem. Educ. 7 (1930) 2829-2849.

[17] C. Liang, C.-F. Huang, N. Mohanty, R.M. Kurakalva, A rapid spectrophotometric determination of persulfate anion in ISCO, Chemosphere 73 (2008) 1540-1543.

[18] L.G. Saywell, B.B. Cunningham, Determination of iron: Colorimetric o-phenanthroline method, Ind. Eng. Chem. Anal. Ed. 9 (1937) 67-69.

[19] US Environmental Protection Agency, Method 551.1 Determination of chlorination disinfection byproducts, chlorinated solvents, and halogenated pesticides/herbicides in drinking water by liquid-liquid extraction and gas chromatography with electron capture detection (1995).

[20] P. Pisitsak, U. Ruktanonchai, Preparation, characterization, and in vitro evaluation of antibacterial sol-gel coated cotton textiles with prolonged release of curcumin, Text. Res. J. 85 (2015) 949.

[21] J. Siepmann, N.A. Peppas, Higuchi equation: Derivation, applications, use and misuse, Int. J. Pharm. 418 (2011) 6-12.

[22] S. Radin, T. Chen, P. Ducheyne, The controlled release of drugs from emulsified, sol gel processed silica microspheres, Biomaterials 30 (2009) 850-858.

[23] N. Roveri, M. Morpurgo, B. Palazzo, B. Parma, L. Vivi, Silica xerogels as a delivery system for the controlled release of different molecular weight heparins, Anal. Bioanal. Chem. 381 (2005) 601-606.

[24] M. Morpurgo, D. Teoli, B. Palazzo, E. Bergamin, N. Realdon, M. Guglielmi, Influence of synthesis and processing conditions on the release behavior and stability of sol–gel derived silica xerogels embedded with bioactive compounds, Il Farmaco 60 (2005) 675-683.

[25] C.J. Brinker, G.W. Scherer, Sol → gel → glass: I. Gelation and gel structure, J. Non-Cryst. Solids 70 (1985) 301322.

[26] R. Chopra, G. Alderborn, F. Podczeck, J.M. Newton, The influence of pellet

shape and surface properties on the drug release from uncoated and coated pellets, Int. J. Pharm. 239 (2002) 171-178.

[27] T.D. Reynolds, S.A. Mitchell, K.M. Balwinski, Investigation of the effect of tablet surface area/volume on drug release from hydroxypropylmethylcellulose controlled-release matrix tablets, Drug Dev. Ind. Pharm. 28 (2002) 457-466.

Part 6

Concluding remarks

This dissertation is focused mainly on the detection of aromatic amines for different applications. Part 2 provides an overview of indole as an indicator of spoilage in shrimp and describes the development of a polymeric film doped with DMAB as a probe for indole. We have coupled the probe with a simple solvent extraction method and demonstrated that both absorbance measurement with a UV-vis spectrometer and the CIELAB measurement with a handheld colorimeter provide adequate sensitivity to detect shrimp decomposition at the early stage as defined by the US FDA. We have obtained an LoD and LoQ of 0.05 and 0.16 μg mL^{-1}, respectively. In addition, a visible naked-eye gradient is observed. The fabrication of the probe is simple, and the ability to pair it with a portable colorimeter is particularly attractive for its use on site. This approach could lead to a rapid test as a less expensive, simpler alternative to the HPLC-fluorescence method currently recommended by the FDA.

We have studied in Part 3 the ability of the probe to analyze aniline and indole simultaneously for potential applications in monitoring of storage and thermal stability of aviation fuels. The response of the probe to aniline is kinetically favored and shows a higher sensitivity than its response to indole. When aniline is present at low concentrations, it does not significantly affect indole determination. However, at higher concentrations, aniline compromises the accuracy of indole analysis by PCR. Further exploration of the saturation of the system may lead to a simultaneous detection of both species on a wider concentration range.

In Part 4, a long-standing discrepancy on the correct structure of the red product between DMAB and indole has been resolved, as we are able to report its crystal structure and confirm the reaction of indole at its β-position with a 2:1 stoichiometry with

DMAB. This has clarified the nature of the Ehrlich reaction, which has been extensively used for a century in diverse applications.

The final part of this dissertation, Part 5, presents a novel approach for ISCO treatment of organic compounds. We have developed persulfate- and Fe^{2+}-containing pellets and demonstrated their ability to decompose TCE from 15 mg L^{-1} to <0.06 mg L^{-1} in 6 h. Moreover, the longest release time is achieved by modifying the pellet size and by loading persulfate into a diatomaceous earth/sol-gel matrix prior to gel formation. The use of diatomaceous earth is an attractive feature for its application on the remediation of groundwater, since this material is inexpensive, widely available, and does not consume persulfate prior to its delivery. Additional studies are needed to extend the release and sustain the activation of persulfate. Different matrix materials such as silica flour and different loads of the chemical could be explored to extend the release. The alternative materials to diatomaceous earth may provide different porosity and tortuosity, directly affecting the release. Since the ratio of the matrix material to persulfate can alter the number of available channels where the release occurs, optimization may determine the best persulfate loading, using maximum release time as a parameter. In addition, preventing Fe^{2+} from reacting with dissolved O_2 in solution would also increase the efficiency of the treatment.

Appendices

Appendix A

Appendix A provides supplemental materials for Part 2.

A1. Additional materials and methods

Fabrication of Film A

It should be pointed out that the spin-coating procedure developed in the current work gives the thinnest film on the substrate as the probe. Neither the change of spin-coating speed nor the volume of the polymer mixture led to a different film. When the spinning speed is reduced from 2,500 to 1,000 rpm, the film is heavier [with a mass gain of 0.13 mg (n = 7, p < 0.05) by a one-tailed t-test] than the probe. In addition, its surface is rougher. We thus did not test this film further. Another attempt in increasing the volume of the polymer mixture to 100 µL in one delivery (under the same spinning speed of 2,500 rpm) showed no difference in the film mass from the probe.

We then studied adding more than one layer of film on the probe. The probe was prepared as described in the main text. It was then dried for 1 h in air. Then 60 µL of the polymer mixture was placed on the film before it was spun at 2,500 rpm, as conducted in the preparation of the probe itself. Afterwards, the film was dried in air overnight before weighing or use. The film shows a mass of 0.85 ± 0.23 mg (mass gain of 0.47 ± 0.24 mg than probe A, n = 7), indicating it is ca. 1.3 times of thickness of the probe. This is labeled Film A.

Fabrication of Film B

Film B was prepared by dropping 25 µL of the polymer mixture onto the glass substrate. The liquid coating was then spread evenly on the surface by a pipet tip. The film was dried in air overnight before weighing or use. This film showed a mass of 1.90 ± 0.29 mg (*n* = 7), 1.3 ± 0.16 mg larger than the probe itself. This film is labeled Film B.

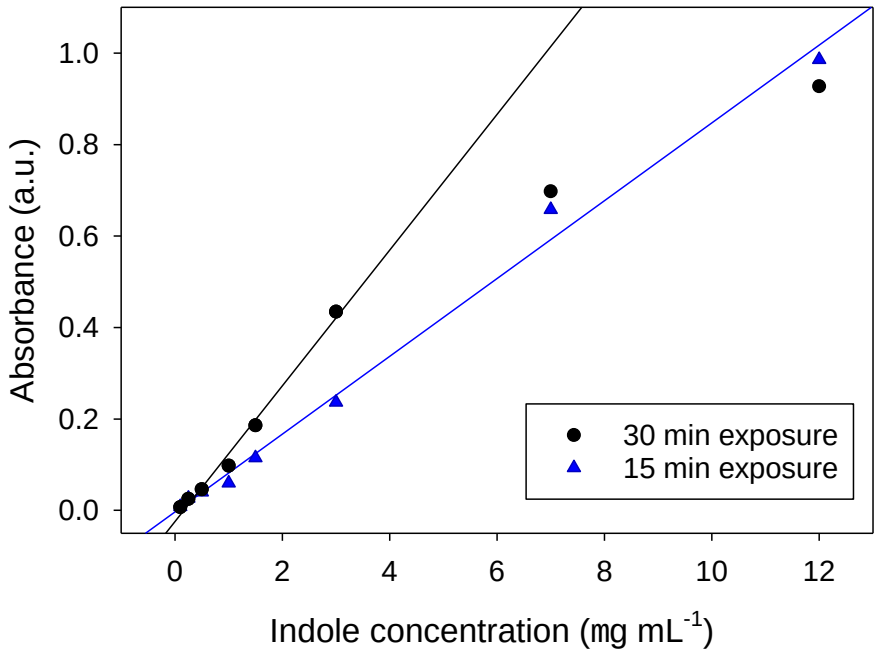

Figure A1. Probe response under different exposure times. A 30-min exposure exhibits a linear range up until 3 µg mL^{-1} (R^2 = 0.989, slope = 0.148) before saturation is observed. A 15-min exposure shows a larger range until 12 µg mL^{-1} (R^2 = 0.993, slope = 0.085) but lower sensitivity.

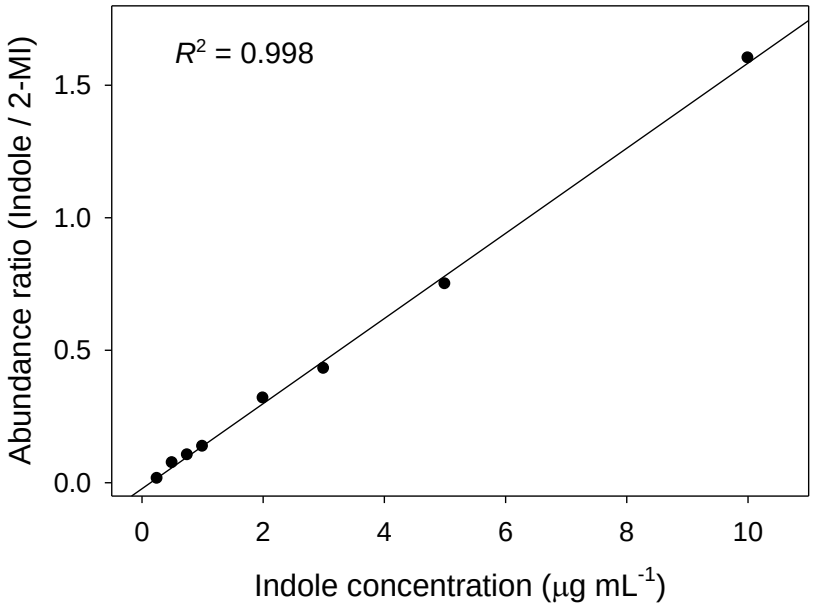

Figure A2. GC-MS calibration plot with standard solutions of indole in petroleum ether.

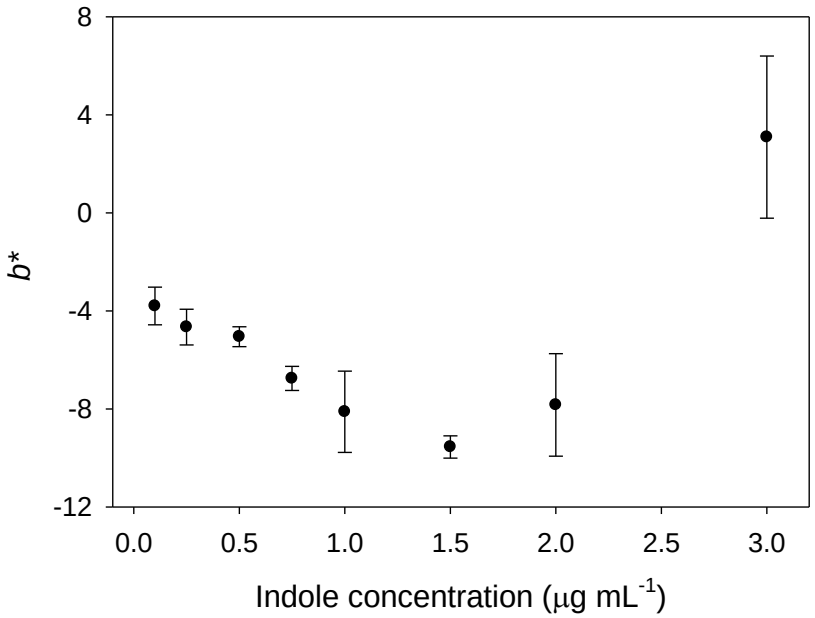

Figure A3. Plot showing *b** axis values after exposure of the probe to indole in the probe to indole in petroleum ether solutions.

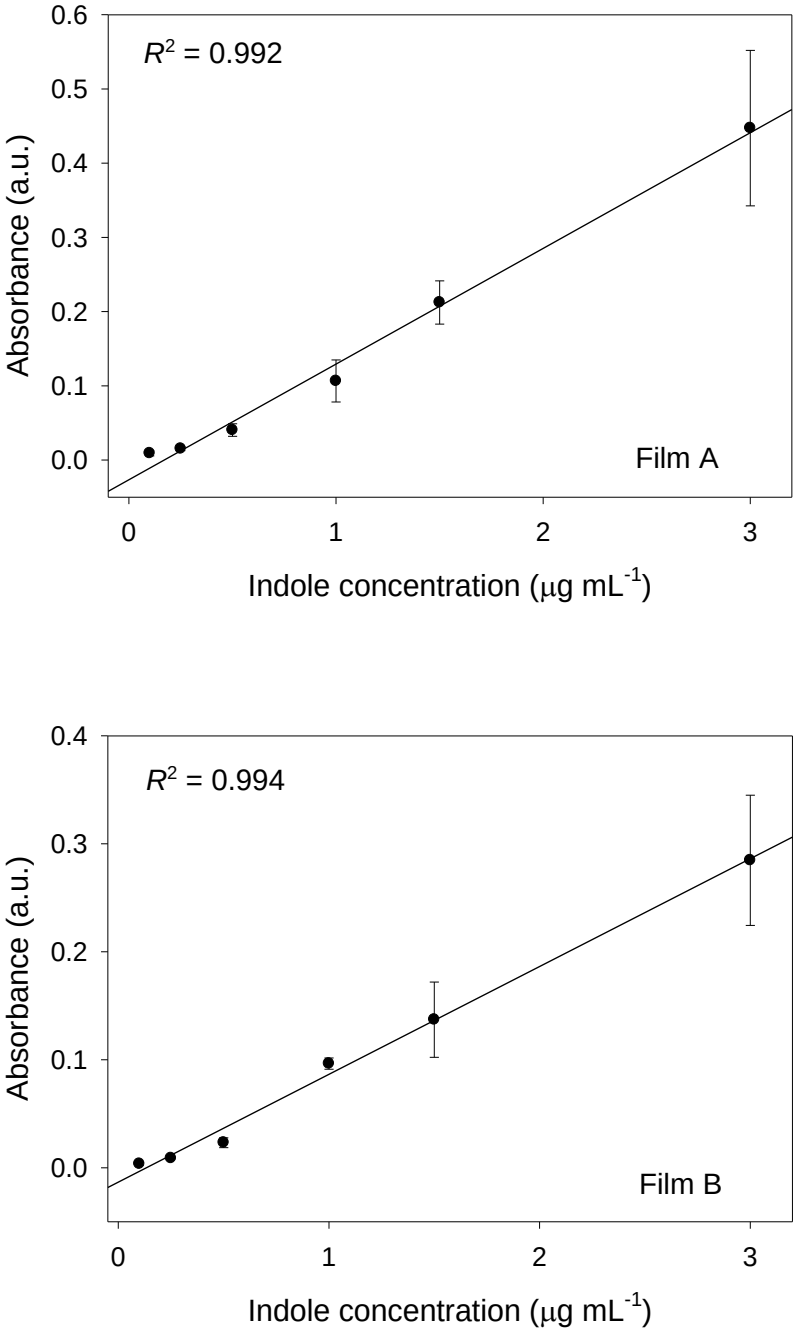

Figure A4. UV-Vis calibration plots for Films A (top) and B (bottom).

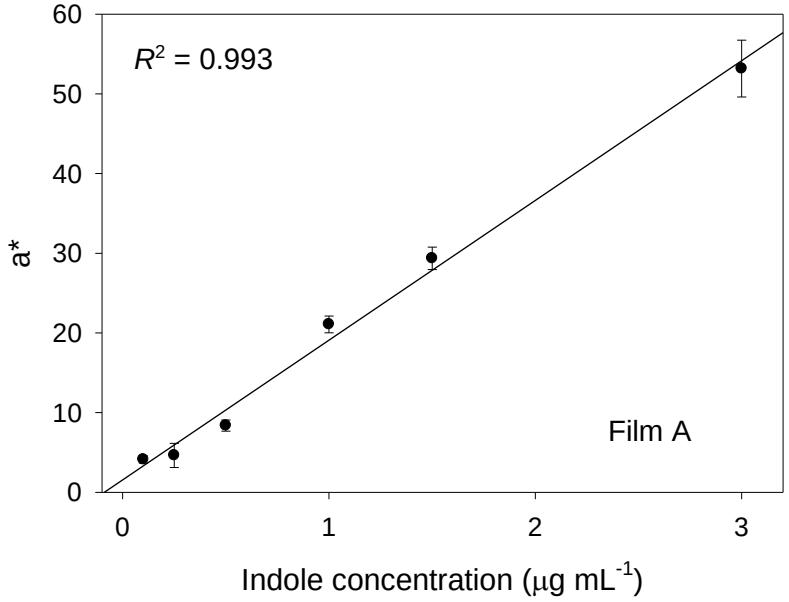

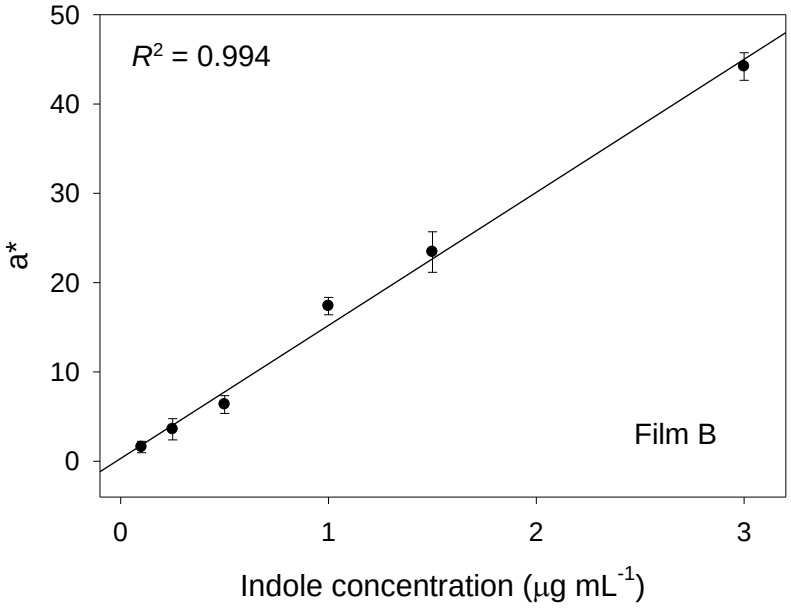

Figure A5. CIELAB calibration plots for Films A (top) and B (bottom).

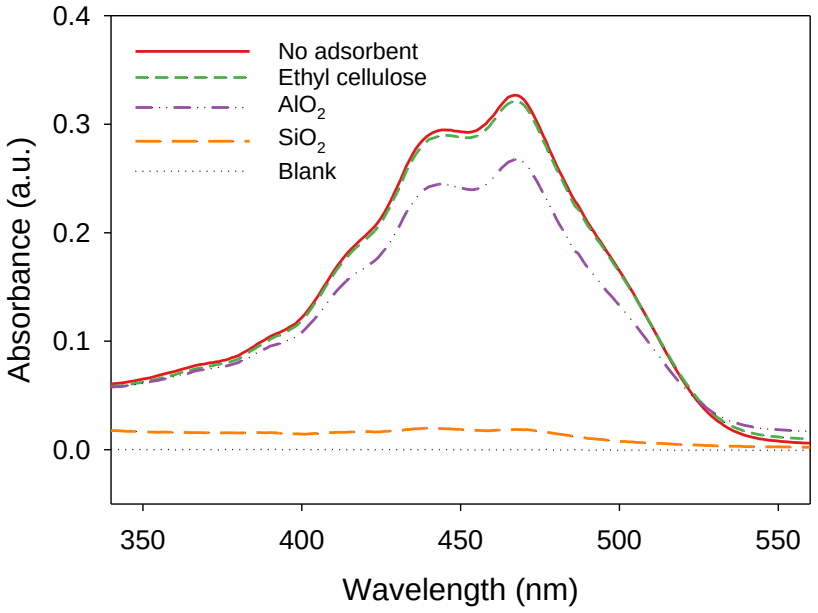

Figure A6. Visible spectra of solutions after extraction of astaxanthin from shrimp. Adsorbent material (20 mg), ethyl cellulose, AlO_2 or SiO_2, was added to 10 mL of the solution and stirred for 30 s. The highest adsorption was observed with SiO_2.

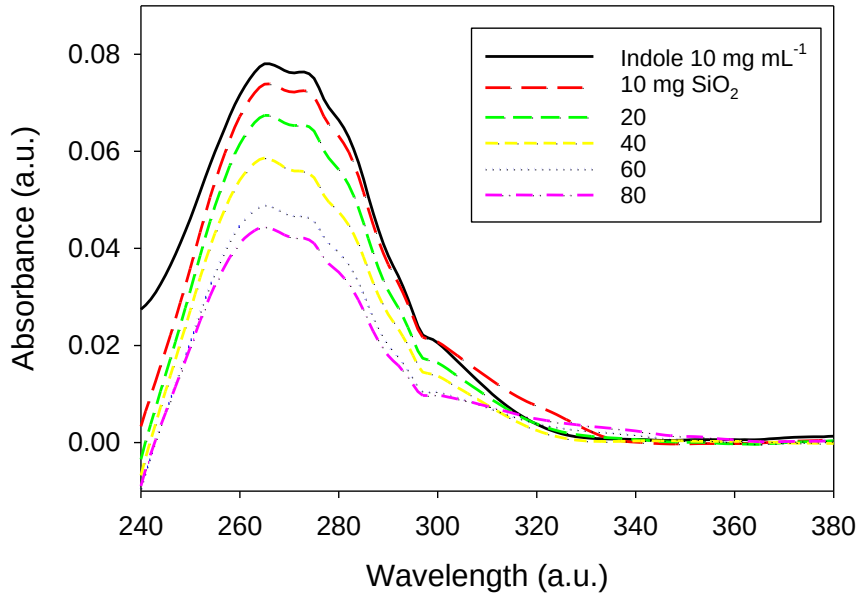

Figure A7. UV-Vis spectra of a solution of indole in petroleum ether (10 µg mL^{-1}) before (black line) and after addition of 10-80 mg of SiO_2.

Table A.1. Preliminary tests for probe polymer matrix

Polymer	Concentration (wt%)	Matrix solvent	Solubility tests
EC	5%	Ethanol/Toluene 1:1	Toluene (s), EtOAc (s), PE (i)
EC	5%	THF	Toluene (s), EtOAc (s), PE (i)
EC	10%	Ethanol/Toluene 1:1	Toluene (s), EtOAc (s), PE (i)
EC	10%	THF	Toluene (s), EtOAc (s), PE (i)
PMMA	5%	Ethanol/Toluene 1:1	PE (i)
PEG	5%	Ethanol/Toluene 1:1	Toluene (s), EtOAc (s), PE (i)
PEG	18%	Ethanol/Toluene 1:2	Toluene (s), EtOAc (ps), PE (i)
PEG	10%	THF	EtOAc (i), PE(i)

Abbreviations: EC, ethyl cellulose (90-100 mPas, TCI America); PMMA, poly(methyl-methacrylate) (MW 120,000, Aldrich); PEG, polyethylene glycol (MW 2,000, TCI); EtOAC, ethyl acetate (certified ACS, Fisher); PE, petroleum ether (certified ACS, Fisher). The insoluble (i) matrices were exposed to 1% indole in the corresponding solvent. Ethyl cellulose films showed readily responded after exposure and used for further simplex optimization.

Appendix B

Appendix B provides supplemental materials for Part 3.

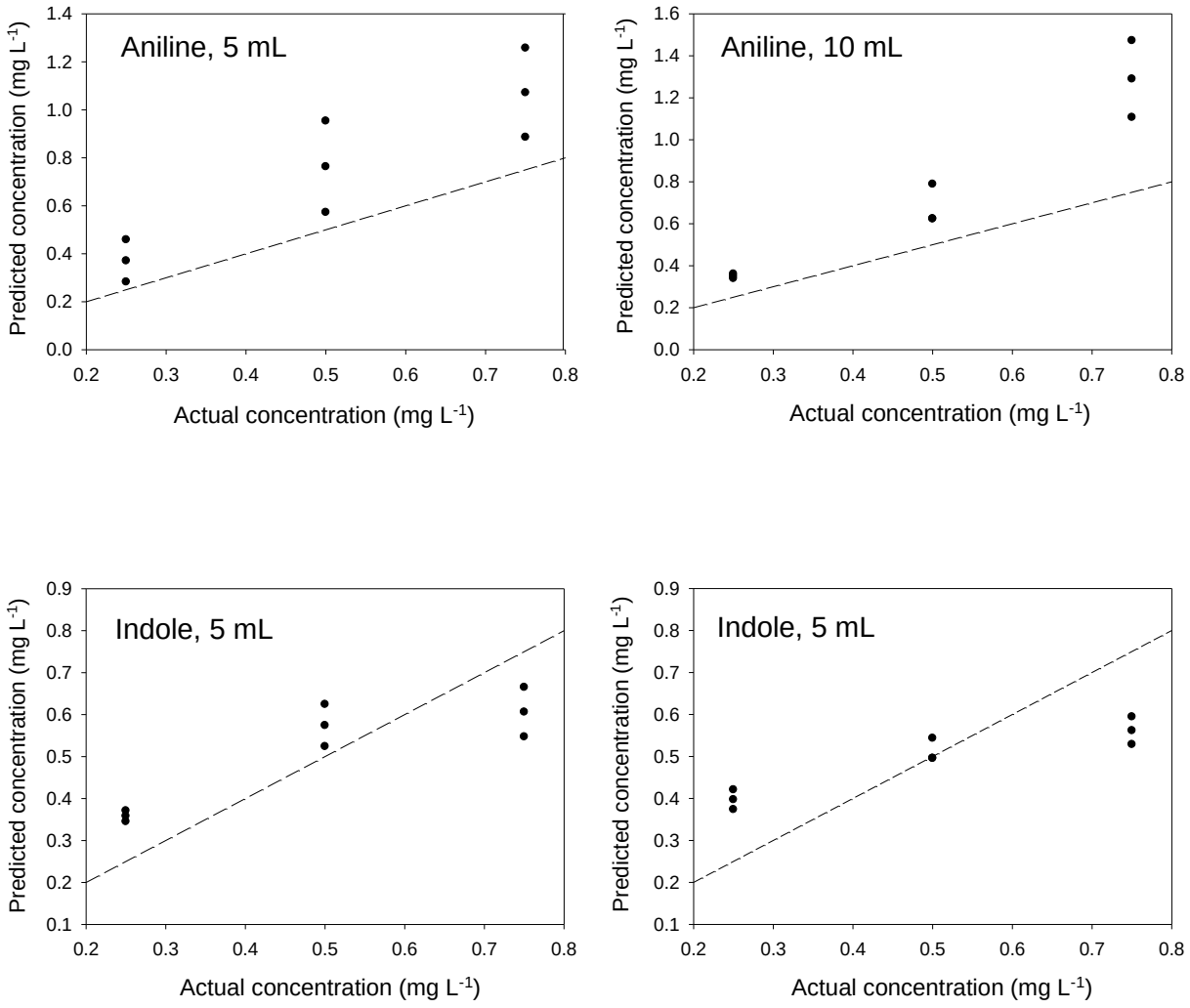

Figure B1. Predictions on validation dataset with CLS calibration for aniline (top) and indole (bottom) for a 15 min exposure time.

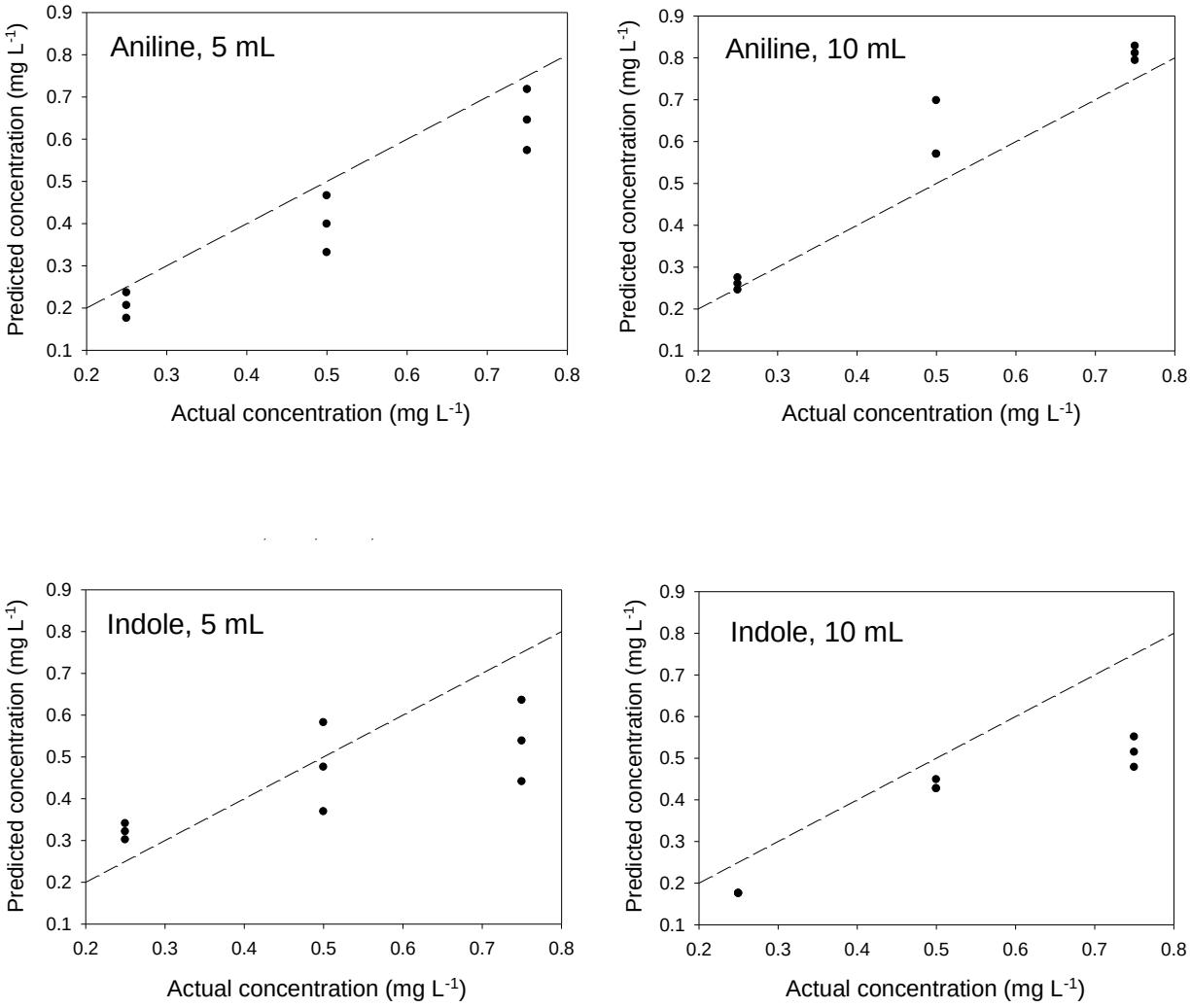

Figure B2. Predictions on validation dataset with CLS calibration for aniline (top) and indole (bottom) for a 30 min exposure time.

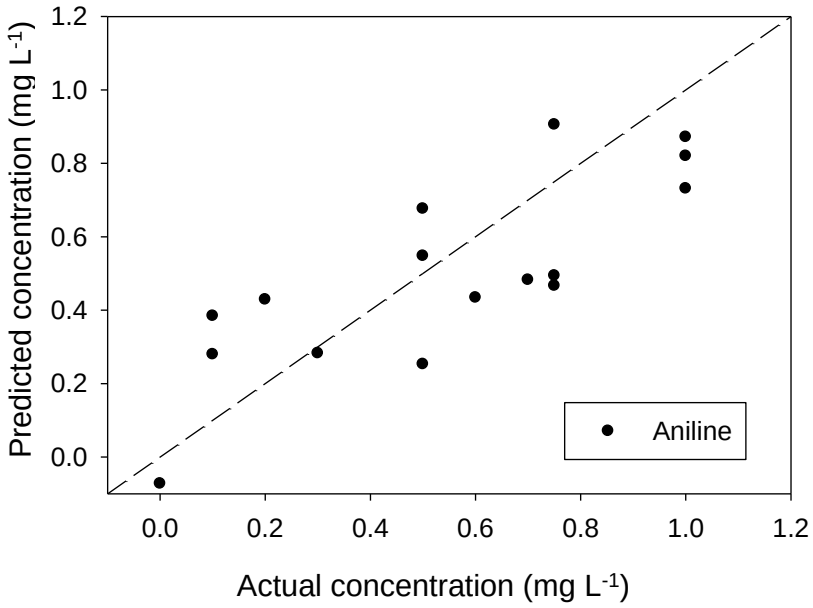

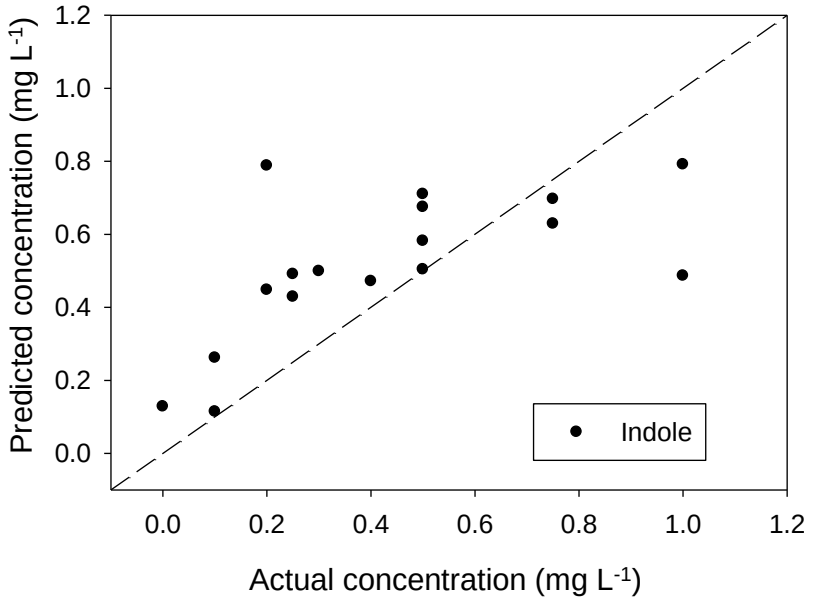

Figure B3. Predictions on validation dataset with PCR calibration for aniline (top) and indole (bottom) for a 30 min exposure. Wavelength range used was 301-701 nm. Six PCs were retained. The equations for the linear fit of aniline and indole are $y = 0.696x + 0.0932$ ($R^2 = 0.607$) and $y = 0.428x + 0.3299$ ($R^2 = 0.404$), respectively.

Appendix C

Appendix C provides supplemental materials for Part 4.

Predicted ^{13}C NMR shifts of indole (135.5, 127.6, 124.1, 121.7, 120.5, 119.6, 111.0, 102.1 ppm, Scheme C.1) by the ChemDraw Professional 2016 program are closed to those reported [^{13}C NMR (101 MHz, $CDCl_3$) 135.9, 128.0, 124.2, 122.12, 120.9, 119.9, 111.1, 102.8 ppm; V. Kanchupalli, D. Joseph, S. Katukojvala. Pyridazine N-oxides as precursors of metallocarbenes: Rhodium-catalyzed transannulation with pyrroles. Org. Lett. 17 (2015), 5878]. The ChemDraw program indicates that the shifts of α and β C atoms in indole are 124.1 and 102.1 ppm, respectively. Although there is no direct correlation between the electron density on an atom and its chemical shift, the upfield shift of the β C atom is consistent with higher electron density on the β C atom than on the α C atom, making the former to be more nucleophilic.

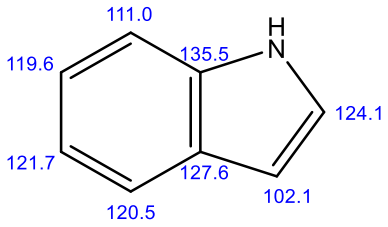

Scheme C.1. Chemical shifts predicted by the ChemDraw program.

Table C.2. Crystal data and structure refinement for β-bis(indolyl)methane

Parameters	Data
Empirical formula	C25 H23 N3
Formula weight	365.46
Temperature	100(2) K
Wavelength	0.71073 Å
Crystal system	Monoclinic
Space group	*P* 21/n
Unit cell dimensions	*a* = 11.4391(12) Å
	b = 10.0716(10) Å
	c = 16.9545(17) Å
Volume	1945.5(3) $Å^3$
Z	4
Density (calculated)	1.248 Mg/m^3
Absorption coefficient	0.074 mm^{-1}
F(000)	776.0
Crystal size	0.06 x 0.05 x 0.04 mm^3
θ range for data collection	2.065 to 28.707°
Index ranges	$-15 \leq h \leq 15$, $-13 \leq k \leq 13$, $-22 \leq l \leq 22$
Reflections collected	22510
Independent reflections	4779 [*R*(int) = 0.0239]
Completeness to θ = 28.707°	94.8%
Absorption correction	Semi-empirical from equivalents
Refinement method	Full-matrix least-squares on F^2
Data / restraints / parameters	4779 / 0 / 255
Goodness-of-fit on F^2	1.129
Final *R* indices [$I > 2\sigma(I)$]	*R*1 = 0.0436, w*R*2 = 0.1467
R indices (all data)	*R*1 = 0.0476, w*R*2 = 0.1400
Largest diff. peak and hole	0.39 and -0.237 e.$Å^{-3}$

Appendix D

Appendix D provides supplemental materials for Part 5.

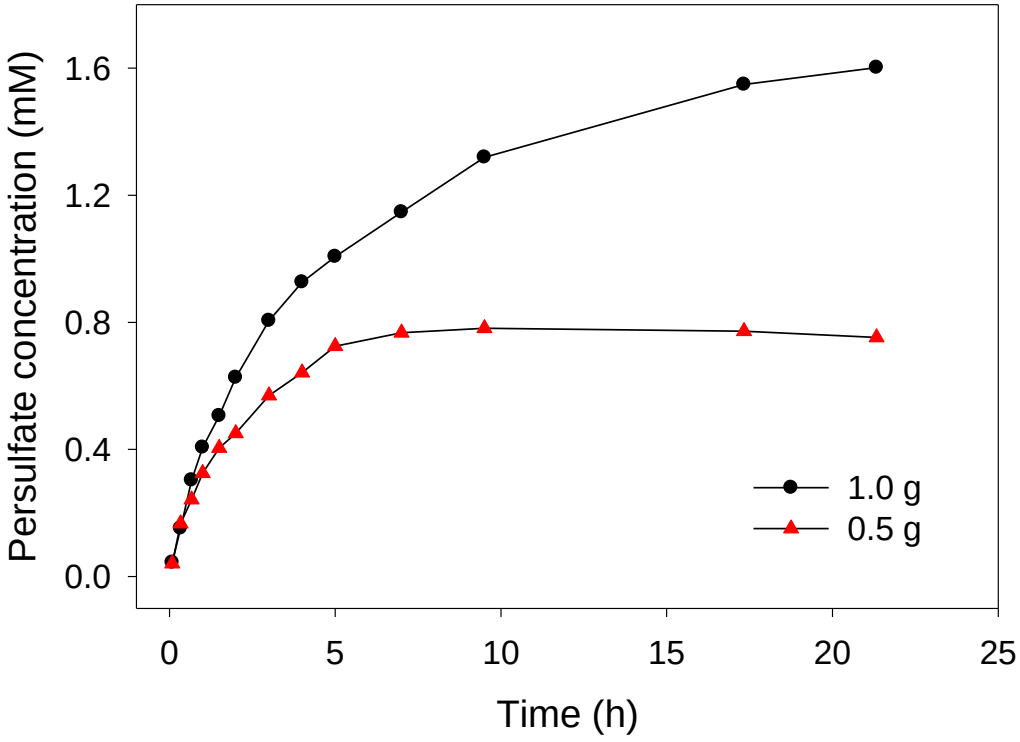

Figure D.1. Release profile for pellets with pre-mixed persulfate.

Vita

Roberto Alan Federico Perez was born in 1988 in Caborca, a city in the Sonoran Desert of northwestern Mexico. After participating in the National Chemistry Olympiad in high school, he started undergraduate studies at the University of Sonora in Hermosillo, Mexico, where he received BSc degree in Food Chemistry in 2011. Roberto then pursued a Graduate Certificate in sustainable development. His capstone project involved the detection of mercury from hidden sources in a clinical laboratory. Roberto graduated in 2013 and started his PhD studies in chemistry in Fall 2013 at the University of Tennessee, Knoxville. He joined the group of Dr. Zi-Ling (Ben) Xue, where he worked on the optical detection of several analytes of interest, and the controlled release of species for chemical oxidation. During the graduate studies, Roberto served as President of the Association of Chemistry Graduate Students, attended the 2016 ACS Summer School in Green Chemistry and Sustainable Energy, and participated in the organization of the International Symposium on Green Chemistry in 2017. Roberto presented his research at the 2016 Pittcon (Pittsburgh Conference on Analytical Chemistry and Applied Spectroscopy) in Atlanta and the 253rd American Chemical Society National Meeting in San Francisco in 2017.